© 2022. Published by The Company of Biologists Ltd | Journal of Cell Science (2022) 135, jcs260042. doi:10.1242/jcs.260042

RESEARCH ARTICLE

MLL regulates the actin cytoskeleton and cell migration by stabilising Rho GTPases via the expression of RhoGDI1

Akash Chinchole[1,2], Kaisar Ahmad Lone[1,3] and Shweta Tyagi[1,*]

ABSTRACT

Attainment of proper cell shape and the regulation of cell migration are essential processes in the development of an organism. The mixed lineage leukemia (MLL or KMT2A) protein, a histone 3 lysine 4 (H3K4) methyltransferase, plays a critical role in cell-fate decisions during skeletal development and haematopoiesis in higher vertebrates. Rho GTPases – RhoA, Rac1 and CDC42 – are small G proteins that regulate various key cellular processes, such as actin cytoskeleton formation, the maintenance of cell shape and cell migration. Here, we report that MLL regulates the homeostasis of these small Rho GTPases. Loss of MLL resulted in an abnormal cell shape and a disrupted actin cytoskeleton, which lead to diminished cell spreading and migration. MLL depletion affected the stability and activity of Rho GTPases in a SET domain-dependent manner, but these Rho GTPases were not direct transcriptional targets of MLL. Instead, MLL regulated the transcript levels of their chaperone protein RhoGDI1 (also known as ARHGDIA). Using MDA-MB-231, a triple-negative breast cancer cell line with high RhoGDI1 expression, we show that MLL depletion or inhibition by small molecules reduces tumour progression in nude mice. Our studies highlight the central regulatory role of MLL in Rho/Rac/CDC42 signalling pathways.

This article has an associated First Person interview with the first author of the paper.

KEY WORDS: Cell migration, Cell shape, H3K4 methylation, MLL, Rho GTPases, RhoGDI1

INTRODUCTION

Actin exists as a monomeric soluble form as well as in filamentous form in cells. The assembly of actin monomers into filaments or polymerisation is brought about by proteins that belong to a family of 23 small G proteins called Rho GTPases. This assembly provides cells with a strong mechanical framework, which allows cells to migrate, maintain a rigid shape and transport cargo (Pollard and Cooper, 2009).

The Rho family of GTPases contains small G proteins that act as molecular switches. Most of them are 'ON' when in a GTP-bound state, and after GTP hydrolysis, they switch back to an 'OFF' state (Goitre et al., 2014). Rho GTPases play an important role in regulating the dynamics of the actin cytoskeleton, cell adhesion, establishing cell polarity and cell migration. Three Rho GTPases are well characterised, namely, RhoA, Rac1 and CDC42, each having unique as well as interdependent roles in signal transduction (Jaffe and Hall, 2005). Constitutively active mutants of RhoA, Rac1 and CDC42 were found to give rise to distinct actin structures in Swiss 3T3 fibroblasts (Nobes and Hall, 1995). Whereas constitutively active RhoA led to the formation of bundles of actin stress fibres, constitutively active Rac1 and CDC42 formed protrusions containing thin sheets of branched actin filaments called lamellipodia and spike-like structures of parallel actin bundles called filopodia (Ridley and Hall, 1992; Ridley et al., 1992; Nobes and Hall, 1995). Cell shape is also governed by the activities of Rho GTPases. Cells of different lineages, such as columnar epithelial cells and stretched and branched neurons during morphogenesis, display a variety of shapes, which are necessary for their functions (Jaffe and Hall, 2005; Paluch and Heisenberg, 2009). Remarkably, cells originating from a single population also exhibit different shapes, owing to dynamics of Rho GTPases and their crosstalk involving their activation and mutual antagonism (Sailem et al., 2014; Zmurchok and Holmes, 2020).

Cell migration is another complex process that is facilitated by the combined action and crosstalk of RhoA, Rac1 and CDC42. Rac1 is activated at the leading edge of migrating cells to form lamellipodia. CDC42 determines the direction of migration (Raftopoulou and Hall, 2004). RhoA regulates focal adhesion assembly, stress-fibre formation and activation of contractile myosin fibres. RhoA also severs old focal adhesion contacts at the rear end of cells, and its inhibition in migrating monocytes causes tail retraction defects and cell elongation (Worthylake et al., 2001). This constitutes a simple model for cell migration, although there is also evidence of crosstalk between these GTPases (Ridley et al., 2003).

The activity of Rho GTPases is very tightly regulated, mainly by three kinds of proteins. Guanine nucleotide exchange factors (GEFs) activate Rho GTPases by catalysing the exchange of GTP to GDP-bound Rho GTPases, GTPase-activating proteins (GAPs) inactivate Rho GTPases by increasing their intrinsic GTPase activity, and guanine nucleotide dissociation inhibitors (GDIs) interact with either GTP- or GDP-bound GTPases, masking their prenyl tails and sequestering them in the cytosol (Jung et al., 2020). In the absence of GDIs, Rho GTPases are targeted for proteasomal degradation (Boulter et al., 2010). Apart from these, Rho GTPases are also regulated by various post-translational modifications that determine their subcellular localisation, activity or stability (Hodge and Ridley, 2016; Navarro-Lérida et al., 2021). Due to the intricate spatiotemporal control of the activity of Rho GTPases and their crucial roles in key pathways, their dysregulation has been implicated in several cancers (Pillé et al., 2005; Cho et al., 2018).

In eukaryotes, su(var)3–9, enhancer-of-zeste, trithorax (SET) 1 (SET1 or KMT2) family proteins introduce the histone 3 lysine 4 (H3K4) tri-, di- and mono-methylation marks (Zhang and

[1]Laboratory of Cell Cycle Regulation, Centre for DNA Fingerprinting and Diagnostics (CDFD), Uppal, Hyderabad 500039, India. [2]Graduate Studies, Manipal Academy of Higher Education, Manipal 567104, India. [3]Graduate Studies, Regional Centre for Biotechnology, Faridabad 121001, India.

*Author for correspondence (shweta@cdfd.org.in)

A.C., 0000-0003-0371-8811; K.A.L., 0000-0001-9132-6476; S.T., 0000-0002-8349-6843

Handling Editor: Michael Way
Received 23 March 2022; Accepted 9 September 2022

Journal of Cell Science (2022) 135, jcs260042. doi:10.1242/jcs.260042

Bergamin, 2012). Humans contain six members in this family including mixed lineage leukaemia (MLL) proteins 1–4, SETD1A and SETD1B. Out of these, the founding member – MLL1 or KMT2A (hereafter referred to as MLL) is the best-characterised protein because of its role in aggressive leukaemia (Patel et al., 2009). MLL, a large nuclear protein, is processed post-translationally into the MLL-N and MLL-C subunits (Hsieh et al., 2003). MLL-N contains several chromatin-binding domains, whereas MLL-C provides the catalytic SET domain and trans-activation domain (TAD) to activate transcription (Ernst et al., 2001). As opposed to the global activity of SETD1A, MLL methylates defined target genes (Wang et al., 2009). Transcriptional maintenance of HOX genes by MLL in the development of mammalian embryos is well documented. MLL is also required for haematopoiesis and skeletal development (Cohn et al., 1997; Hess et al., 1997). A previous study showed that MLL-null mice did not survive beyond embryonic day 10.5 due to failure of continuous transcriptional maintenance of genes during development (Yu et al., 1998).

Here, we describe the role of MLL in the regulation of the activity and stability of the Rho GTPases RhoA, Rac1 and CDC42. MLL-depleted cells displayed an atypical cell shape and loss of actin fibres resulting in defective cell spreading and migration. We found that the stabilisation of Rho GTPase levels depends on the catalytic SET domain of MLL; however, MLL depletion did not affect their transcript levels. We show that MLL regulates the stability of Rho GTPases by transcriptional activation of RhoGDI1 (also known as ARHGDIA) using its methyltransferase activity. Using xenograft experiments, we show that targeting the methyl transferase activity of MLL using the small-molecule inhibitor OICR-9429 reduced the size of tumours formed from the triple-negative breast cancer (TNBC) cell line MDA-MB-231. Our findings characterise MLL as an upstream regulator of the RhoA, Rac1 and CDC42 GTPases, and identify MLL as a potential novel therapeutic target for triple-negative breast cancer.

RESULTS

Loss of MLL causes changes in cell shape and in the actin cytoskeleton

Mammalian cells attain various complex shapes. To understand the role of MLL in regulating cell shape, we performed RNAi experiments using specific MLL siRNAs (Ali et al., 2014) and probed immunoblots with an anti-MLL antibody (Fig. 1A; Fig. S1A). The cells were subjected to indirect immunofluorescence staining (IF) using anti-α-tubulin antibodies. We observed that human osteosarcoma U2OS cells depleted of MLL assumed an elongated shape compared to control siRNA-treated cells (Fig. 1B). Ongoing studies from our laboratory indicate that MLL depletion does affect *de novo* microtubule polymerisation from the microtubule-organising centre (S. Chodisetty and S.T., unpublished). However, we could not detect any distinct microtubule organisation defects in MLL siRNA-treated cells, except that they bunched together in elongated parts, probably due to cell shape (Fig. 1B, see panels d–f). Apart from microtubules, cell shape is also governed by the actin cytoskeleton and intermediate filaments (Luxenburg and Zaidel-Bar, 2019). Therefore, we stained the cells with rhodamine dye-conjugated phalloidin, a peptide toxin known to bind filamentous actin (F-actin) with high affinity. Phalloidin-stained actin stress fibres could be clearly visualised in control cells (Fig. 1C, panels a–c,a′–c′; Fig. S1B). In contrast, in MLL-depleted cells, we observed a dramatic loss of visually discernible actin stress fibres as well as changes in cell shape (Fig. 1C; Fig. S1C). Based on a previous RNAi screen (Pascual-Vargas et al., 2017), we could make out the following prominent cell shapes in control siRNA-treated U2OS cells: (1) fan, (2) triangular and (3) circular (Fig. 1C; Fig. S1B). When cells were clumped, without a clear shape, we classified these as ‘compact’. In contrast, MLL-depleted cells exhibited two or three prominent protrusions and were classified as ‘spindly’ (Fig. 1C, panels d,e,d′,e′; Fig. S1C, panels a,b) or ‘triangular’ (Fig. 1C, panels g,h,g′,h′; Fig. S1C, panels d,e). The triangular shape observed for MLL-depleted cells differed from that seen in control cells as they exhibited elongated protrusions on one side [with a number of distinct filopodia (Fig. 1C, panels g,h,g′,h′) or no filopodia (Fig. S1C, panels d,e)]. Therefore, we made the distinction in the two shapes by classifying them as ‘triangular normal’ (‘N’) (Fig. 1C, panels a,b; Fig. S1B, panels d,e) or ‘triangular abnormal’ (‘A’) (Fig. 1C, panels g,h,g′,h′; Fig. S1C, panels d,e). Notably, when circular shapes were observed for MLL-depleted cells, the diameter of the cell was much smaller (compare Fig. S1B, panels g,h to Fig. S1C, panels g,h). To make sure that these observed cell shapes were not an artifact of the siRNA used, we used two different, previously used MLL siRNAs (Ali et al., 2014). As shown, treatment with both MLL siRNAs yielded similar counts in cell shape (Fig. 1D; Fig. S1D–I). We observed that, the frequency of fan-shaped and triangular-normal cells was significantly lower in MLL siRNA-treated cells (Fig. S1D,E), whereas the frequency of spindly and triangular-abnormal cells was significantly higher (Fig. S1G,H). The percentages of cells that were circular or compact were similar in all samples (Fig. S1F,I). Next, we tried to observe the correlation of cell shape to the presence or absence of actin fibres. However, this analysis was not feasible as we did not have a sufficient number of cells in some populations to make a statistical comparison. Nonetheless, irrespective of their shape, across all cell-shape categories, we observed a substantial decrease in the number of actin stress fibres in MLL siRNA-treated cells (Fig. 1E). Taken together, our findings indicate that MLL depletion affects actin stress-fibre formation as well as cell shape.

Depletion of MLL alters cell spreading and cell migration

The extracellular matrix (ECM) composition influences downstream actin cytoskeleton remodelling (Reymond et al., 2012a). In fact, substrates coated with ECM components, such as fibronectin, are often used to mimic tissue environments characteristic of human cancer metastases (Reymond et al., 2012a). Rho GTPases and the actin cytoskeleton play a crucial role in cell spreading on ECM-coated surfaces. Therefore, we tested whether the ability of cells to spread on ECM-coated surfaces is affected due to loss of MLL. Our results show that there was a significant loss of area occupied by the spread cells upon MLL knockdown (Fig. 2A,B). Interestingly, we also observed that within 4 h of spreading on fibronectin-coated surfaces, MLL-depleted cells adopted an elongated shape (similar to that seen on uncoated glass surfaces). We quantified these shapes by measuring circularity ($c=4\pi A/P^2$, where A is the area and P the perimeter; $c=1$ for perfect circle, $c<1$ for elongated objects) of cells and found a significant decrease in circularity upon loss of MLL (Fig. 2C). We also measured the aspect ratio (ratio of the major axis to the minor axis; aspect ratio>1 for elongated objects), which showed a significant increase in MLL siRNA-treated cells compared to control cells (Fig. 2D). Taken together with the data in Fig. 1, these observations point to a role of MLL in the regulation of cell shape.

As the cell shape and actin cytoskeleton were dramatically perturbed upon knockdown of MLL, we suspected that loss of MLL would also affect cell migration. To test our hypothesis, we performed transwell migration assays. Upon treatment with two MLL-specific shRNAs, but not with control shRNA, we observed

Journal of Cell Science (2022) 135, jcs260042. doi:10.1242/jcs.260042

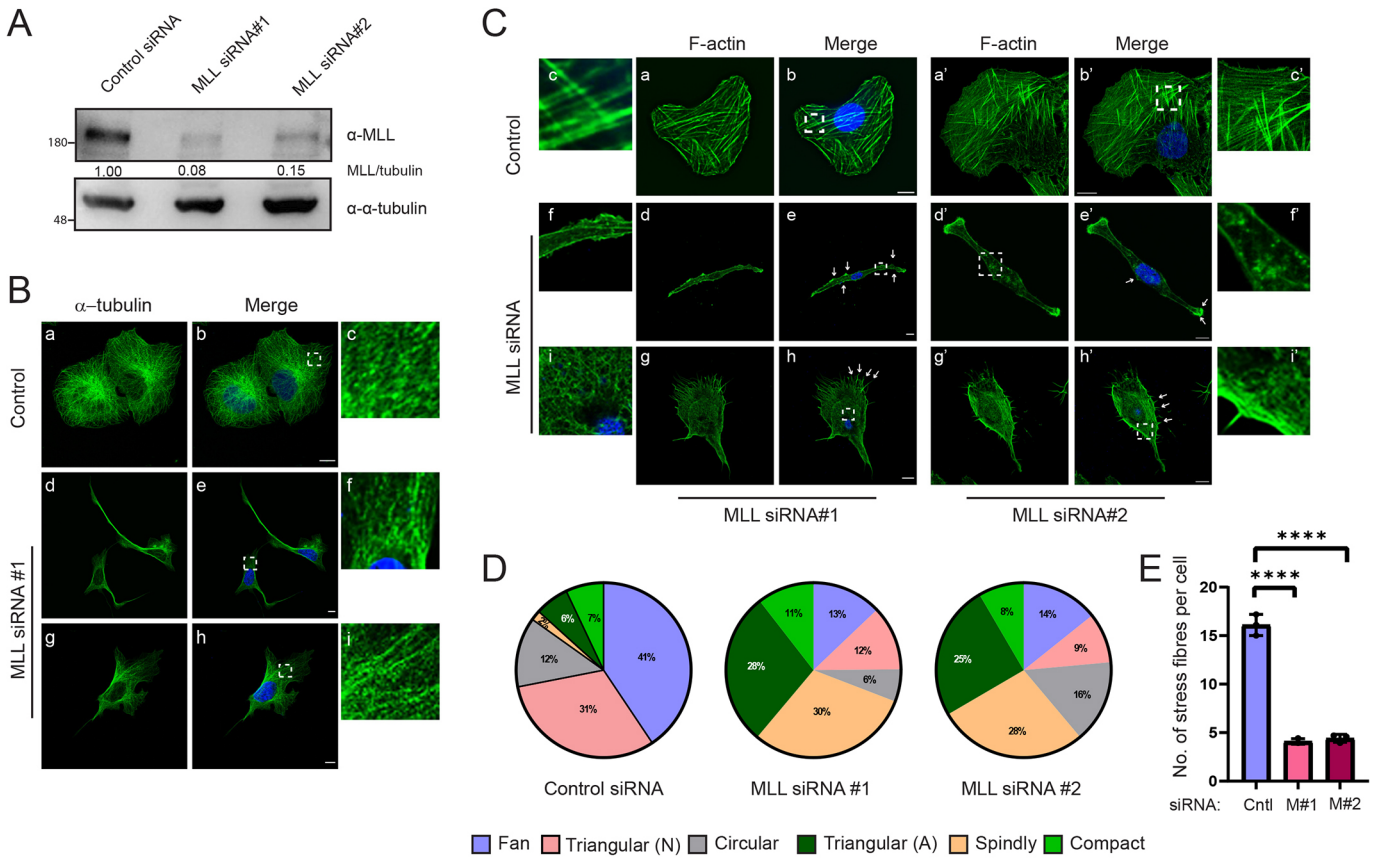

Fig. 1. Loss of MLL affects cell shape and actin cytoskeleton. (A) U2OS cells, treated with control siRNA, MLL siRNA#1 and MLL siRNA#2 for 72 h were lysed and immunoblotted. Blots were probed with anti-MLL and anti-α-tubulin antibody as indicated. The MLL/tubulin ratios are indicated. (B,C) Control and MLL siRNA-treated U2OS cells were fixed and used for immunofluorescence (IF). Cells were stained using anti-α-tubulin (B, green) antibody or rhodamine-conjugated phalloidin (C, green). The nucleus was stained using DAPI (blue). White arrows in C, panels e,e′ indicate small protrusions and those in panels h,h′ indicate spine-like actin-rich filopodia. Panels c,f,i,c′,f′,i′ show magnified views of the boxed regions in panels b,e,h,b′,e′,h′, respectively. Scale bars: 10 µm. (D,E) Shape of the cells (D) or number of stress fibres in cells (E) treated with different siRNAs from (C) were quantified from three independent experiments as shown. Data represents mean±s.d. ****P<0.0001, one-way ANOVA with Dunnett's multiple comparisons test. F-actin, filamentous actin; Cntl, control; M#1, MLL siRNA#1; M#2, MLL siRNA#2.

reduced cell migration in U2OS cells (Fig. 2E–G; Fig. S2A). We also tested cell migration upon MLL downregulation in the epithelial TNBC cell line MDA-MB-231 (Fig. 2H), and observed results similar to those obtained in the osteosarcoma epithelial cells (Fig. 2G).

Thrombin not only activates RhoA, Rac1 and CDC42 (Azim et al., 2000; van Nieuw Amerongen et al., 2000), but also stimulates cell migration by different mechanisms (Radjabi et al., 2008). As MLL-depleted U2OS cells showed reduced migration, we wanted to know whether stimulation of these cells with thrombin over longer durations affects cell migration. We found a significant increase in cell migration in control cells upon thrombin treatment (Fig. 2I, compare bar 1 to bar 3). However, this difference was not apparent in MLL-depleted cells (Fig. 2I, compare bar 2 to bar 4), indicating that MLL-depleted cells were insensitive to stimulation by thrombin. Taken together, our studies indicated that MLL knockdown perturbed the actin cytoskeleton, which was associated with changes in cell shape and reduced cell migration.

MLL or Rho GTPase depletion causes loss of actin dynamics and lamellipodia

Our observations of elongated cells with poor F-actin fibres and reduced cell migration are reminiscent of studies describing loss of RhoA family members (Vega et al., 2011; Reymond et al., 2012b). Thus, to compare the changes in actin cytoskeleton and cell shape that we observed here, we performed experiments to knockdown RhoA, Rac1 and CDC42, three of the best-characterised Rho GTPases involved in actin cytoskeleton remodelling (Etienne-Manneville and Hall, 2002), by using previously published siRNAs (Boulter et al., 2010; Reymond et al., 2012b; see Materials and Methods, Fig. 3A–C). We observed elongated cells upon RhoA and CDC42 siRNA treatments, similar to those seen upon MLL knockdown (Fig. 1C, Fig. 3D; Fig. S2B). Although cell elongation upon loss of Rac1 has been reported previously (Guo et al., 2006), we did not observe this phenotype in our studies (Fig. 3D; Fig. S2B). This might be due to the use of Rac1 knockout (KO) mouse embryonic fibroblasts in the previous study (Guo et al., 2006), in which Rac1 expression was completely abolished, as opposed to siRNA treatment here (Fig. 3B).

We observed a significant reduction in actin stress fibres upon depletion of Rho GTPases (Fig. 3D,E). In contrast, control siRNA-treated cells displayed distinct numerable actin stress fibres. Rac1 siRNA-treated cells exhibited few prominent actin stress fibres (Fig. 3D, compare panel c to panel i); however, when counted, the numbers were significantly less than in control cells (Fig. 3D,E). Loss of Rac1 leads to a dramatic decrease of the dorsal but not the ventral stress fibres (Kovac et al., 2013). This explained the diminished number of stress fibres upon Rac1 depletion even if a

Journal of Cell Science (2022) 135, jcs260042. doi:10.1242/jcs.260042

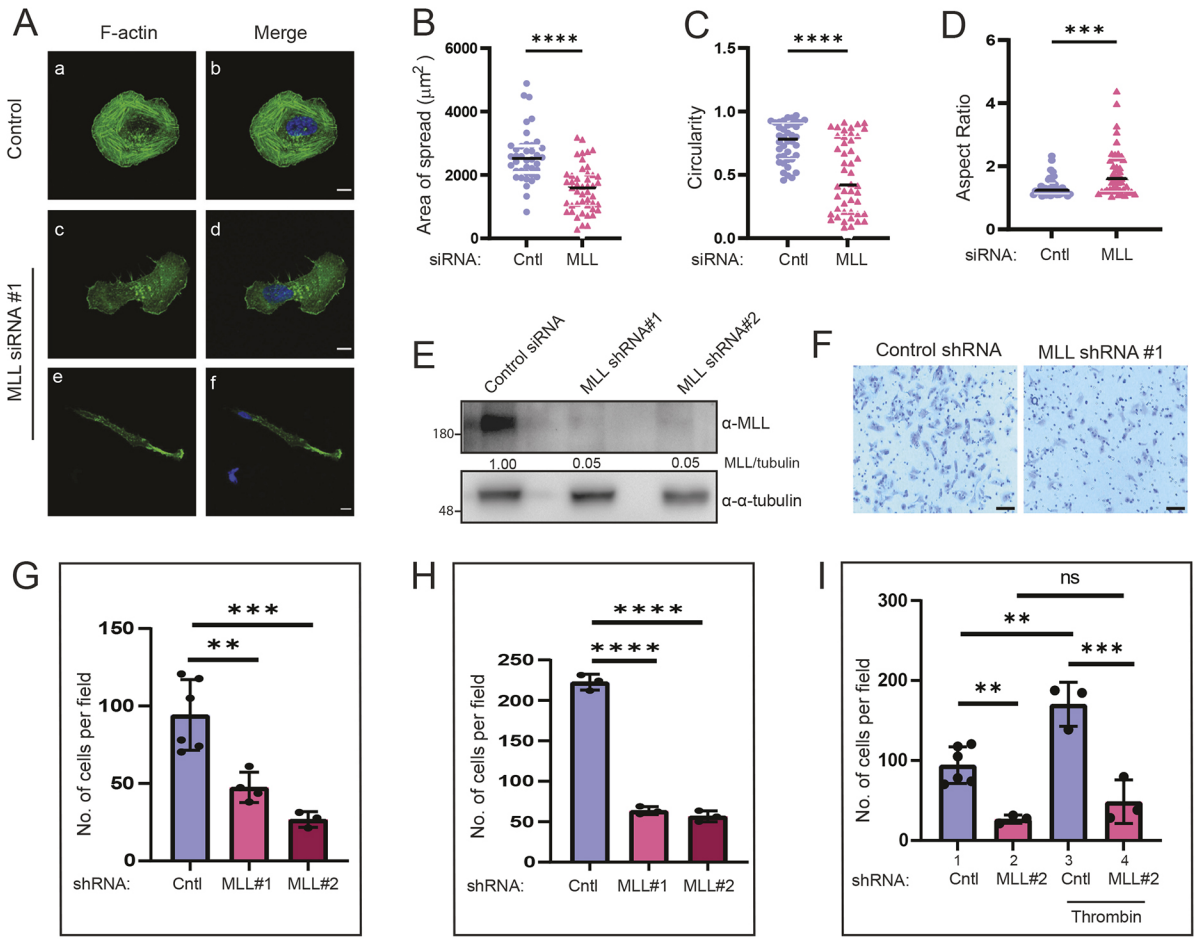

Fig. 2. Depletion of MLL alters cell spreading and cell migration. (A) Representative IF images of U2OS cells, treated with control or MLL siRNA#1 for 72 h, and plated on fibronectin-coated coverslips for 4 h. Phalloidin (green) and DAPI (blue) staining is shown. Scale bars: 10 µm. (B–D) Quantifications of area of spread (B), circularity (C) and aspect ratio (D) of control or MLL siRNA-treated cells. Data are represented as violin plot with all the data points and the median. ****P<0.0001, ***P<0.0004 (Student's unpaired two-tailed t-test; n=40 cells and N=2 experiments). (E) Immunoblotting of lysates from U2OS cells treated with two different MLL shRNAs, probed with anti-MLL and anti-tubulin antibodies, is shown. The MLL/tubulin ratios are indicated. (F) U2OS cells were treated with control or MLL shRNA#1 for 48 h and transwell migration (Boyden chamber) assay was performed. Bright-field images show migrated cells upon treatment with the indicated shRNAs. Scale bars: 50 µm. (G,H) Quantifications for the number of U2OS (G) and MDA-MB-231 (H) cells migrated per field. Data are represented as mean±s.d. **P=0.0046, ***P=0.0006 (G); ****P<0.0001 (H) (one-way ANOVA with Dunnett's multiple comparisons test; N=3 experiments). (I) U2OS cells treated with control or MLL shRNA#2 were incubated in medium containing thrombin (4 U/ml) for 48 h and seeded for transwell migration assay. Quantifications for the number of cells migrated per field is shown. For ease of comparison, data from G of control and MLL shRNA#2 treatments are replotted here. Data are represented as mean±s.d. **P=0.007 (bar 2) and 0.003 (bar 3); ***P=0.0002; ns, not significant, P=0.65 (one-way ANOVA with Tukey's multiple comparisons test; N=3 experiments).

few prominent stress fibres remained. MLL depletion caused similar reduction in actin stress fibres to that seen individually with RhoA, Rac1 and CDC42 depletion (Fig. 3E, Nobes and Hall, 1995; Guo et al., 2006; Vega et al., 2011; Huang et al., 2016). Thus, our results here indicated that MLL might regulate one or possibly more Rho GTPases.

As all three major Rho GTPases being studied here showed defects in actin cytoskeleton assembly, we decided to use this assay to determine which domain of MLL is involved in this process. As transcription is the major activity ascribed to this protein, we focused on the nine-amino-acid TAD, which promotes cooperative binding of coactivators to augment synergistic gene activation (Ernst et al., 2001), and the SET domain, which is required for its H3K4 histone methyltransferase activity (Fig. S2C). We used previously described U2OS cells stably expressing various FLAG-tagged mutants of MLL (Fig. S2C,D) (Ali et al., 2014; Malik et al., 2022 preprint for the TAD cell line). Depletion of endogenous MLL in these cell lines was achieved by treatment with a siRNA targeting the 3′ UTR of the *MLL* transcript (siRNA#2, Fig. 1A), such that recombinant MLL expression was unaffected. Consistent with previous experiments, the number of actin stress fibres showed a reduction in wild-type U2OS cells upon treatment with MLL siRNA#2 (compare Fig. 3F to Fig. 1E). When the expression of the MLL protein was reconstituted, actin stress fibres were rescued but not to the same levels as those of wild-type U2OS cells (Fig. 3F). However, no further change was observed in stress-fibre numbers after cells were treated with siRNA#2, indicating that actin stress-fibre reduction could be specifically assigned to MLL depletion. Out of the two transcription-promoting domains of MLL, the absence of the SET domain but not TAD resulted in the reduction of actin stress fibres, suggesting that the methylation activity of MLL promoted actin stress-fibre formation (Fig. 3F).

As the actin cytoskeleton diminished with the loss of MLL, we wanted to explore whether actin dynamics in the cells were also affected. The primary driving force behind the motility and shape changes in cells depends on the dynamics of actin, which can be

Journal of Cell Science (2022) 135, jcs260042. doi:10.1242/jcs.260042

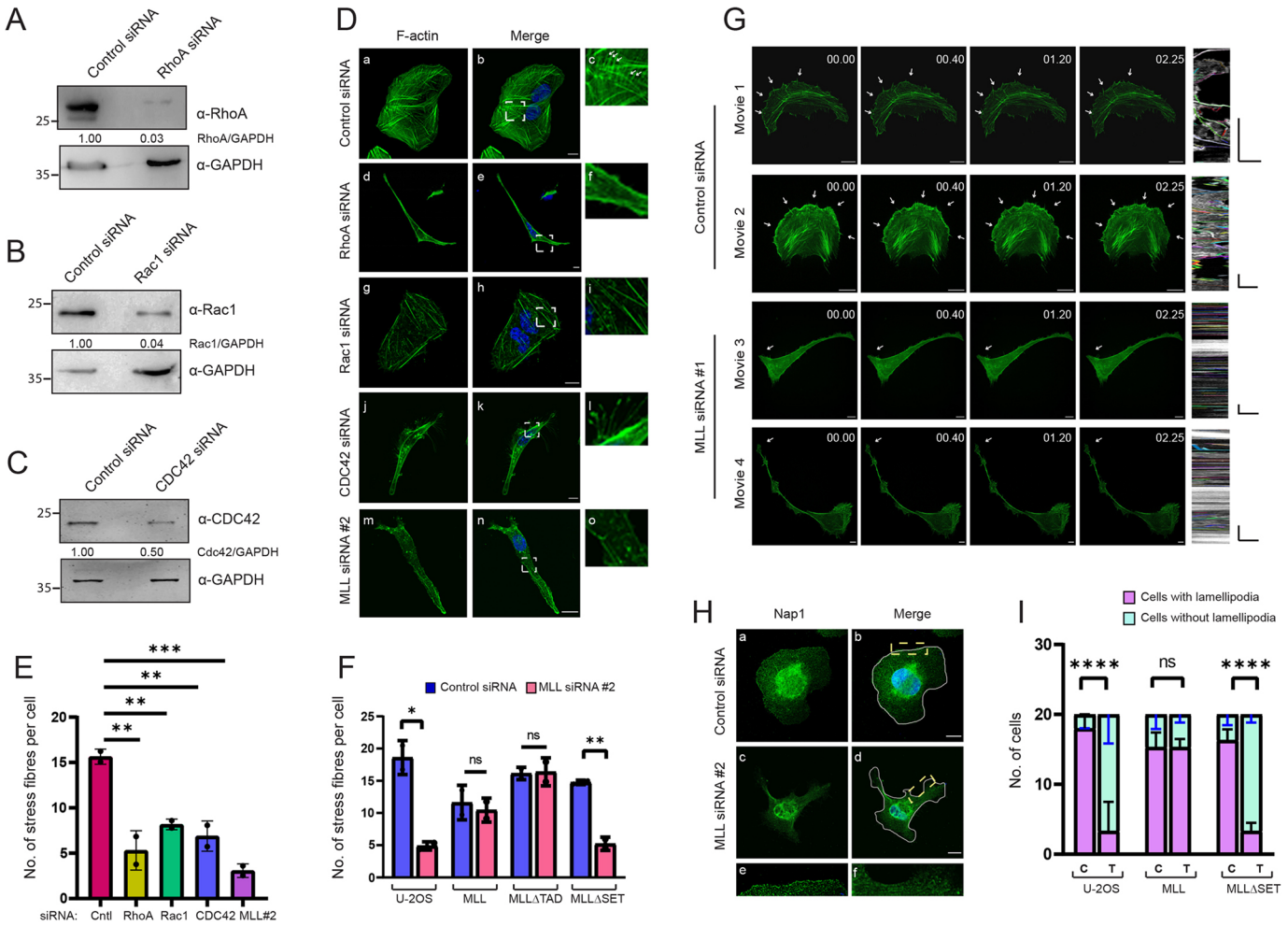

Fig. 3. MLL and Rho GTPase depletion causes loss of actin dynamics and lamellipodium formation. (A–C) Immunoblotting of whole-cell lysates of U2OS cells treated with control, RhoA, Rac1 and CDC42 siRNAs and probed with the respective antibodies are shown. GAPDH was used as a loading control. (D) IF of U2OS cells treated with the indicated siRNAs for 72 h. The cells were stained with phalloidin (green) and DAPI (blue). White arrows in panel c indicate fine actin stress fibres. (E) Quantification of the number of stress fibres in cells treated with the respective siRNAs from D. ***P<0.001; **P=0.001 (RhoA), 0.003 (Rac1) and 0.001(CDC42) (one-way ANOVA with Dunnett's multiple comparisons test; n=40 cells and N=2 experiments). (F) Quantification of the number of stress fibres in control U2OS cells, and in U2OS expressing various mutants of MLL, treated with control or MLL#2 siRNAs. Datas in wild-type U2OS are the same as E and replotted here. **P=0.006; *P=0.019; ns, not significant, P=0.66 (MLL) and 0.89 (MLLΔTAD) (Student's unpaired two-tailed t-test; n=40 cells and N=2 experiments). (G) U2OS cells expressing GFP–Lifeact were treated with control or MLL#1 siRNAs for 72 h, then imaged in SIM time-lapse mode at 5 s intervals. Representative images are shown with the time indicated in the mm.ss format (also see Movies 1–4). White arrows in the panels highlight regions with high actin dynamics. Kymographs are shown on left and the coloured lines therein indicate the particles selected for quantifying the average track velocities. (H) Formation of lamellipodia in control (panels a,b) and MLL-depleted (panels c,d) U2OS cells. Cell boundaries are marked in white in panel b,d, whereas magnified views of the dashed boxes are shown in panels e,f. (I) Number of cells with and without lamellipodia were quantified in cells treated with control or MLL#2 siRNAs. ****P<0.0001; ns, not significant, P>0.99. Downward error bars (blue) are shown for cells without lamellipodia and upward error bars (black) for cells with lamellipodia. (two-way ANOVA; n=60 cells and N=3 experiments). Data represent mean±s.d. Scale bars: 10 µm (D,G,H); 90 s (horizontal bars for kymographs in G), 10 µm (vertical bars for kymographs in G). 'C' denotes control and 'T' denotes MLL siRNA treatment; ΔTAD, trans-activation domain deletion; ΔSET, SET domain deletion.

polymerised into different networks and structures and rapidly depolymerised (Blanchoin et al., 2014). To study actin dynamics in real time, we made use of GFP–Lifeact, which binds to filamentous actin in live cells (Riedl et al., 2008). U2OS cells expressing GFP–Lifeact displayed well-formed lamellipodia, with rapid spreading and ruffling (Fig. 3G; Movies 1 and 2), but these were absent in MLL-depleted cells (Fig. 3G; Movies 3 and 4). In fact, the actin dynamics in MLL siRNA-treated cells almost came to a halt. Consistent with our previous observations, MLL-depleted cells were elongated and exhibited numerous filopodia along the length of the cells (Fig. 3G). The particle velocity estimated by generating kymographs (Fig. 3G, right panels) from the live-cell movies showed that the average track velocities reduced drastically in MLL-depleted cells (Fig. S2E). These experiments confirmed the role of MLL in regulating actin dynamics in the cell.

Rac1 is a key regulator of lamellipodium extension (Ridley et al., 1992). Our RhoA and CDC42-depleted cells displayed cell shapes similar to those seen upon MLL depletion, but Rac1-depleted cells had different cell shapes. Thus, to ascertain that MLL influenced Rac1 functions, we checked for lamellipodium formation in MLL-depleted cells (Fig. 3H). We used the Nck-associated protein 1 (Nap1 or NCKAP1), a part of the WAVE regulatory complex, as a marker for lamellipodia. Nap1 migrates to the tips of membrane protrusions like lamellipodia upon Rac1 activation (Steffen et al., 2004). We observed a prominent lamellipodium in control siRNA-treated cells, which displayed Nap1 enriched at its tip (Fig. 3H),

Journal of Cell Science (2022) 135, jcs260042. doi:10.1242/jcs.260042

whereas fewer MLL siRNA-treated cells formed lamellipodia, and the membrane protrusions that formed did not show Nap1 staining at the tips (Fig. 3H,I). We further assessed whether the MLL SET domain was also involved in the regulation of Rac1 function. Indeed, expression of the full-length MLL protein, but not of the SET domain-deleted mutant, rescued lamellipodium formation (Fig. 3I). Similarly, cell migration was also compromised for cells expressing the SET domain-deleted mutant of MLL (Fig. S2F), indicating that MLL regulates the various functions of Rho GTPases by its histone methyltransferase activity.

RhoA, Rac1 and CDC42 are essential for cell spreading on fibronectin in different cell types (Reymond et al., 2012b; Yang et al., 2020). As we found defects in fibronectin spreading upon MLL depletion, we wanted to study whether similar spreading defects were observed upon Rho GTPase knockdown. Consistent with previous reports, depletion of Rho GTPases led to significant impairment in cell spreading on fibronectin-coated surfaces (Fig. S3A,B), but we did not observe any significant change in aspect ratio and circularity of cells (Fig. S3C,D), as was observed upon MLL depletion (Fig. 2C,D). These results indicate that, similar to MLL-depleted cells, the Rho GTPase-depleted cells are slow to spread on fibronectin-coated surfaces but do not show cell elongation in the observed time. It is possible that upon MLL depletion, we might be observing the collective effects of more than one Rho GTPase, which could lead to a more severe cell-shape phenotype than individual Rho GTPase depletion.

Loss of MLL leads to reduction of Rho GTPase protein stability and activity

Our actin stress-fibre, lamellipodium and cell migration assays indicated that MLL might regulate the three Rho GTPases. To find out how MLL might confer this regulation, we decided to check the cellular levels of these GTPases upon MLL depletion. MLL knockdown resulted in a dramatic loss of total endogenous protein levels of RhoA, Rac1 and CDC42, quantified over multiple experiments in U2OS cells (Fig. 4A). We made similar observations in MDA-MB-231 cells (Fig. S4A). To check whether this reduction in total protein translated to loss of activity of these Rho GTPases, we tested for active GTPases in our system.

Classical Rho GTPases like RhoA, Rac1 and CDC42 act like molecular switches. To study their activities, we used previously established assays utilising their binding to effector domains (Ota et al., 2007;Ito et al., 2018). Due to technical difficulties in detecting the endogenous Rho GTPases in this assay, we expressed RhoA, Rac1 and CDC42 as green fluorescent protein (GFP) fusion proteins. An anti-GFP antibody was used to detect all three GTPases, which also removed the impact of differential affinities of antibodies specific to RhoA, Rac1 and CDC42 on our assay. Upon MLL depletion, we saw a striking loss of active and total protein levels of RhoA, Rac1 and CDC42 (Fig. 4B,C). Our results imply that MLL-depleted cells undergo a decrease in total protein levels of Rho GTPases, which manifests as a decrease in the active protein levels, leaving the cell with a very small pool of active Rho GTPases.

As MLL is an established transcription co-activator; we thought MLL might transcriptionally regulate Rho GTPase expression. Therefore, we checked the transcript levels of *RHOA*, *RAC1* and *CDC42* after MLL depletion. Although *MLL* mRNA levels were reduced by 70–75% in our experiments, we did not find any significant change in the expression of *RHOA* and *CDC42* upon MLL depletion (Fig. 4D). Even though the relative expression of *RAC1* was reduced upon MLL knockdown, it was not sufficient to cause near-complete reduction of protein levels as seen in Fig. 4A. Our results thus indicate that MLL regulates the protein levels but not the transcript levels of Rho GTPases.

Downregulation of MLL affects the protein and transcript levels of RhoGDI1

Unchanged *RHOA*, *RAC1* and *CDC42* transcript levels upon MLL knockdown prompted us to search for a causal factor that affects the stability of all three Rho GTPases. A literature search revealed that depletion of RhoGDI1 affected the protein levels of major Rho GTPases, including the ones being studied here (Boulter et al., 2010). To ascertain whether MLL knockdown affects RhoGDI1, we checked RhoGDI1 protein levels in control and MLL-depleted cells. As shown in Fig. 5A, the levels of RhoGDI1 were considerably reduced upon MLL knockdown. We also used the CRISPR-Cas9 system to generate inducible MLL-knockout (iKO) HEK293 cell lines (Fig. S4B). RhoGDI1 protein levels were significantly reduced in two independent MLL iKO clones (Fig. 5B; Fig. S4C). Finally, we tested our hypothesis by performing a dose-dependent depletion of MLL. Upon transfecting increasing amounts of the MLL shRNA#2 plasmid, we observed a gradation in decrease of MLL protein levels (Fig. S4D, panel a). These changes were accompanied by a corresponding gradation in decrease in RhoGDI1 protein levels as well as those of RhoA, Rac1 and CDC42 (Fig. S4D), indicating that MLL regulated RhoGDI1 protein levels to regulate these RhoGTPases.

To determine whether RhoGDI1 is a transcriptional target of MLL, we measured its transcript levels in MLL siRNA-treated cells. *MLL* levels were reduced by more than 60% and we observed a corresponding decrease in the *RHOGDI1* transcript (Fig. 5C). Although RhoGDI1 is the most abundant and ubiquitously expressed member of the GDI family, we also tested transcript levels of *RHOGDI2* (*ARHGDIB*) and *RHOGDI3* (*ARHGDIG*), primarily expressed in haematopoietic cells and the brain, respectively (Gorvel et al., 1998). These transcripts showed no significant change upon loss of MLL (Fig. 5C), indicating that MLL specifically regulated RhoGDI1 in these cells. Next, we asked whether, similar to the Rho GTPase-regulated phenotypes studied above, MLL-mediated regulation of *RHOGDI1* transcript was also SET domain dependent. Indeed, expression analysis of *RHOGDI1* indicated that its levels were restored in the presence of the MLL full-length protein, but decreased in the absence of the SET domain-deleted MLL mutant (Fig. 5D). Based on our results, it is likely that RhoGDI1 is the common denominator in the regulation of Rho GTPases by MLL.

Up to 95% of the cellular levels of RhoA, Rac1 and CDC42 are maintained by RhoGDI1 (Boulter et al., 2010). We confirmed these findings by generating stable KOs of RhoGDI1 in U2OS cells by genome editing. We used two individual clones for our experiments, both of which showed complete KO of RhoGDI1 (Fig. 5E; Fig. S4F). As expected, the protein levels of RhoA, Rac1 and CDC42 were highly diminished in these cell lines (Fig. S4E,G), indicating that RhoGDI1 indeed regulated Rho GTPase protein levels. We also compared the numbers of stress fibres in control and RhoGDI1 (KO#1) cells. Consistent with the absence of the three GTPases, we found that the numbers of stress fibres were drastically reduced in both RhoGDI1 KO cell lines (Fig. 5F,G). Previous reports indicated that the loss of RhoGDI1 is associated with a mild phenotype (Boulter et al., 2010). As these studies were based on the siRNA knockdown of RhoGDI1, we depleted RhoGDI1 using siRNA (Fig. S5A). RhoGDI1-depleted cells displayed very few actin stress fibres, similar to RhoGDI1 KO cells (compare Fig. 5F,G

Journal of Cell Science (2022) 135, jcs260042. doi:10.1242/jcs.260042

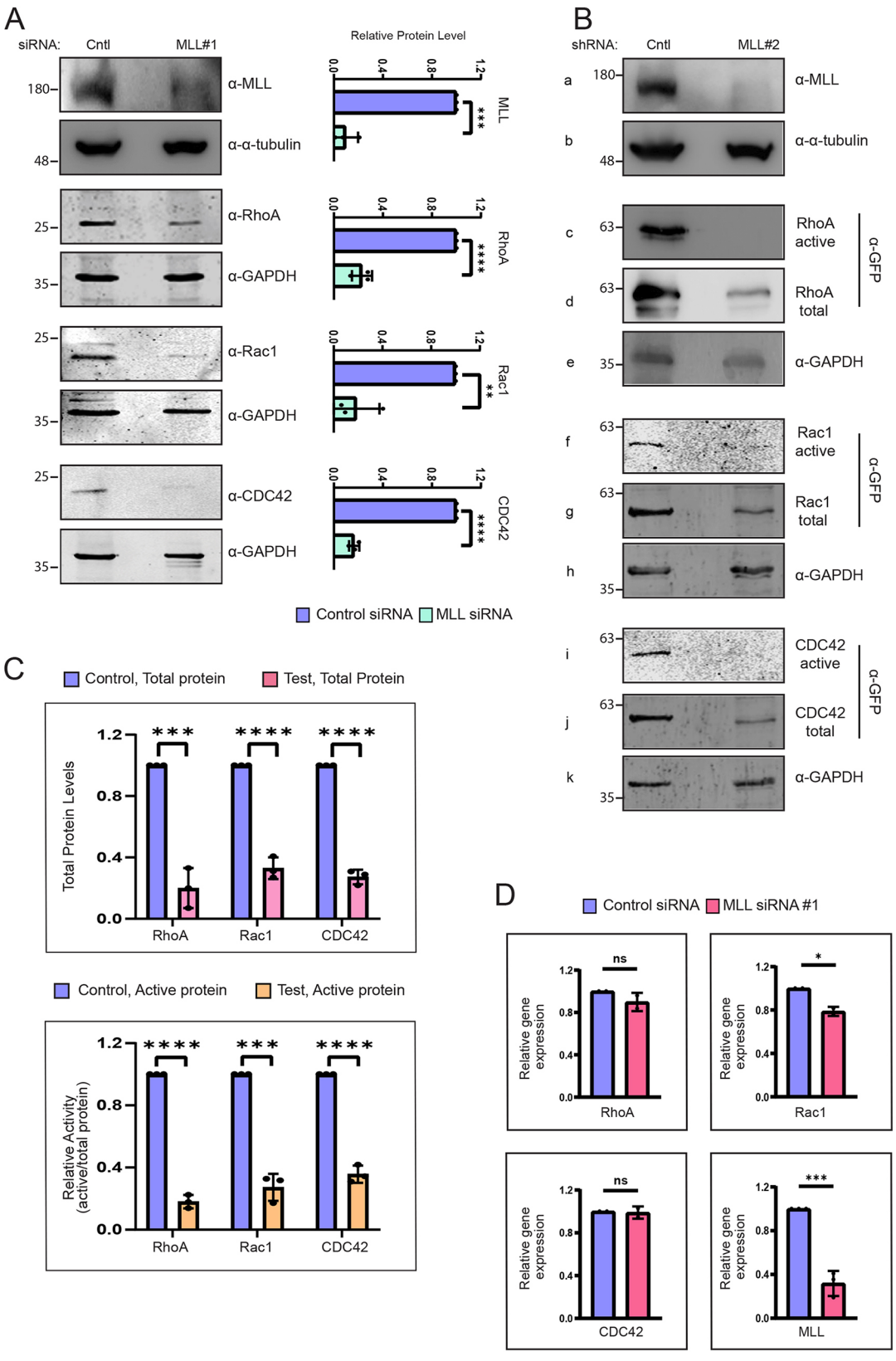

Fig. 4. See next page for legend.

to Fig. S5B,C) and there was a significant reduction in the area of spread of these cells (Fig. S5D,E). We found no change in the circularity and aspect ratios of these cells (Fig. S5F,G), similar to what was seen for Rho GTPase knockdown. In contrast, RhoGDI1 KO cells showed significant spreading defects (Fig. 5H) as well as significant increase in circularity, and, hence, reduction in the aspect ratio (Fig. 5I,J). Our results indicate that transient knockdown as well as stable knockout of RhoGDI1 have similar effects on stress-

Journal of Cell Science (2022) 135, jcs260042. doi:10.1242/jcs.260042

Fig. 4. Loss of MLL affects stability and activity of Rho GTPases. (A) Immunoblotting of lysates from U2OS cells treated with control or MLL#1 siRNAs, probed with the indicated antibodies, is shown. Graphs on the right show the relative protein levels (with respect to the loading control). ****P<0.0001 for RhoA and CDC42; ***P=0.0001 and **P=0.0017 for MLL and Rac1, respectively (Student's unpaired two-tailed t-test, N=3 experiments). (B) U2OS cells stably expressing GFP-tagged RhoA, Rac1 or CDC42 were either treated with control or MLL#2 shRNAs for 72 h. The cells were then lysed and subjected to pull-down using GST-tagged effector domains (see Materials and Methods). Immunoblot analysis indicate endogenous protein levels of MLL (panel a) and α-tubulin (panel b). Total protein levels (panels d,g,j) and active (GTP-bound) protein levels (panels c,f,i) of the indicated Rho GTPases, probed with anti-GFP antibody are shown. The blots shown in panels e,h,k, were probed with anti-GAPDH antibody. (C) Densitometric analyses of immunoblots from B of total protein levels relative to loading control (upper panel) and relative activity (ratio of active to total protein levels) upon depletion of MLL are shown. ****P<0.0001; ***P<0.005 (Student's unpaired two-tailed t-test, N=3 experiments). (D) RT-qPCR analysis of gene expression upon MLL depletion. Relative gene expression was calculated using the −ΔΔCt method. *P=0.018 (Rac1); ***P<0.001 (MLL); ns, not significant, P=0.23 (RhoA) and 0.80 (CDC42) (Student's unpaired two-tailed t-test, N=2 experiments). Data represent mean±s.d.

fibre formation and cell spreading as does MLL loss (compare Fig. 1E, Fig. 5G and Fig. S5C; Fig. 2B, Fig. 4H and Fig. S5E). However, transient RhoGDI1 depletion but not its knockout had a more severe effect on cell shape, similar to MLL depletion (compare Fig. S5B, Fig. 5F and Fig. 1C). Taken together, our results show that MLL modulates the protein levels of RhoA, Rac1 and CDC42 by regulating the transcript levels of *RHOGDI1*.

MLL binds to the *RHOGDI1* promoter to bring about H3K4 trimethylation

Based on our results, we propose that RhoGDI1 might be a transcriptional target of MLL. To determine whether this regulation is direct, we performed chromatin immunoprecipitation (ChIP) experiments and analysed MLL binding on RhoGDI promoters. Our transcript data showed that MLL only affected the transcript levels of *RHOGDI1* and not *RHOGDI2* or *RHOGDI3* (Fig. 5C). To confirm these observations, based on the RNA polymerase II enrichment in the UCSC genome browser (Barski et al., 2007), we chose the upstream and promoter regions of all three RhoGDIs as shown (Fig. 6A). We selected a well-characterised MLL target, *HOXA9*, as a positive control and *CD4*, a gene that is not expressed in the chosen cells, as a negative control. IgG was used as an antibody control. We performed the ChIP experiments in transformed (HEK293T) cells. We also used non-transformed human lung fibroblasts IMR-90 cells, immortalized by expression of telomerase reverse transcriptase (IMR-90tert) for these experiments. ChIP-PCR analyses in these two cell lines indicated that, consistent with our transcript data, MLL showed significant enrichment only on the *RHOGDI1* promoter but not the *RHOGDI2* and *RHOGDI3* promoters (Fig. 6B,C; Fig. S6A). This enrichment of MLL correlated with the presence of H3K4 dimethylation (H3K4me2) and trimethylation (H3K4me3) marks on the *RHOGDI1* promoter (Fig. 6D,E; Fig. S6B,C). Curiously, we also observed the presence of H3K4me2 marks on the *RHOGDI3* promoter in both cell lines (Fig. S5B,C). However, these were not accompanied by the H3K4me3 marks, suggesting that these promoters might not be actively transcribed in these cell lines.

Our data so far indicate that MLL regulates RhoGDI1 transcription by its histone methyltransferase activity. To confirm our hypothesis, we used our MLL iKO cells to perform ChIP experiments. The MLL levels were severely reduced in iKO cells compared to the control cells (Fig. 6F). Consistent with our hypothesis, the H3K4me3 and H3K4me2 marks were correspondingly reduced on the *RHOGDI1* promoter (Fig. 6G; Fig. S6D). Thus, our results indicate that MLL specifically regulates RhoGDI1 by methylating its promoter and activating transcription.

Exogenous expression of RhoGDI1 can rescue some phenotypes associated with loss of MLL

MLL is a transcriptional regulator of hundreds of genes (Wang et al., 2009). However, our findings indicate that the phenotypes related to cell shape and migration studied here might be due to the loss of the major Rho GTPases, which are in turn governed by the transcript or protein levels of RhoGDI1. Therefore, we wanted to test whether restoration of RhoGDI1 protein levels in MLL-depleted cells could rescue Rho GTPase protein levels and cell-shape, cell-migration and actin stress-fibre formation defects. To answer this question, we conditionally expressed RhoGDI1 by drug induction. We could clearly detect RhoGDI1–GFP upon induction with doxycycline (Fig. S7A), which was absent in the uninduced control cells. We then transfected these cells with control and MLL siRNAs and probed for RhoGDI1–GFP as well as endogenous RhoGDI1 (Fig. 7A). Although endogenous RhoGDI1 protein levels diminished substantially in MLL-depleted cells, exogenous RhoGDI1–GFP expression was unaffected (Fig. 7A, compare panels c and d). In line with our hypothesis, we next checked the protein levels of RhoA, Rac1 and CDC42 in the RhoGDI1–GFP cell line in control and MLL siRNA-treated cells. We observed that exogenous expression of RhoGDI1–GFP was able to restore the endogenous expression of RhoA, Rac1 and CDC42 proteins despite MLL siRNA treatment, at levels comparable to those seen in control cells (Fig. 7A). These results indicate that RhoGDI1 was indeed the major factor responsible for regulating RhoA, Rac1 and CDC42 protein levels upon loss of MLL. Given that the major Rho GTPase levels were restored in the cell, we performed cell migration assays in RhoGDI1–GFP-expressing cells using control and MLL shRNAs. As reported before, we observed reduced cell migration upon MLL shRNA treatment (Fig. 2G,H, Fig. 7B,C) in U2OS cells. Surprisingly, control shRNA-treated cells expressing RhoGDI1–GFP also showed reduced cell migration compared to control U2OS cells. This was likely the indirect consequence of the sequestration of active Rho GTPases by overexpressed RhoGDI1 (Golding et al., 2019). However, when MLL was depleted using shRNA in these cells, cells migrated faster (Fig. 7B,C). Even though the cell migration was not restored to the levels seen in wild-type cells, our results suggest that RhoGDI1 is a key factor affecting cell migration upon MLL depletion.

Misregulated expression of RhoGDI1 is associated with many different cancers. Notably, upregulated expression of RhoGDI1 in certain cancers is associated with enhanced invasion, metastasis and chemoresistance (Fritz et al., 1999; Hondermarck et al., 2001; Zhang et al., 2005). We noted that MDA-MB-231 cells exhibited high expression of RhoGDI1 (Fig. S7B). The MDA-MB-231 cell line is commonly used to model late-stage TNBC (Betapudi et al., 2006). To assess whether our findings here might have clinical relevance, we used the small-molecule inhibitor OICR-9429, which binds specifically to WDR5 and inhibits its interaction with MLL, thereby inhibiting the methyltransferase activity of the MLL complex (Grebien et al., 2015), for the treatment of these TNBC cells. Treating MDA-MB-231 cells with 25 µM OICR-9429 for 72 h significantly reduced the expression of RhoGDI1 transcripts (Fig. 7D). Similar to MLL RNAi treatment, OICR-9429 treatment also resulted in fewer migrating cells compared to control cells in

Journal of Cell Science (2022) 135, jcs260042. doi:10.1242/jcs.260042

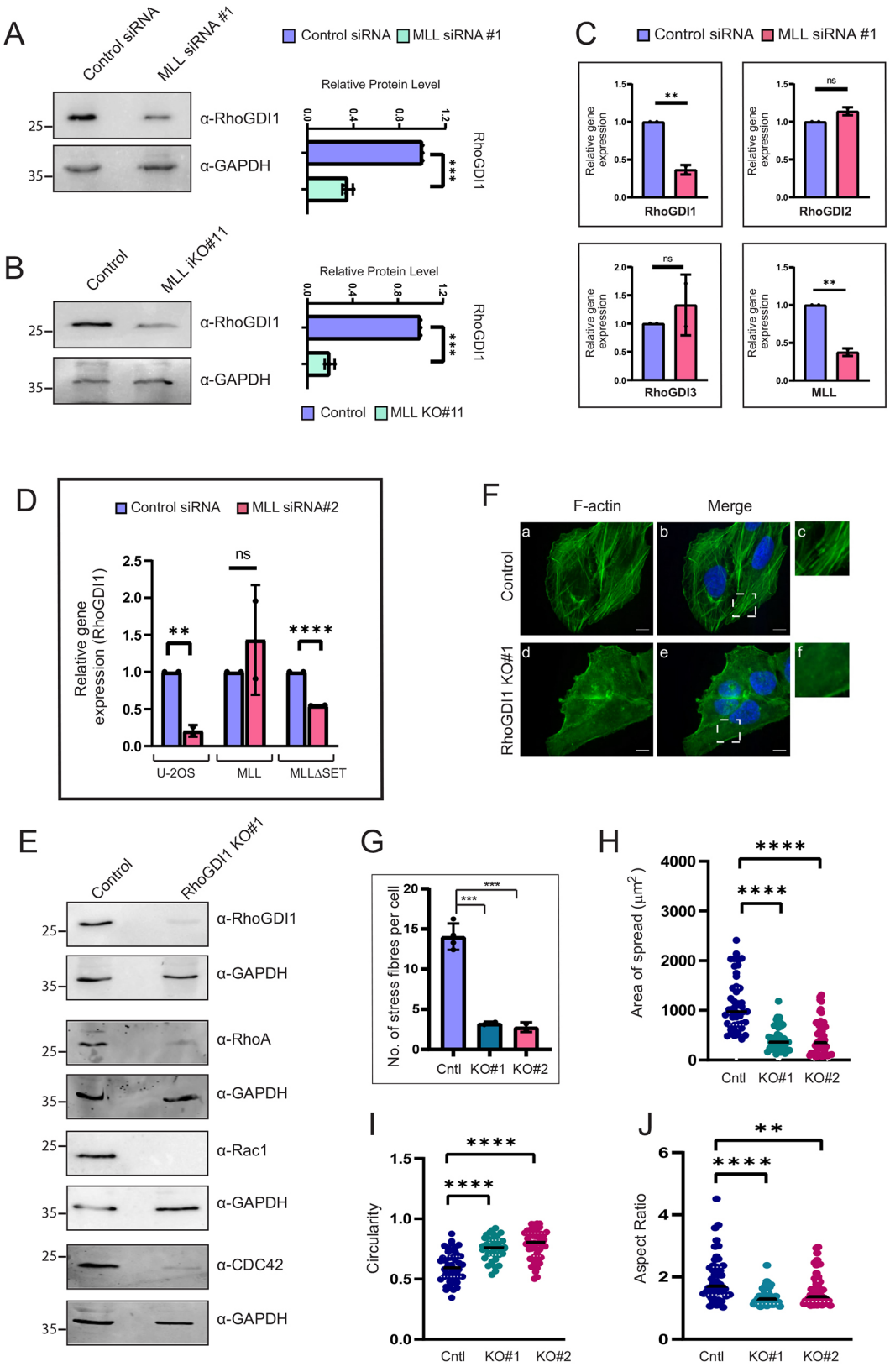

Fig. 5. See next page for legend.

transwell migration assays (Fig. 7E). To investigate the efficacy of OICR-9429 treatment or depletion of MLL on TNBC *in vivo*, we performed xenograft assays in nude mice. MDA-MB-231 cells were treated with either MLL or RhoGDI1 shRNA and engrafted in the breasts of female nude mice by subcutaneous injection. MLL or RhoGDI1 shRNA-treated cells showed substantially small tumour sizes compared to the control set (Fig. 7F; Fig. S7C). Similarly, in mice engrafted with MDA-MB-231 cells, intravenous injections

Fig. 5. Downregulation of MLL affects the protein and transcript levels of RhoGDI1. (A,B) Whole-cell lysates from control and MLL-depleted U2OS cells (A) and HEK293 control (Cas9-expressing cells) and MLL iKO#11 clonal cells (B) were immunoblotted and probed with antibodies against RhoGDI1 and GAPDH. Graphs indicate the quantifications of relative protein levels shown in A and B. ****P<0.0001 (A); ***P=0.0009 (B). (Student's unpaired two-tailed t-test, N=3 experiments). (C) RT-qPCR analysis of gene expression upon MLL siRNA depletion. **P=0.005 (RhoGDI1) and 0.003 (MLL); P=0.06 (RhoGDI2) and 0.47 (RhoGDI3) (Student's unpaired two-tailed t-test, N=2 experiments). (D) RT-qPCR analysis of gene expression of *RHOGDI1* in wild-type U2OS and U2OS cells stably expressing various mutants of MLL upon depletion of endogenous MLL using siRNA#2. ns, not significant, P=0.50 for MLL; **P=0.005 and ****P<0.0001 (Student's unpaired two-tailed t-test, N=2 experiments). (E) Whole-cell lysates of control U2OS and RhoGDI1 knockout (KO#1) cells were immunoblotted and probed as shown. (F) IF images of control U2OS and RhoGDI1 KO#1 cells are shown. Cells are stained with phalloidin. Scale bars: 10 µm. (G) Quantification of the number of stress fibres per cell in control U2OS, RhoGDI1 KO#1 and KO#2 clonal cell lines. ***P<0.001 (one-way ANOVA with Dunnett's multiple comparisons test; n=80 cells and N=4 experiments for control, and n=40 cells and N=2 experiments for RhoGDI1 KO clones #1 and #2). (H–J) Quantification of area of spread (H), circularity (I) and aspect ratio (J) of U2OS and RhoGDI1 KO clones #1 and #2 spread on fibronectin-coated coverslips. ****P<0.0001, **P=0.0025 for RhoGDI1 KO clone #2 (J) (one-way ANOVA with Dunnett's multiple comparisons test; n=40 cells and N=2 experiments). Data represent mean±s.d.

with 4 mg/kg OICR-9429 showed a significant reduction in the size of tumours compared to those injected with vehicle (Fig. 7G). Taken together, our results identify MLL as a potential new target to treat TNBC (or other cancers) with upregulated expression of RhoGDIs.

DISCUSSION

MLL regulates cell shape, the actin cytoskeleton and cell motility

Here, we report the role of MLL in the regulation of cell shape and migration as a consequence of regulating the actin cytoskeleton via stabilisation of Rho GTPases. MLL or MLL complex proteins, such as WDR5 and Dpy30, have been deemed important for cell migration (Wang et al., 2018; Malek et al., 2017; He et al., 2019; Zhang et al., 2020; Artinger et al., 2013). Similarly, different family members like MLL2 and MLL3, through different targets and modes, affect cancer cell motility and survival (Xia et al., 2015; Issaeva et al., 2007). Rho GTPase signalling is central to the formation and maintenance of the actin cytoskeleton. In MLL-rearranged leukaemia, at least 18 MLL fusion partners are involved in Rho GTPase signalling (Marschalek, 2016). Many of them are GEFs and GAPs, highlighting the importance of crosstalk in Rho GTPase signalling and of MLL in cancer. The fusion of MLL with these proteins might give the leukaemic cells a selective advantage in anchorage and metastasis by altered actin dynamics. In support of this hypothesis, knockdown of the MLL–AF6 fusion protein led to dramatic changes in cell shape and actin cytoskeleton in the human acute monocytic leukaemia cell line SHI1 (Tregnago et al., 2020). We observe similar cell-shape phenotypes upon loss of MLL and three Rho GTPases, suggesting that MLL regulates these Rho GTPases directly or indirectly.

MLL is responsible for the homeostasis of Rho GTPases by transcriptional activation of RhoGDI1

Our study revealed the role of MLL in the stabilisation of endogenous as well as overexpressed RhoA, Rac1 and CDC42 proteins. We performed our activity assays with overexpressed Rho GTPases, which is not a norm but has been reported (Shi et al., 2017; Zhou et al., 2010). However, the stoichiometry and equilibrium of RhoGDI1-bound Rho proteins have been found to change with the overexpression of any one Rho GTPase (Boulter et al., 2010). Nonetheless, our assays showed reduced Rho GTPase activity upon MLL knockdown, which was consistent with our other observations showing defects in the actin cytoskeleton, lamellipodium formation, actin dynamics and cell spreading following MLL loss. Remarkably, all three Rho GTPase proteins studied here are at the epicentre of extensive signalling pathways. Regulatory proteins that can modulate their active or total protein levels can influence various cellular processes. In agreement with this, overexpression of human MLL in murine c-Kit+/Cd41+ embryonic stem cells increases the frequency of cells with multi-lineage differentiation capacity by stimulating Rac/Rho/integrin signalling pathways rather than conventional MLL targets like HOX genes (Yang et al., 2020). Thus, this study underscores the wider influence of MLL on cellular pathways that are controlled by Rho GTPase signalling.

Rho GTPases are stabilised by three RhoGDIs. RhoGDI1 is ubiquitously expressed, and its knockdown leads to reduced protein stability of RhoA, Rac1 and CDC42 (Boulter et al., 2010). Our experiments show that RhoGDI1 levels are transcriptionally regulated by MLL-mediated H3K4 trimethylation. Apart from the regulation of its protein levels, how the activity of RhoGDI1 is regulated still needs to be unravelled. For example, how certain cancers sustain high RhoGDI1 expression is still unknown. Overexpression of RhoGDI1 is toxic for certain cell types (Miura et al., 1993; this study). However, RhoGDI1 is highly expressed in many cancers, conferring tumour cells with high metastatic and invasive potential and drug resistance (Fritz et al., 1999; Hondermarck et al., 2001; Zhang et al., 2005). Even though protein levels of RhoA, Rac1 and CDC42 were rescued after induced overexpression of RhoGDI1, the stress fibres were not replenished. On the contrary, consistent with previous findings, we found defective actin polymerisation and cell shape in cells expressing GFP–RhoGDI1 (Fig. S7D; Miura et al., 1993). It is likely that RhoGDI1 overexpression stabilised overall Rho GTPase protein levels but extracted the active forms from the membrane (Golding et al., 2019). Similarly, cells expressing the MLL full-length protein showed reduced numbers of actin stress fibres and cell migration (Fig. 3F; Fig. S2F) compared to control U2OS cells. Even though these effects were not as drastic as RhoGDI1 expression (compare Fig. S2F to Fig. 7C), we speculate that these might be a consequence of an increase in RhoGDI1 expression upon MLL ectopic expression. Supporting our hypothesis, previous studies show that RhoGDI1 overexpression causes migration defects (Yu et al., 2012). Collectively, these observations imply that appropriate expression of RhoGDI1 in cells is of utmost importance and any variation can lead to undesirable consequences.

MLL depletion causes a reduction in the size of xenografts

TNBCs, which account for 15% of total breast cancer cases, are characterised by high proliferative rates, greater brain metastases, early onset and poor prognosis (Dangi and Firodiya, 2012). These tumour cells do not express receptors for oestrogen, progesterone or the ERBB2 protein, making them resistant to conventional hormone treatment regimens with no definite treatment available. MDA-MB-231 is one such TNBC-derived cell line with high RhoGDI1 expression and is a model for studying breast cancer *in vivo*. We show that the grafting of MDA-MB-231 cells with MLL and RhoGDI1 depletion produces smaller tumours in nude mice. Although MLL fusion proteins vastly deregulate the gene expression profiles of the transformed cells, sustenance of leukaemogenesis in these cells still requires one functional allele of MLL. Thus, targeting

Journal of Cell Science (2022) 135, jcs260042. doi:10.1242/jcs.260042

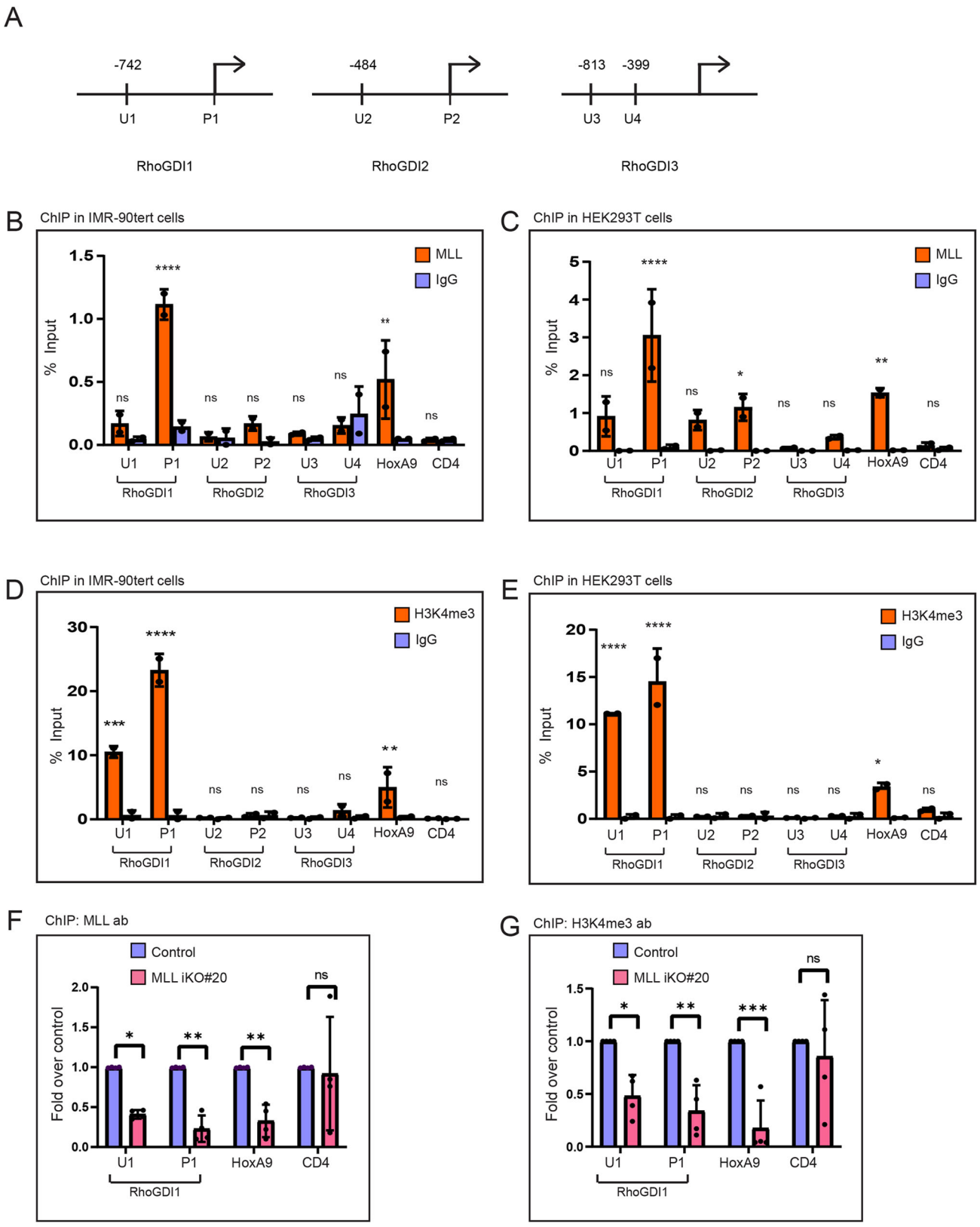

Fig. 6. See next page for legend.

the catalytic activity of MLL with small-molecule inhibitors has yielded considerable success in treating cancer in mouse models (Ye et al., 2019; Thiel et al., 2010; Ansari et al., 2013). We chose a non-peptide inhibitor of the MLL–WDR5 interaction, OICR-9429, which has already been reported to treat various cancers in mouse models (Grebien et al., 2015; Carugo et al., 2016). In OICR-9429-treated MDA-MB-231 cells, we report significant reduction of gene expression of *RHOGDI1*, translating into reduced size of xenografts

Fig. 6. MLL binds to the *RHOGDI1* promoter to deposit the H3K4 trimethylation mark. (A) Schematic of regions of genes for which the primers for ChIP assay were designed. Primers in promoters region are denoted by 'P' and upstream region by 'U'. Considering the transcription start site as +1, the exact base positions of the respective upstream primers are indicated. (B,C) ChIP assay was performed using anti-MLL and IgG antibodies in IMR-90tert (B) and HEK293T (C) cell lines. The primers used are indicated in the graphs. (D,E) ChIP assay was performed using anti-H3K4me3 and IgG antibodies in IMR-90tert (D) and HEK293T (E) cell lines. (F,G) ChIP assay was performed using anti-MLL (F) and anti-H3K4me3 (G) antibodies in HEK293 control (Cas-9 expressing) and MLL KO clone #20 cell lines. The immunoprecipitated DNA was quantified with RT-qPCR and the results are plotted as the percentage enrichment relative to the input. Data represent mean±s.d. Two-way ANOVA was used. ns: not significant, $P>0.05$; *$P\leq0.05$; **$P\leq0.01$; ***$P\leq0.001$; ****$P\leq0.0001$. All experiments were done at least twice.

formed from these cells in nude mice. Taken together, our results indicate a new target for treatment of TNBC using a small-molecule inhibitor affecting the catalytic activity of MLL. We believe similar approaches can be utilised for treating other cancers showing overexpression of Rho GTPases and RhoGDIs.

MATERIALS AND METHODS

Cloning

Complementary DNA (cDNA) encoding *RHOA*, *RAC1*, *CDC42* and *RHOGDI1* was amplified from cDNA generated from the human osteosarcoma U2OS cell line using Phusion polymerase (New England Biolabs, M0530). These cDNAs were cloned into a XhoI-linearised pCDNA vector (a gift from Dr Jacqueline Lees, Koch institute, Massachusetts, USA), with GFP at the N-terminus, yielding GFP–RhoA, GFP–Rac1, GFP–CDC42 and GFP–RhoGDI1 constructs. For ectopic inducible expression of RhoGDI1 in U2OS cells, we deleted the Cas9 gene from the pCW-Cas9 vector (Addgene #50661, deposited by Eric Lander and David Sabatini; Wang et al., 2014), and incorporated an EcoRI site in its place by inverse PCR. GFP–RhoGDI1 (PCR amplified from pCDNA GFP–RhoGDI1) was then cloned into the EcoRI sites using the In-Fusion HD cloning kit (Takara, 639649) creating pCW-GFP-RhoGDI1. RhoGDI1 sgRNA1 (5′-CAGGCCAGTCACCACGACGT-3′) and sgRNA2 (5′-CCCCAACGTCCCCAACGTCG-3′) were cloned in LentiCRISPRv2 (Addgene #52961, deposited by Feng Zhang; Sanjana et al., 2014) in the BsmBI sites. MLL sgRNA1 (5′-CGAACATGGCGCACAGCTGT-3′) and MLL sgRNA2 (5′-CAGCGGGGCTGGGGTTCCAG-3′) were cloned into Lentiguide-puro vector (Addgene #52963, deposited by Feng Zhang; Sanjana et al., 2014) in the BsmBI site. RhoGDI1 shDNA1 (5′-CGTCTAACCATGATGCCTTAA-3′), RhoGDI1 shDNA2 (5′-TCCGGGTTAACCGAGAGATAG-3′), MLL shDNA1 (5′-CTACCA-ACCCTAAACCCTG-3′), MLL shDNA2 (5′-GCCTCCATCAACAGAA-AGGAT-3′) and control shDNA (5′-GCGCGATAGCGCTAATAATTT-3′) were cloned in the PLKO.1 vector (Merck, SHC001V) in the KpnI and EcoRI sites. All constructs were verified by sequencing. GST-tagged Rho-binding domain (RBD) of rhotekin and p21-binding domain (PBD) of p21 activated kinase 1 for pulldowns of GTP-bound RhoA and CDC42/Rac1, respectively, were a gift from Dr Keith Burridge (University of North Carolina, Chapel Hill, NC, USA). The pCMV-LifeAct-TagGFP2 vector was a gift from Dr Rashna Bhandari (CDFD, Hyderabad, India).

Cell culture, transfection and stable cell-line generation

All cell lines were authenticated by STR profiling and checked for contamination. A549 cells was a gift from Dr Anand Ramteke (Tezpur University, Assam, India). Cells were grown in Dulbecco's modified Eagle's medium (DMEM, HiMedia, AT186) supplemented with 10% fetal bovine serum (Thermo Fisher Scientific, 26140095), L-glutamine and penicillin/streptomycin. U2OS cells stably expressing GFP-tagged RhoA, Rac1, CDC42 and RhoGDI1 were obtained by transfecting cells with polyethylene imine (PEI; Polysciences, 23966-2). MDA-MB-231 cells expressing control, MLL and RhoGDI1 shRNA were obtained by lentiviral transduction as described before (Van Lidth de Jeude et al., 2015). The transduced and transfected cells were selected using 4 µg/ml puromycin and maintained using 2 µg/ml puromycin (Gibco, 11138-03). Drug-resistant colonies were tested for recombinant gene expression by immunoblotting. Two different RhoGDI1 sgRNAs were transfected in U2OS cells. Serial dilution was done to obtain single cell colonies after puromycin (4 µg/ml) treatment. Colonies were screened for RhoGDI1 KO by western blotting.

For our experiments, we generated an inducible MLL knockout in HEK293 cells. To achieve this, a doxycycline-inducible Cas9 expression vector (pCW-Cas9) was modified by replacing the puromycin resistance gene with blasticidin resistance gene, taken from LentiCas9-Blast (Addgene #52962, deposited by Feng Zhang; Sanjana et al., 2014) to create the pCW-Cas9-Blast vector. The pCW-Cas9-Blast vector was packaged as a lentivirus and HEK293 cells were transduced with these viral particles. Cas9-positive colonies were selected with 5 µg/ml blasticidin (Invitrogen, R21001). Once single colonies were selected by screening for Cas9 expression (upon induction with 2 µg/ml doxycycline; Sigma-Aldrich, D9891) by western blotting, these colonies were transduced with both MLL sgRNA (described above) viral particles. Cells were selected with puromycin (2 µg/ml). Single colonies were screened for loss of MLL expression by western blotting, and two clones were selected for further analysis (#11 and #20). MLL knockout was initiated by inducing cells with 4 µg/ml doxycycline for 7 days. MLL knockout was confirmed with western blotting, before proceeding for ChIP experiments.

To make GFP–RhoGDI1 cell lines, U2OS cells were transfected with pCW-GFP-RhoGDI1 and selected by 4 µg/ml puromycin. Single-cell-derived colonies were induced with 2 µg/ml doxycycline and screened for RhoGDI1 expression by western blotting.

siRNA and shRNA transfections

siRNA transfections were performed as described previously (Tyagi and Herr, 2009). Cells were harvested 72 h after the first transfection and either used for RNA extraction, fixed for immunofluorescence studies, or lysed in SDS Laemmli buffer and subjected to western blotting. Control siRNA (5′-CGUCGCGGAAUACUUCGA-3′), MLL siRNA#1 (5′-AAGGAAAG-CAUUACUGAGAAAUU-3′) and MLL siRNA#2 (5′-ACGAAAGACT-GAATGTAAAUU-3′) were purchased from GE Dharmacon as described before (Ali et al., 2014). Previously described siRNAs against RhoA (5′-GAACUAUGUGGCAGAUAUCUU-3′), Rac1 (5′-CGGCACCAUG-UCCCAACAUU-3′), CDC42 (5′-GGAGAACCAUAUACUCUUGUU-3′) and RhoGDI1 (5′-UCAAUCUUGACGCCUUUCCUU-3′) were purchased from Sigma-Aldrich (Boulter et al., 2010; Reymond et al., 2012b). The shRNAs described above were transfected using PEI in U2OS cells. For transwell migration assays, cells were subjected to one round of shRNA transfection. For pulling down active forms of Rho GTPases, cells were subjected to two rounds of shRNA transfection at 24 h intervals. For dose-dependent MLL knockdown, U2OS cells in 10 cm plates were treated with 10 µg (one round of transfection), 20 µg (two rounds of 10 µg DNA transfections, 24 h apart) or 30 µg (three rounds of 10 µg DNA transfections, 24 h apart) of control (scrambled) or MLL shDNAs and incubated for 72 h. Post incubation, cells were harvested and lysed, and the lysates were analysed by immunoblotting.

RNA isolation and real-time quantitative PCR

RNA was extracted either by the Trizol (Ambion, 15596018) extraction method or Directzol RNA Miniprep kit (Zymo Research, R 2050). Approximately 2 µg of the total RNA was used to prepare cDNA using Superscript III reverse transcriptase (Invitrogen, 1808005) and cDNA was used for real-time quantitative PCR (RT-qPCR) using the SYBR Green kit (Thermo Fisher Scientific, F416L). Each sample was run in triplicate. The amplification was performed and detected using the 7500 Real Time PCR system (Applied Biosystems). Transcripts were normalised to the housekeeping gene GAPDH by using the $-\Delta\Delta CT$ method for determining relative gene expression (Livak and Schmittgen, 2001). The primers used for PCR amplifications are described in Table S1.

Protein pulldowns

Lysates of GFP–RhoA-expressing cells, treated with control or MLL shRNAs, were prepared by lysing cells in NETN buffer (100 mM NaCl,

Journal of Cell Science (2022) 135, jcs260042. doi:10.1242/jcs.260042

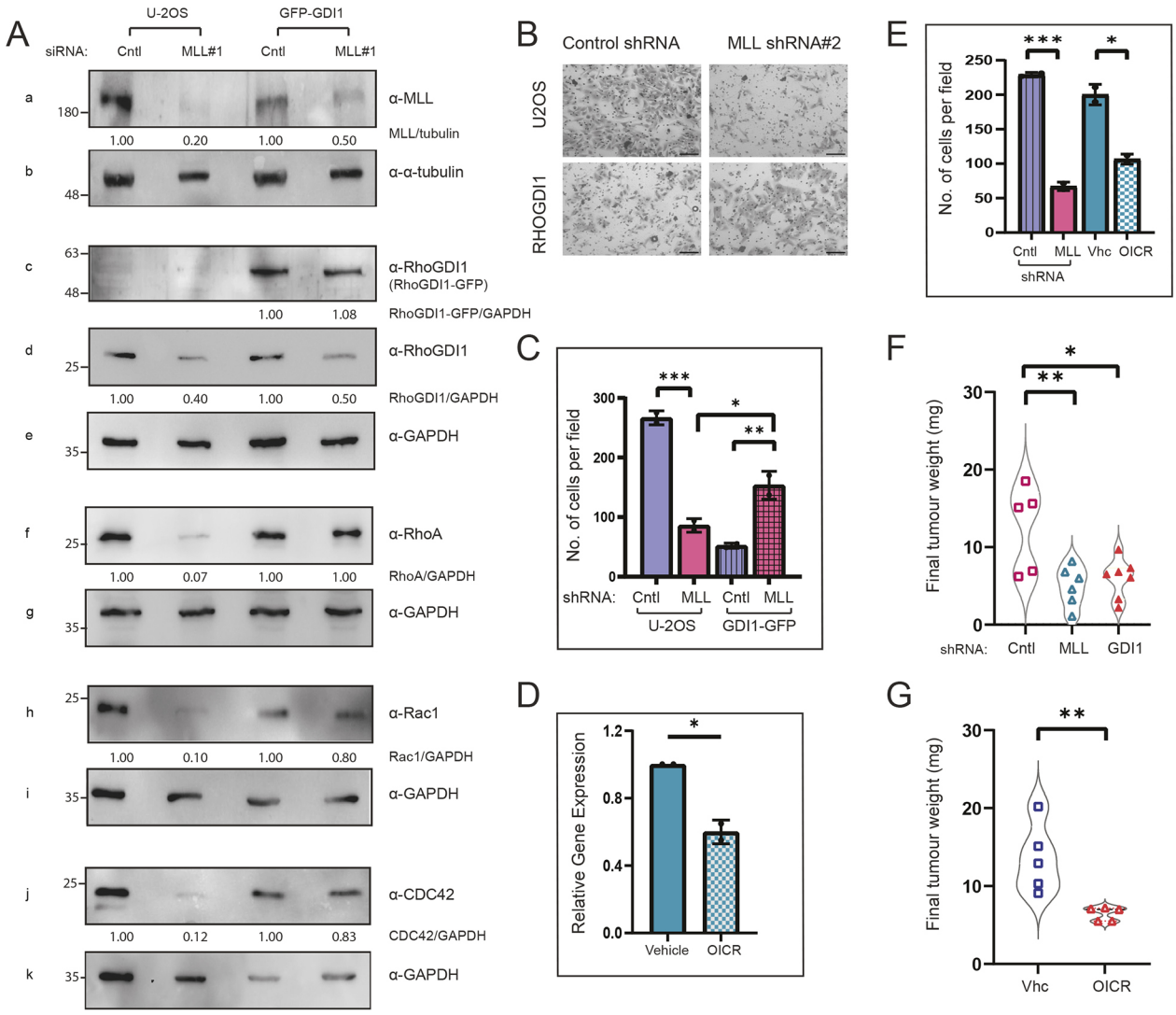

Fig. 7. Exogenous expression of RhoGDI1 can rescue some phenotypes associated with loss of MLL. (A) Western blot analysis of whole-cell lysates from U2OS cells as well as the GFP–RhoGDI1 cell line, treated with control and MLL#1 siRNAs for 72 h. The blots were probed with the indicated antibodies. (B) Wild-type U2OS cells and GFP–RhoGDI1-expressing cells were treated with control and MLL#2 shRNAs, and seeded for transwell migration assay. Bright-field images for migrated cells were captured at 10× magnification. Scale bars: 50 µm. (C) Quantification for the number of cells that migrated in B. **P*=0.0214; ***P*=0.005; ****P*<0.001 (one-way ANOVA with Dunnett's multiple comparisons test; *N*=2 experiments). (D) RT-qPCR analysis of gene expression of *RHOGDI1* in MDA-MB-231 cells upon treatment with 25 µM OICR-9429. Data represent mean±s.d. **P*=0.0323 (Student's unpaired two-tailed *t*-test; *N*=2 experiments). (E) MDA-MB-231 cells were treated with control (Cntl) or MLL#2 shRNAs for 48 h, or vehicle (Vhc, DMSO) or 25 µM OICR-9429 for 72 h, used for transwell migration assay and the number of migrated cells were quantified. Data represent mean±s.d. **P*=0.0153; ****P*=0.0008; (Student's unpaired two-tailed *t*-test; *N*=2 experiments). (F) Tumours obtained from xenografts of MDA-MB-231 cells, treated with control, MLL#2 or RhoGDI1#2 shRNAs were harvested, weighed and plotted. **P*=0.014; ***P*=0.007 (one-way ANOVA with Dunnett's multiple comparisons test; *n*=5, 6 and 7 animals for control, MLL and RhoGDI1 shRNA treatment groups, respectively). (G) Tumours obtained after treatment with vehicle (DMSO) or 4 mg/kg OICR-9429 were harvested, weighed and plotted. Data represent violin plots with all datapoints. ***P*=0.008 (Student's unpaired two-tailed *t*-test; *n*=5 animals each).

20 mM Tris-HCl pH 8, 0.5 mM EDTA and 0.5% Nonidet P-40) in the presence of protease inhibitors and PMSF, and incubated with GST-tagged RBD immobilised on glutathione beads (Sigma-Aldrich, G4510) respectively, for 2 h at 4°C. Lysates of GFP–Rac1- or GFP–CDC42-expressing cells were similarly prepared and incubated with GST-tagged PBD immobilised on glutathione beads. The beads were washed with wash buffer (50 mM Tris-HCl pH 7.4, 100 mM KCl, 0.05% Nonidet P-40) and used for immunoblot analysis.

Immunoblotting

Immunoblotting was performed on nitrocellulose (Amersham, 10600003) or PVDF (Amersham, 10600023) membranes. Transfer was done using a Tris-glycine transfer buffer containing 10% methanol for 2 h at 225 mA. The membranes were blocked using 5% skimmed milk in PBS with 0.1% Tween 20 and probed with either of the following primary antibodies overnight at 4°C: anti-RhoA (St. John's Laboratories, 95442, 1:100), anti-CDC42 (St. John's Laboratories, 191678, 1:100), anti-Rac1 (Abcam, 33186, 1:5000), anti-GAPDH (Cloud Clone Corp., PAB932Hu01, 1:5000), anti-tubulin (Sigma-Aldrich, T5168, 1:10,000) and anti-RhoGDI1 (St. John's Laboratories, 22675, 1:5000). For imaging in the LI-COR imaging system, the following fluorescently labelled secondary antibodies were used at 1:10,000 dilution: goat anti-mouse IR dye 800 CW (LI-COR, 926-33210), goat anti-rabbit IR dye 800 CW (LI-COR, 926-32211), goat anti-mouse IR dye 680 CW (LI-COR, 926-68020) and goat anti-rabbit IR dye 680 CW (LI-COR, 926-68021). For imaging in a chemiluminescence system, horse radish peroxidase (HRP)-conjugated secondary antibodies raised either in mouse (Bio-Rad, 170-6516) or rabbit (Bio-Rad, 170-6515) were used at 1:10,000 dilution. See Fig. S8 for whole blots used in the figures.

Generation of the MLL_C antibody

A GST-tagged fragment of MLL_C containing amino acids 2718–3280, named MLL D1, was utilised for antibody generation. The protein was produced as described in Ali et al. (2017). GST–MLL D1 was eluted in elution buffer [50 mM Tris-Cl, pH 8.8, 30 mM reduced glutathione (Sigma-Aldrich, G4251)] for 2 h at 4°C. The elute was dialysed overnight at 4°C in dialysis buffer (120 mM NaCl, 2 mM $MgCl_2$, 10% glycerol, 20 mM HEPES pH 7.9). The antibody was generated in rabbit at Bioklone Biotech, Chennai, India. Subsequently, the specificity of the antibody was checked by transfection of MLL-specific siRNAs/shRNAs and western blotting of cell lysates (see Fig. 1A, Fig. 2E, Fig. S1A).

Immunofluorescence

Unless they were used for fibronectin spreading assay, cells were grown on coverslips for immunofluorescence experiments. After the appropriate treatment, cells were fixed either with 4% paraformaldehyde (Sigma-Aldrich, 158127) solution prepared in PBS at room temperature for 10 min for rhodamine-conjugated phalloidin (Thermo Fisher Scientific, R415) staining, or with 10% trichloroacetic acid (Amresco, 133) at 4°C for 10 min for anti-Nap1 antibody (St. John's Laboratories, 114120, 1:100) staining. Permeabilisation of cells prior to phalloidin and antibody staining was done using 0.2% Triton X-100 (Amresco, 0694). The cells were then incubated with phalloidin or anti-NAP1 antibody for 1 h at room temperature. When staining for NAP1, the anti-rabbit Alexa Fluor 488 secondary antibody (Invitrogen, A 11034, 1:500) was used. The coverslips were then washed with a solution of 4′,6-diamidino-2-phenylindole (DAPI; Sigma-Aldrich, D9542), mounted on slides and visualised under a Zeiss LSM 700 confocal microscope or a Leica SP8 confocal microscope.

For quantification of stress fibres, images were opened in ImageJ and the numbers of stress fibres were counted manually by using the multipoint selection tool. The numbers of cells that were used to calculate stress fibres were also noted. The numbers of stress fibres per cell were expressed as a ratio of the sum of all the stress fibres obtained in the experiment to the number of cells imaged. The presence or absence of lamellipodia in the cells was determined visually by the presence or absence of membrane staining of Nap1 in cells. The number of cells with and without lamellipodia were then plotted.

For time-lapse imaging, U2OS cells expressing pCMV-LifeAct-TagGFP2 vector were seeded on a glass-bottomed dish. siRNA transfections were carried out as discussed above. After incubation, cells were imaged in Zeiss Elyra 7 microscope in lattice structured illumination microscopy (SIM) mode at 5 s interval for 2 min 25 s. Kymographs of these images were generated using the inbuilt FiJi plugin 'Multi Kymograph' and selecting line width as '5'. Analysis of kymographs was done as described previously (Jakobs et al., 2019). Average track velocities thus generated were plotted as scattered plots using GraphPad Prism and significance analysis was performed.

Cell-spreading assay

Coverslips were incubated with 200 µg/ml fibronectin (Sigma-Aldrich, F2006) dissolved in PBS and coated on coverslips for 30–45 min at room temperature in aseptic conditions. The solution was removed and coverslips were rinsed with DMEM or PBS. For fibronectin spreading assay, cells were directly seeded in six-well plates and, after completion of siRNA treatment (72 h), cells were trypsinised and 10^5 cells were reseeded on fibronectin-coated coverslips for 4 h before fixing for immunofluorescence. For quantifications of area of spread, circularity and aspect ratio, images were opened in ImageJ. The edges of the cells were marked using the freehand selection tool. The 'Shape Descriptor' plugin was used to calculate area of spread, circularity and aspect ratio of the regions of interest. These data were saved in Excel files and used for plotting graphs in GraphPad Prism.

Transwell migration assay

U2OS or MDA-MB-231 cells, after MLL shRNA or OICR-9429 treatment, were trypsinised and counted using a haemocytometer. For thrombin treatment, U2OS cells treated with control or MLL shRNAs were incubated in DMEM containing 4 U/ml thrombin (Sigma-Aldrich, T4648) for 48 h. For OICR-9429 treatment, MDA-MB-231 cells seeded in six-well plates were treated with 25 µM OICR-9429 for 72 h. Control cells in the same experiments were treated with DMSO. U2OS GFP–RhoGDI1 cells were additionally treated with 2 µg/ml doxycycline. 10^5 cells from the above-mentioned treatments were suspended in 200 µl of DMEM containing 1% fetal bovine serum. The cell suspension was carefully added to the cell culture inserts (BD falcon 353097). These inserts were immediately placed in the wells of 24-well plates containing complete medium and incubated for 24 h at 37°C in a CO_2 incubator. After incubation, the cells that had migrated to the outer surfaces of the inserts were fixed using 4% paraformaldehyde for 10 min and stained using 5% Crystal Violet stain in methanol for 1 h. The number of cells migrated were imaged using a Zeiss Axiovert microscope under a 10× objective, and the number of cells in an image was quantified using the multipoint selection tool of ImageJ and averaged. The average number of cells that migrated in two different experiments were plotted using GraphPad Prism software.

ChIP

ChIP experiments were done as previously described (Zargar et al., 2018) with some minor modifications. The following antibodies were used for our ChIP assays, anti-H3K4me2 (Abcam, ab32356), anti-H3K4me3 (Millipore, 07-473 or Abcam, ab8580), anti-H3 (Abcam, ab1791), IgG (Millipore, 12-370), all at a concentration of 2 µg per 10 million cells. RT-qPCR was done to calculate Ct values. Percentage enrichment over the input was calculated using the formula: percentage enrichment=$100\times2^{x-y}$, where x is the Ct value for input adjusted for dilution factor and y is the Ct value for the immunoprecipitated samples. For ChIP in MLL iKO cells, fold change over control was calculated using the formulae 2^{x-y} of test/2^{x-y} of control, where x and y are the Ct values of input and immunoprecipitates. The ABI 7500 system was used for RT-qPCR. The primer sequences used are listed in the Table S2.

Animal experiments

All animal experiments were performed after being approved by the Centre for DNA Fingerprinting and Diagnostics (CDFD) institutional animal ethics committee (protocol number EAF/ST/25/2021). For the studies, 6- to 8-week-old $FOXN1^{-/-}$ female nude mice were used. For xenograft assays, MDA-MB-231 cells were transduced with control, MLL or RhoGDI1 shRNAs containing lentiviruses and subjected to brief puromycin treatment (4 µg/ml) after 24 h. About 48 h post transduction, 10^6 cells suspended in 100 µl of 1:1 mixture of Matrigel (Corning, 354254) and PBS were injected subcutaneously in one of the breasts of each female nude mice. Tumour growth was monitored every 10 days. Mice were euthanised and tumours were harvested on day 40 and their weights measured. For OICR-9429 treatment, the study was done as described previously (Zhou et al., 2021). Tumours were induced in female nude mice as described using MDA-MB-231 cells. When tumours reached the size of 50 mm^3 (in approximately 1 week), mice were grouped randomly. One group of mice was administered 4 mg/kg OICR-9429 and the other with DMSO intravenously for seven alternate days. Mice were euthanised after 40 days from the beginning of the experiment. Tumours were harvested and their weights measured. The injections were performed by CDFD animal facility staff, who were blinded for the study.

Statistical analysis

For all the statistical analyses, 95% confidence interval was applied. GraphPad Prism software was used to determine statistical significance. For simple comparison between two sets, Student's unpaired two-tailed *t*-test was applied. For multiple comparisons, one-way ANOVA with Dunnett's multiple comparisons test (except Fig. 2I where one-way ANOVA with Tukey's multiple comparisons test was) or two-way ANOVA was implemented as indicated. The significance of each test is mentioned in the respective figure legends in the form of *P*-values.

Acknowledgements

We thank A. Karole for cloning control and MLL shRNAs and I. Kaur for sharing time on the LI-COR imaging system.

Competing interests

The authors declare no competing or financial interests.

Author contributions
Conceptualization: A.N.C., S.T.; Methodology: A.N.C.; Validation: A.N.C., K.A.L.; Investigation: A.N.C., K.A.L.; Resources: S.T.; Writing - original draft: A.N.C.; Supervision: S.T.; Project administration: S.T.; Funding acquisition: S.T.

Funding
A.N.C. is a recipient of Junior and Senior Research Fellowships of the University Grants Commission, India toward the pursuit of a PhD degree from Manipal University. K.A.L. is a recipient of Junior and Senior Research Fellowships of the Council of Scientific and Industrial Research, India toward the pursuit of a PhD degree from the Regional Centre for Biotechnology. This work was supported by grants from the Department of Biotechnology, Ministry of Science and Technology, India to S.T. (BT/PR34385/BRB/10/1829/2019), Department of Science and Technology, Ministry of Science and Technology, India to S.T. (EMR/2016/000406), The Wellcome Trust DBT India Alliance Senior Fellowship to S.T. (IA/S/18/2/503981) and CDFD core funds.

Peer review history
The peer review history is available online at https://journals.biologists.com/jcs/article-lookup/doi/10.1242/jcs.260042.reviewer-comments.pdf.

References

Ali, A., Veeranki, S. N. and Tyagi, S. (2014). A SET-domain-independent role of WRAD complex in cell-cycle regulatory function of mixed lineage leukemia. *Nucleic Acids Res.* **42**, 7611-7624. doi:10.1093/nar/gku458

Ali, A., Veeranki, S. N., Chinchole, A. and Tyagi, S. (2017). MLL/WDR5 complex regulates Kif2A localization to ensure chromosome congression and proper spindle assembly during mitosis. *Dev. Cell* **41**, 605-622.e7. doi:10.1016/j.devcel.2017.05.023

Ansari, K. I., Kasiri, S. and Mandal, S. S. (2013). Histone methylase MLL1 has critical roles in tumor growth and angiogenesis and its knockdown suppresses tumor growth in vivo. *Oncogene* **32**, 3359-3370. doi:10.1038/onc.2012.352

Artinger, E. L., Mishra, B. P., Zaffuto, K. M., Li, B. E., Chung, E. K. Y., Moore, A. W., Chen, Y., Cheng, C. and Ernst, P. (2013). An MLL-dependent network sustains hematopoiesis. *Proc. Natl. Acad. Sci. USA* **110**, 12000-12005. doi:10.1073/pnas.1301278110

Azim, A. C., Barkalow, K., Chou, J. and Hartwig, J. H. (2000). Activation of the small GTPases, rac and cdc42, after ligation of the platelet PAR-1 receptor. *Blood* **95**, 959-964. doi:10.1182/blood.V95.3.959.003k22_959_964

Barski, A., Cuddapah, S., Cui, K., Roh, T.-Y., Schones, D. E., Wang, Z., Wei, G., Chepelev, I. and Zhao, K. (2007). High-resolution profiling of histone methylations in the human genome. *Cell* **129**, 823-837. doi:10.1016/j.cell.2007.05.009

Betapudi, V., Licate, L. S. and Egelhoff, T. T. (2006). Distinct roles of nonmuscle myosin II isoforms in the regulation of MDA-MB-231 breast cancer cell spreading and migration. *Cancer Res.* **66**, 4725-4733. doi:10.1158/0008-5472.CAN-05-4236

Blanchoin, L., Boujemaa-Paterski, R., Sykes, C. and Plastino, J. (2014). Actin dynamics, architecture, and mechanics in cell motility. *Physiol. Rev.* **94**, 235-263. doi:10.1152/physrev.00018.2013

Boulter, E., Garcia-Mata, R., Guilluy, C., Dubash, A., Rossi, G., Brennwald, P. J. and Burridge, K. (2010). Regulation of Rho GTPase crosstalk, degradation and activity by RhoGDI1. *Nat. Cell Biol.* **12**, 477-483. doi:10.1038/ncb2049

Carugo, A., Genovese, G., Seth, S., Nezi, L., Rose, J. L., Bossi, D., Cicalese, A., Shah, P. K., Viale, A., Pettazzoni, P. F. et al. (2016). In vivo functional platform targeting patient-derived xenografts identifies WDR5-Myc association as a critical determinant of pancreatic cancer. *Cell Rep.* **16**, 133-147. doi:10.1016/j.celrep.2016.05.063

Cho, H. J., Kim, J. T., Lee, S.-J., Hwang, Y. S., Park, S. Y., Kim, B.-Y., Yoo, J., Hong, K. S., Min, J.-K., Lee, C.-H. et al. (2018). Protein phosphatase 1B dephosphorylates Rho guanine nucleotide dissociation inhibitor 1 and suppresses cancer cell migration and invasion. *Cancer Lett.* **417**, 141-151. doi:10.1016/j.canlet.2018.01.002

Cohn, M. J., Patel, K., Krumlauf, R., Wilkinson, D. G., Clarke, J. D. and Tickle, C. (1997). Hox9 genes and vertebrate limb specification. *Nature* **387**, 97-101. doi:10.1038/387097a0

Dangi, C. B. S. and Firodiya, A. (2012). Triple-negative breast cancer and it's therapeutic options. *Int. J. Pharma Bio Sci* **3**, 130-160. doi:10.1016/S1470-2045(07)70074-8

Ernst, P., Wang, J., Huang, M., Goodman, R. H. and Korsmeyer, S. J. (2001). MLL and CREB bind cooperatively to the nuclear coactivator CREB-binding protein. *Mol. Cell. Biol* **21**, 2249-2258. doi:10.1128/MCB.21.7.2249-2258.2001

Etienne-Manneville, S. and Hall, A. (2002). Rho GTPases in cell biology. *Nature* **420**, 629-635. doi:10.1038/nature01148

Fritz, G., Just, I. and Kaina, B. (1999). Proteomics of breast cancer for marker discovery and signal pathway profiling. *Int. J. Cancer* **81**, 682-687. doi:10.1002/(SICI)1097-0215(19990531)81:5<682::AID-IJC2>3.0.CO;2-B

Goitre, L., Trapani, E., Trabalzini, L. and Retta, S. F. (2014). The ras superfamily of small GTPases: the unlocked secrets. *Methods Mol. Biol* **1120**, 1-18. doi:10.1007/978-1-62703-791-4_1

Golding, A. E., Visco, I., Bieling, P. and Bement, W. M. (2019). Extraction of active rhoGTPases by rhoGDI regulates spatiotemporal patterning of rhogtpases. *Elife* **8**, e50471. doi:10.7554/eLife.50471

Gorvel, J. P., Chang, T. C., Boretto, J., Azuma, T. and Chavrier, P. (1998). Differential properties of D4/LyGDI versus RhoGDI: phosphorylation and rho GTPase selectivity. *FEBS Lett.* **422**, 269-273. doi:10.1016/S0014-5793(98)00020-9

Grebien, F., Vedadi, M., Getlik, M., Giambruno, R., Grover, A., Avellino, R., Skucha, A., Vittori, S., Kuznetsova, E., Smil, D. et al. (2015). Pharmacological targeting of the Wdr5-MLL interaction in C/EBPα N-terminal leukemia. *Nat. Chem. Biol.* **11**, 571-578. doi:10.1038/nchembio.1859

Guo, F., Debidda, M., Yang, L., Williams, D. A. and Zheng, Y. (2006). Genetic deletion of Rac1 GTPase reveals its critical role in actin stress fiber formation and focal adhesion complex assembly. *J. Biol. Chem.* **281**, 18652-18659. doi:10.1074/jbc.M603508200

He, F.-X., Zhang, L.-L., Jin, P.-F., Liu, D.-D. and Li, A.-H. (2019). DPY30 regulates cervical squamous cell carcinoma by mediating epithelial-mesenchymal transition (EMT). *Onco. Targets. Ther.* **12**, 7139-7147. doi:10.2147/OTT.S209315

Hess, J. L., Yu, B. D., Li, B., Hanson, R. and Korsmeyer, S. J. (1997). Defects in yolk sac hematopoiesis in Mll-null embryos. *Blood* **90**, 1799-1806. doi:10.1182/blood.V90.5.1799

Hodge, R. G. and Ridley, A. J. (2016). Regulating Rho GTPases and their regulators. *Nat. Rev. Mol. Cell Biol.* **17**, 496-510. doi:10.1038/nrm.2016.67

Hondermarck, H., Vercoutter-Edouart, A.-S., Révillion, F., Lemoine, J., El-Yazidi-Belkoura, I., Nurcombe, V. and Peyrat, J.-P. (2001). Proteomics of breast cancer for marker discovery and signal pathway profiling. *Proteomics* **1**, 1216-1232. doi:10.1002/1615-9861(200110)1:10<1216::AID-PROT1216>3.0.CO;2-P

Hsieh, J. J.-D., Ernst, P., Erdjument-Bromage, H., Tempst, P. and Korsmeyer, S. J. (2003). Proteolytic cleavage of MLL generates a complex of N- and C-terminal fragments that confers protein stability and subnuclear localization. *Mol. Cell. Biol.* **23**, 186-194. doi:10.1128/MCB.23.1.186-194.2003

Huang, Z., Zhang, L., Chen, Y., Zhang, H., Zhang, Q., Li, R., Ma, J., Li, Z., Yu, C., Lai, Y. et al. (2016). Cdc42 deficiency induces podocyte apoptosis by inhibiting the Nwasp/stress fibers/YAP pathway. *Cell Death Dis.* **7**, e2142. doi:10.1038/cddis.2016.51

Issaeva, I., Zonis, Y., Rozovskaia, T., Orlovsky, K., Croce, C. M., Nakamura, T., Mazo, A., Eisenbach, L. and Canaani, E. (2007). Knockdown of ALR (MLL2) reveals ALR target genes and leads to alterations in cell adhesion and growth. *Mol. Cell. Biol.* **27**, 1889-1903. doi:10.1128/MCB.01506-06

Ito, H., Morishita, R. and Nagata, K.-I. (2018). Functions of Rhotekin, an effector of Rho GTPase, and Its binding partners in mammals. *Int. J. Mol. Sci.* **19**, 2121. doi:10.3390/ijms19072121

Jaffe, A. B. and Hall, A. (2005). Rho GTPases: biochemistry and biology. *Annu. Rev. Cell Dev. Biol.* **21**, 247-269. doi:10.1146/annurev.cellbio.21.020604.150721

Jakobs, M. A., Dimitracopoulos, A. and Franze, K. (2019). KymoButler, a deep learning software for automated kymograph analysis. *Elife* **8**, e42288. doi:10.7554/eLife.42288

Jung, H., Yoon, S. R., Lim, J., Cho, H. J. and Lee, H. G. (2020). Dysregulation of rho gtpases in human cancers. *Cancers* **12**, 1179. doi:10.3390/cancers12051179

Kovac, B., Teo, J. L., Mäkelä, T. P. and Vallenius, T. (2013). Assembly of non-contractile dorsal stress fibers requires α-actinin-1 and Rac1 in migrating and spreading cells. *J. Cell Sci.* **126**, 263-273. doi:10.1242/jcs.115063

Livak, K. J. and Schmittgen, T. D. (2001). Analysis of relative gene expression data using real-time quantitative PCR and the 2–ΔΔCT Method. *Methods* **25**, 402-408. doi:10.1006/meth.2001.1262

Luxenburg, C. and Zaidel-Bar, R. (2019). From cell shape to cell fate via the cytoskeleton — insights from the epidermis. *Exp. Cell Res.* **378**, 232-237. doi:10.1016/j.yexcr.2019.03.016

Malek, R., Gajula, R. P., Williams, R. D., Nghiem, B., Simons, B. W., Nugent, K., Wang, H., Taparra, K., Lemtiri-Chlieh, G., Yoon, A. R. et al. (2017). TWIST1-WDR5-hottip regulates Hoxa9 chromatin to facilitate prostate cancer metastasis. *Cancer Res.* **77**, 3181-3193. doi:10.1158/0008-5472.CAN-16-2797

Malik, K. K., Sridhara, S. C., Lone, K. A., Katariya, P. D. and Tyagi, S. (2022). MLL family members regulate H3K4 methylation to ensure CENP-A assembly at human centromeres. *bioRxiv*. doi:10.1101/2022.06.20.496844

Marschalek, R. (2016). Classification of mixed-lineage leukemia fusion partners predicts additional cancer pathways. *Ann. Lab. Med.* **36**, 85-100. doi:10.3343/alm.2016.36.2.85

Miura, Y., Kikuchi, A., Musha, T., Kuroda, S., Yaku, H., Sasaki, T. and Takai, Y. (1993). Regulation of morphology by rho p21 and its inhibitory GDP/GTP exchange protein (rho GDI) in Swiss 3T3 cells. *J. Biol. Chem.* **268**, 510-515. doi:10.1016/S0021-9258(18)54180-6

Navarro-Lérida, I., Sánchez-Álvarez, M. and del Pozo, M. Á. (2021). Post-translational modification and subcellular compartmentalization: emerging concepts on the regulation and physiopathological relevance of RhoGTPases. *Cells* **10**, 1990. doi:10.3390/cells10081990

Nobes, C. D. and Hall, A. (1995). Rho, Rac, and Cdc42 GTPases regulate the assembly of multimolecular focal complexes associated with actin stress fibers, lamellipodia, and filopodia. *Cell* **81**, 53-62. doi:10.1016/0092-8674(95)90370-4

Ota, T., Maeda, M., Murakami, M., Takegami, T., Suto, S. and Tatsuka, M. (2007). Activation of Rac1 by Rho-guanine nucleotide dissociation inhibitor-β with defective isoprenyl-binding pocket. *Cell Biol. Int.* **31**, 92-96. doi:10.1016/j.cellbi.2006.09.002

Paluch, E. and Heisenberg, C. P. (2009). Biology and physics of cell shape changes in development. *Curr. Biol.* **19**, R790-R799. doi:10.1016/j.cub.2009.07.029

Pascual-Vargas, P., Cooper, S., Sero, J., Bousgouni, V., Arias-Garcia, M. and Bakal, C. (2017). RNAi screens for Rho GTPase regulators of cell shape and YAP/TAZ localisation in triple negative breast cancer. *Sci. Data* **4**, 1-13. doi:10.1038/sdata.2017.18

Patel, A., Dharmarajan, V., Vought, V. E. and Cosgrove, M. S. (2009). On the mechanism of multiple lysine methylation by the human mixed lineage leukemia protein-1 (MLL1) core complex. *J. Biol. Chem.* **284**, 24242-24256. doi:10.1074/jbc.M109.014498

Pillé, J. Y., Denoyelle, C., Varet, J., Bertrand, J. R., Soria, J., Opolon, P., Lu, H., Pritchard, L.-L., Vannier, J. P., Malvy, C. et al. (2005). Anti-RhoA and Anti-RhoC siRNAs inhibit the proliferation and invasiveness of MDA-MB-231 breast cancer cells in vitro and in vivo. *Mol. Ther.* **11**, 267-274. doi:10.1016/j.ymthe.2004.08.029

Pollard, T. D. and Cooper, J. A. (2009). Actin, a central player in cell shape and movement. *Science* **326**, 1208-1212. doi:10.1126/science.1175862

Radjabi, A. R., Sawada, K., Jagadeeswaran, S., Eichbichler, A., Kenny, H. A., Montag, A., Bruno, K. and Lengyel, E. (2008). Thrombin induces tumor invasion through the induction and association of matrix metalloproteinase-9 and β1-integrin on the cell surface. *J. Biol. Chem.* **283**, 2822-2834. doi:10.1074/jbc.M704855200

Raftopoulou, M. and Hall, A. (2004). Cell migration: Rho GTPases lead the way. *Dev. Biol.* **265**, 23-32. doi:10.1016/j.ydbio.2003.06.003

Reymond, N., Riou, P. and Ridley, A. J. (2012a). Rho GTPases and cancer cell transendothelial migration. *Methods Mol. Biol.* **827**, 123-142. doi:10.1007/978-1-61779-442-1_9

Reymond, N., Im, J. H., Garg, R., Vega, F. M., Borda d'Agua, B., Riou, P., Cox, S., Valderrama, F., Muschel, R. J. and Ridley, A. J. (2012b). Cdc42 promotes transendothelial migration of cancer cells through β1 integrin. *J. Cell Biol.* **199**, 653-668. doi:10.1083/jcb.201205169

Ridley, A. J. and Hall, A. (1992). The small GTP-binding protein rho regulates the assembly of focal adhesions and actin stress fibers in response to growth factors. *Cell* **70**, 389-399. doi:10.1016/0092-8674(92)90163-7

Ridley, A. J., Paterson, H. F., Johnston, C. L., Diekmann, D. and Hall, A. (1992). The small GTP-binding protein rac regulates growth factor-induced membrane ruffling. *Cell* **70**, 401-410. doi:10.1016/0092-8674(92)90164-8

Ridley, A. J., Schwartz, M. A., Burridge, K., Firtel, R. A., Ginsberg, M. H., Borisy, G., Parsons, J. T. and Horwitz, A. R. (2003). Cell migration: integrating signals from front to back. *Science* **302**, 1704-1709. doi:10.1126/science.1092053

Riedl, J., Crevenna, A. H., Kessenbrock, K., Yu, J. H., Neukirchen, D., Bista, M., Bradke, F., Jenne, D., Holak, T. A., Werb, Z. et al. (2008). Lifeact: a versatile marker to visualize F-actin. *Nat. Methods* **5**, 605-607. doi:10.1038/nmeth.1220

Sailem, H., Bousgouni, V., Cooper, S. and Bakal, C. (2014). Cross-talk between Rho and Rac GTPases drives deterministic exploration of cellular shape space and morphological heterogeneity. *Open Biol.* **4**, 130132. doi:10.1098/rsob.130132

Sanjana, N. E., Shalem, O. and Zhang, F. (2014). Improved vectors and genome-wide libraries for CRISPR screening. *Nat. Methods* **11**, 783-784. doi:10.1038/nmeth.3047

Shi, G. X., Yang, W. S., Jin, L., Matter, M. L. and Ramos, J. W. (2017). RSK2 drives cell motility by serine phosphorylation of LARG and activation of Rho GTPases. *Proc. Natl. Acad. Sci. USA* **115**, E190-E199. doi:10.1073/pnas.1708584115

Steffen, A., Rottner, K., Ehinger, J., Innocenti, M., Scita, G., Wehland, J. and Stradal, T. E. B. (2004). Sra-1 and Nap1 link Rac to actin assembly driving lamellipodia formation. *EMBO J.* **23**, 749-759. doi:10.1038/sj.emboj.7600084

Stringer, B. W., Day, B. W., D'Souza, R. C. J., Jamieson, P. R., Ensbey, K. S., Bruce, Z. C., Lim, Y. C., Goasdoué, K., Offenhäuser, C., Akgül, S. et al. (2019). A reference collection of patient-derived cell line and xenograft models of proneural, classical and mesenchymal glioblastoma. *Sci. Rep.* **9**, 4902. doi:10.1038/s41598-019-41277-z

Thiel, A. T., Blessington, P., Zou, T., Feather, D., Wu, X., Yan, J., Zhang, H., Liu, Z., Ernst, P., Koretzky, G. A. et al. (2010). MLL-AF9-induced leukemogenesis requires coexpression of the wild-type Mll allele. *Cancer Cell* **17**, 148-159. doi:10.1016/j.ccr.2009.12.034

Tregnago, C., Da Ros, A., Porcù, E., Benetton, M., Simonato, M., Simula, L., Borella, G., Polato, K., Minuzzo, S., Borile, G. et al. (2020). Thioridazine requires calcium influx to induce MLL-AF6-rearranged AML cell death. *Blood Adv.* **4**, 4417-4429. doi:10.1182/bloodadvances.2020002001

Tyagi, S. and Herr, W. (2009). E2F1 mediates DNA damage and apoptosis through HCF-1 and the MLL family of histone methyltransferases. *EMBO J.* **28**, 3185-3195. doi:10.1038/emboj.2009.258

Van Lidth de Jeude, J. F., Vermeulen, J. L. M., Montenegro-Miranda, P. S., Van den Brink, G. R. and Heijmans, J. (2015). A protocol for lentiviral transduction and downstream analysis of intestinal organoids. *J. Vis. Exp.* **98**, 52531. doi:10.3791/52531

van Nieuw Amerongen, G. P., van Delft, S., Vermeer, M. A., Collard, J. G. and van Hinsbergh, V. W. (2000). Activation of RhoA by thrombin in endothelial hyperpermeability: role of Rho kinase and protein tyrosine kinases. *Circ. Res.* **87**, 335-340. doi:10.1161/01.RES.87.4.335

Vega, F. M., Fruhwirth, G., Ng, T. and Ridley, A. J. (2011). RhoA and RhoC have distinct roles in migration and invasion by acting through different targets. *J. Cell Biol.* **193**, 655-665. doi:10.1083/jcb.201011038

Wang, P., Lin, C., Smith, E. R., Guo, H., Sanderson, B. W., Wu, M., Gogol, M., Alexander, T., Seidel, C., Wiedemann, L. M. et al. (2009). Global analysis of H3K4 methylation defines MLL family member targets and points to a role for MLL1-mediated H3K4 methylation in the regulation of transcriptional initiation by RNA polymerase II. *Mol. Cell. Biol.* **29**, 6074-6085. doi:10.1128/MCB.00924-09

Wang, T., Wei, J. J., Sabatini, D. M. and Lander, E. S. (2014). Genetic screens in human cells using the CRISPR-Cas9 system. *Science* **343**, 80-84. doi:10.1126/science.1246981

Wang, P., Dreger, M., Madrazo, E., Williams, C. J., Samaniego, R., Hodson, N. W., Monroy, F., Baena, E., Sánchez-Mateos, P., Hurlstone, A. et al. (2018). WDR5 modulates cell motility and morphology and controls nuclear changes induced by a 3D environment. *Proc. Natl. Acad. Sci. USA* **115**, 8581-8586. doi:10.1073/pnas.171940511

Worthylake, R. A., Lemoine, S., Watson, J. M. and Burridge, K. (2001). RhoA is required for monocyte tail retraction during transendothelial migration. *J. Cell Biol.* **154**, 147-160. doi:10.1083/jcb.200103048

Xia, M., Xu, L., Leng, Y. and Gao, F. (2015). Downregulation of MLL3 in esophageal squamous cell carcinoma is required for the growth and metastasis of cancer cells. *Tumour Biol.* **36**, 605-613. doi:10.1007/s13277-014-2616-3

Yang, W., Trahan, G. D., Howell, E. D., Speck, N. A., Jones, K. L., Gillen, A. E., Riemondy, K., Hesselberth, J., Bryder, D. and Ernst, P. (2020). Enhancing hematopoiesis from murine embryonic stem cells through MLL1-induced activation of a Rac/Rho/Integrin signaling axis. *Stem Cell Rep.* **14**, 285-299. doi:10.1016/j.stemcr.2019.12.009

Ye, X., Zhang, R., Lian, F., Zhang, W., Lu, W., Han, J., Zhang, N., Jin, J., Luo, C., Chen, K. et al. (2019). The identification of novel small-molecule inhibitors targeting WDR5-MLL1 interaction through fluorescence polarization based high-throughput screening. *Bioorganic Med. Chem. Lett.* **29**, 638-645. doi:10.1016/j.bmcl.2018.12.035

Yu, B. D., Hanson, R. D., Hess, J. L., Horning, S. E. and Korsmeyer, S. J. (1998). MLL, a mammalian trithorax-group gene, functions as a transcriptional maintenance factor in morphogenesis. *Proc. Natl. Acad. Sci. USA* **95**, 10632-10636. doi:10.1073/pnas.95.18.10632

Yu, J., Zhang, D., Liu, J., Li, J., Yu, Y., Wu, X. R. and Huang, C. (2012). RhoGDI SUMOylation at Lys-138 increases its binding activity to Rho GTPase and its inhibiting cancer cell motility. *J. Biol. Chem.* **287**, 13752-13760. doi:10.1074/jbc.M111.337469

Zargar, Z. U., Kimidi, M. R. and Tyagi, S. (2018). Dynamic site-specific recruitment of RBP2 by pocket protein p130 modulates H3K4 methylation on E2F-responsive promoters. *Nucleic Acids Res.* **46**, 174-188. doi:10.1093/nar/gkx961

Zhang, P. and Bergamin, E. (2012). The many facets of MLL1 regulation. *Biopolymers* **99**, 136-145. doi:10.1002/bip.22126

Zhang, B., Zhang, Y., Dagher, M.-C. and Shacter, E. (2005). Rho GDP dissociation inhibitor protects cancer cells against drug-induced apoptosis. *Cancer Res.* **65**, 6054-6062. doi:10.1158/0008-5472.CAN-05-0175

Zhang, Y., Ji, T., Ma, S. and Wu, W. (2020). MLL1 promotes migration and invasion of fibroblast-like synoviocytes in rheumatoid arthritis by activating the TRIF/NF-κB signaling pathway via H3K4me3 enrichment in the TLR4 promoter region. *Int. Immunopharmacol.* **82**, 106220. doi:10.1016/j.intimp.2020.106220

Zhou, Y. T., Chew, L. L., Lin, S.-C. and Low, B. C. (2010). The BNIP-2 and Cdc42GAP homology (BCH) domain of p50RhoGAP/Cdc42GAP sequesters RhoA from inactivation by the adjacent GTPase-activating protein domain. *Mol. Biol. Cell* **21**, 3232-3246. doi:10.1091/mbc.e09-05-0408

Zhou, Q., Chen, X., He, H., Peng, S., Zhang, Y., Zhang, J., Cheng, L., Liu, S., Huang, M., Xie, R. et al. (2021). WD repeat domain 5 promotes chemoresistance and Programmed Death-Ligand 1 expression in prostate cancer. *Theranostics* **11**, 4809-4824. doi:10.7150/thno.55814

Zmurchok, C. and Holmes, W. R. (2020). Simple Rho GTPase dynamics generate a complex regulatory landscape associated with cell shape. *Biophys. J.* **118**, 1438-1454. doi:10.1016/j.bpj.2020.01.035

Journal of Cell Science (2022) 135, jcs260042. doi:10.1242/jcs.260042

Journal of Cell Science

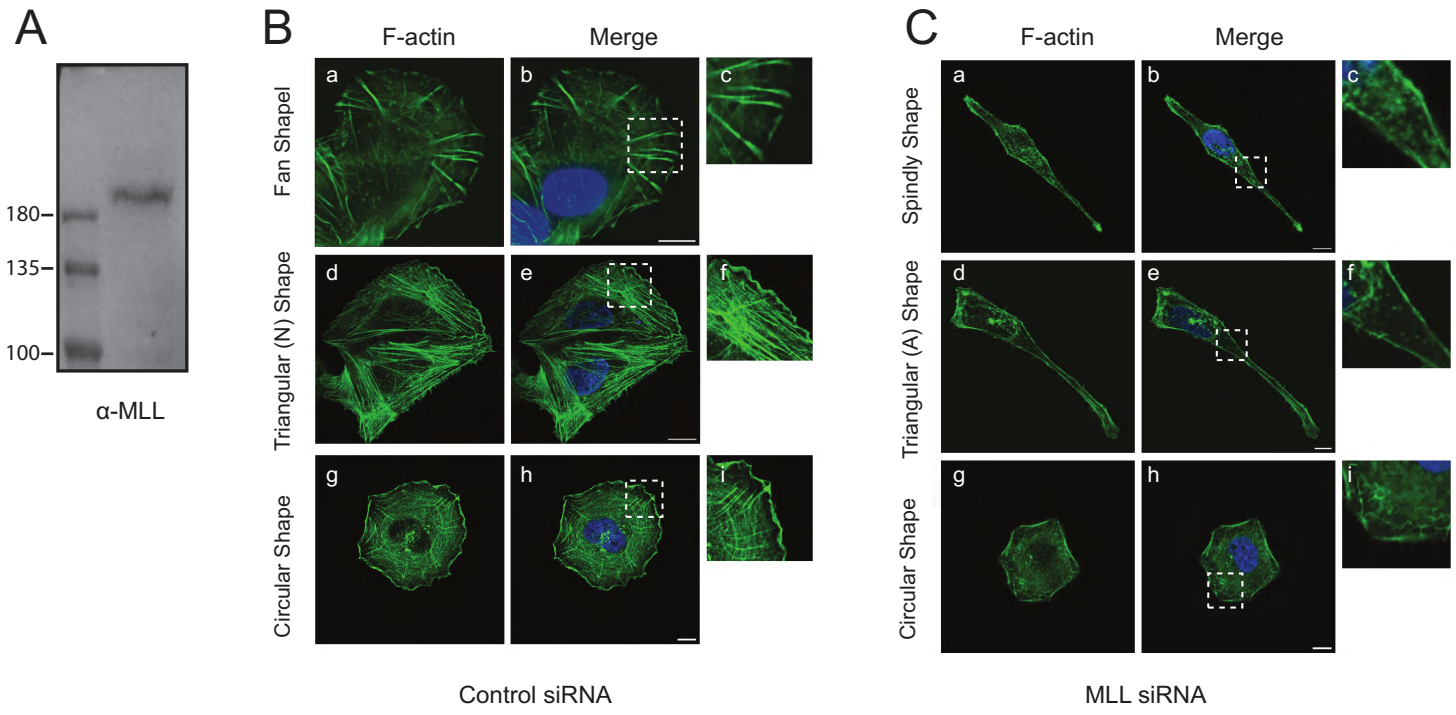

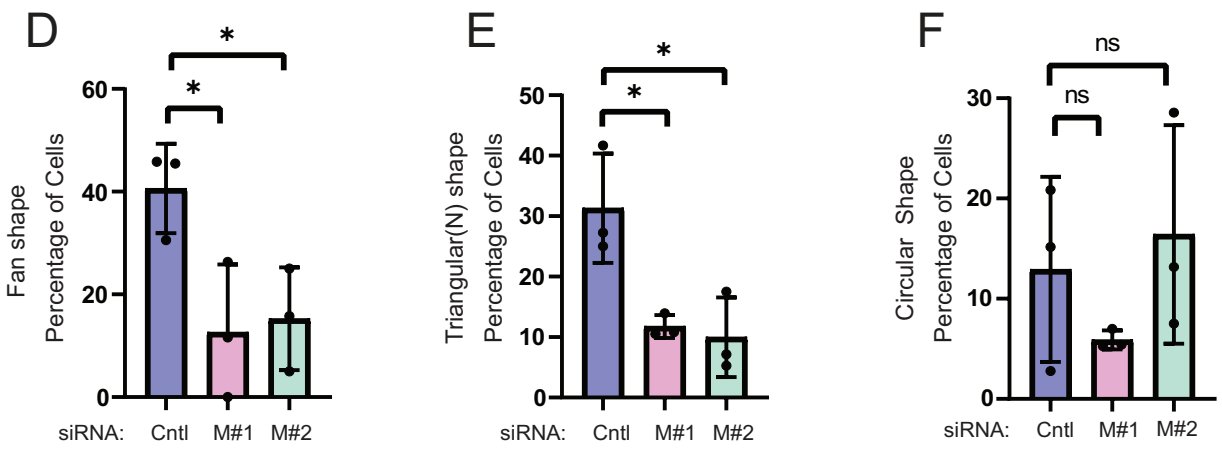

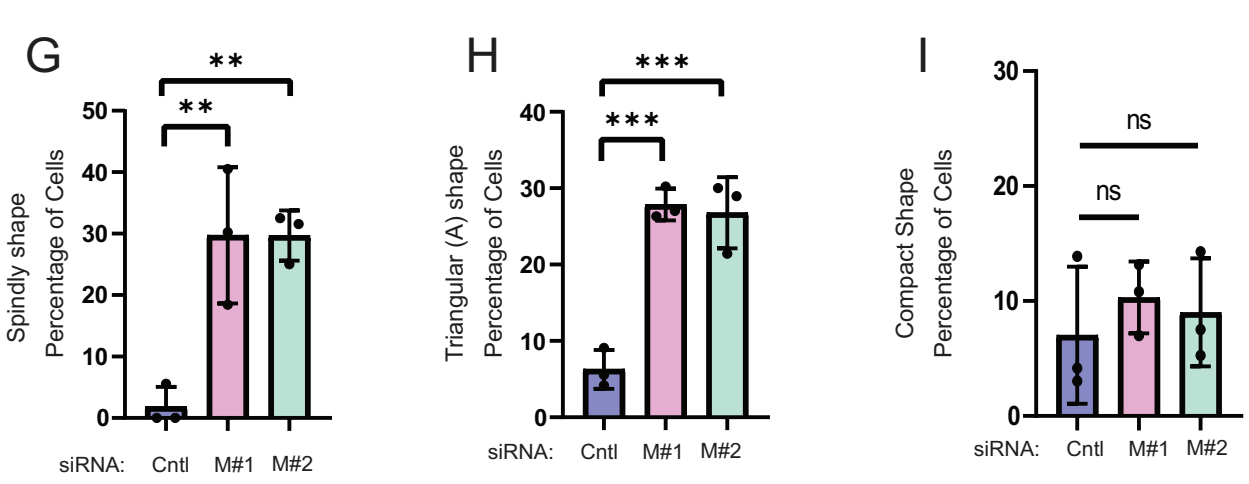

Fig. S1. Loss of MLL affects cell shape and actin cytoskeleton.

(A) U2OS cells were lysed and immunoblotted. Blot was then probed with in-house generated MLL antibody. Molecular weights are indicated on the left. **(B-C)** U2OS cells treated with control or MLL siRNA were fixed and used for immunofluorescence and stained with rhodamine conjugated phalloidin to mark filamentous actin (green). Nucleus was stained using DAPI (blue). Representative images from control (**B**) and MLL (**C**) siRNA-treated cells exhibiting three major shapes are displayed, which are quantified in Figure **1D** as well as here. Images from individual MLL siRNA treatments are shown in Figure **1C**. Panels c,f,I, show magnified views of the boxed regions in panels b,e,h, respectively. Scale bars: 10 µm. **(D-I)** Quantification of percentage of cells showing different cell shapes from **B-C**. Data represents mean ± SD. *P = 0.0339 and 0.0493 **(D)**, *P = 0.0188 and 0.0128 **(E)**, ns P = 0.5140 and 0.8304 **(F)**, **P = 0.0052 each **(G)**, *** P = 0.0004 and 0.0005 **(H)**, ns P =0.6284 and 0.8323 **(I)** for M#1 and M#2 respectively. One way ANOVA with Dunnett's multiple comparisons test was performed. F-actin, filamentous-actin; Cntl, control; M#1, MLL siRNA1; M#2, MLL siRNA#2; Triangular (N), Triangular (Normal); Triangular (A), Triangular (Abnormal).

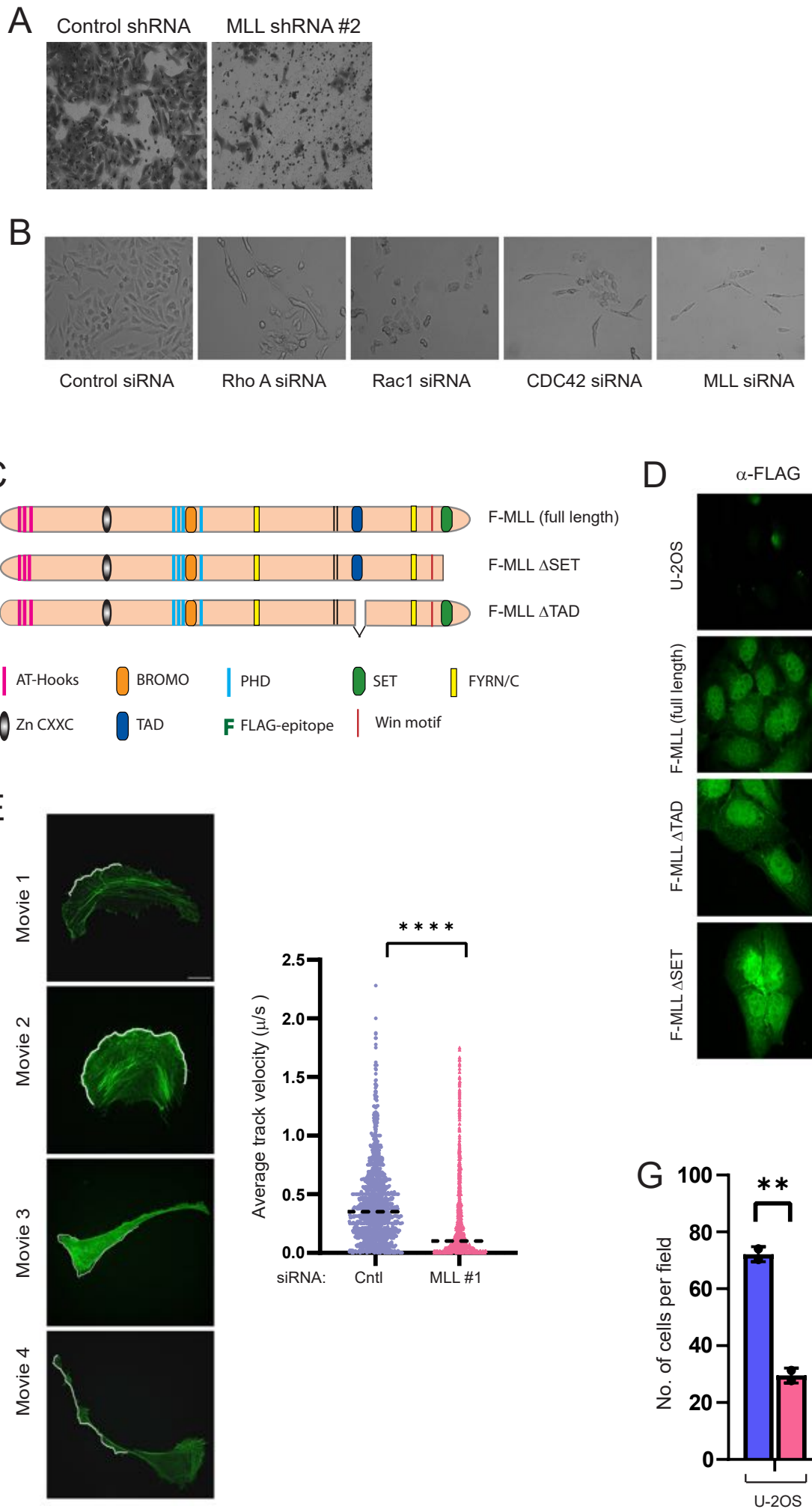

Fig. S2. Depletion of MLL alters cell-spreading and cell migration.

(A) U2OS cells were treated with control or MLL shRNA#2 for 48 h and transwell migration (Boyden chamber) assay was performed. Bright field images show migrated cells upon treatment with respective shRNAs as indicated. (**B**) Bright field images of U2OS cells treated with various siRNAs (indicated below the images) for 72 h. Images were captured in Zeiss Axiovert 40 CFL at 10X magnification. (**C**) Schematic of domain architecture of FLAG epitope tagged full length MLL and its different mutants used for the rescue experiments is shown. F-MLL (full length) denotes FLAG epitope tagged MLL protein with all its domains intact whereas F-MLLΔSET and ΔTAD denote recombinant MLL protein devoid of its transcription effector— SET or transactivation —domain respectively. Domains of MLL which impart it chromatin binding capabilities are shown as indicated: AT hooks bind to minor grove of DNA, Zinc finger (Zn) CXXC domain helps in recognition of unmethylated CpG islands, Bromodomains (Bromo) are essential for protein-protein interactions, plant homeodomain (PHD) of MLL help it to read histone marks. The 'FY' rich N-terminal (FYRN) and 'FY' rich C-terminal (FYRC) domains are required for heterodimerization of MLL_N with MLL_C subunits. WDR5 interacting (Win) motif is responsible for interacting with WDR5. (**D**) U2OS and U2OS cells expressing full length MLL and its various mutants tagged with FLAG epitope tag were fixed for immunofluorescence. Cells were stained with anti-FLAG antibody (green) to detect recombinant MLL expression and nucleus was stained with DAPI. Scale bars: 10 µm. (**E**) Live cell movies of U2OS cells expressing GFP–Lifeact from Figure **3G** were utilised for generating kymographs shown in panel on the left. Region used for kymograph generation are marked in white. Scale bars: 10 µm. Average track velocities from same time-lapse images in Figure **3G** are shown. ****P <0.0001, (Student's unpaired two-tailed t test; n = 44 movies for each siRNA from 3 experiments). **(F)** U2OS cells and U2OS expressing various mutants of MLL were treated with control and MLL shRNA#2 for 48 h and 10^5 cells were seeded for transwell migration assay. Quantifications for number of cells migrated per field of image is shown. Data are represented as mean ± SD. **P =0.004 (U2OS) and 0.003 (SET) ns, P =0.4 respectively (Student's unpaired two-tailed t test; m=2 experiments). ns, not significant; cntl, control.

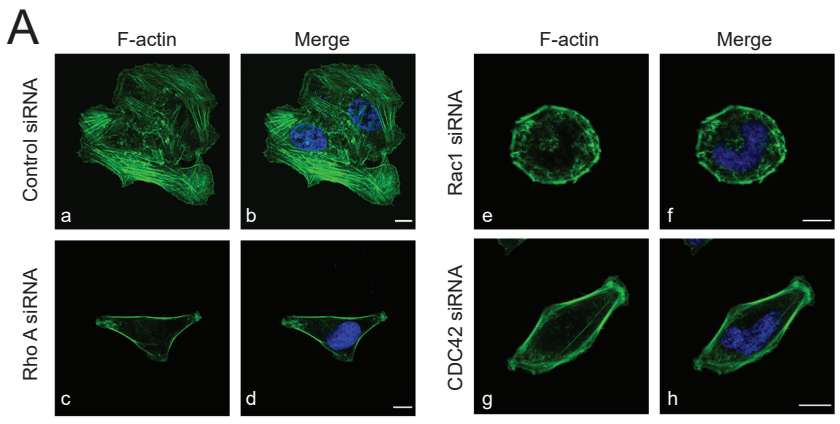

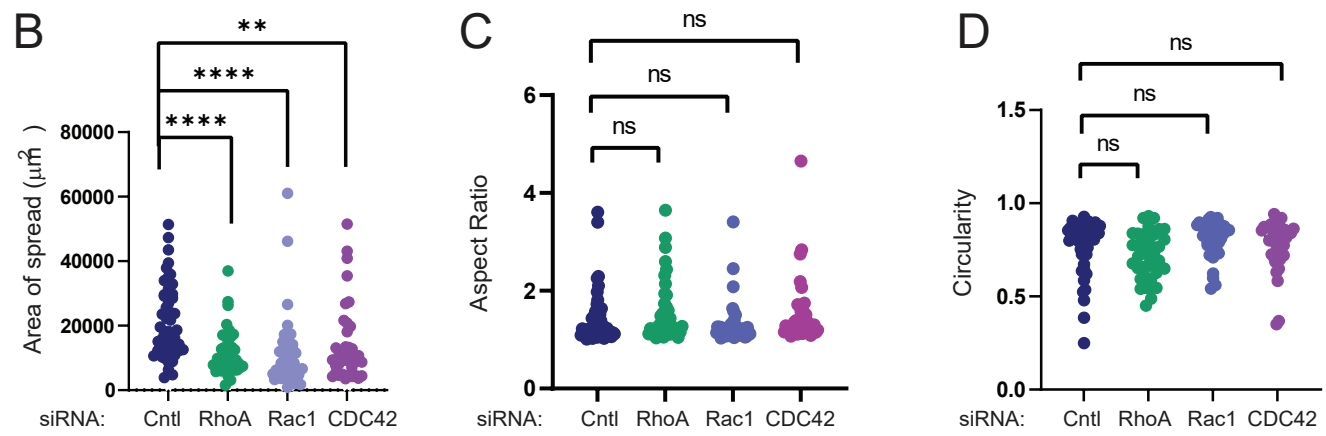

Fig. S3. Rho GTPases depletion alters cell-spreading.

(**A**) Fibronectin spreading of control U2OS cells (panels a and b) and U2OS cells upon knock down of Rho GTPases: RhoA (panels c and d), RAC1 (panels e and f) and CDC42 (panels g and h). The cells were stained with rhodamine-conjugated phalloidin to mark F-actin (green) and DAPI to mark nucleus (blue). Scale bars: 10 μm. (**B**) Quantification of area of spread of cells treated with respective siRNAs. Data represents violin plot with all the data points. ***P =0.0005 for RhoA siRNA, ****P <0.0001 for RAC1 siRNA and **P =0.001 for CDC42 siRNA-treated cells respectively. (**C**) Quantification of aspect ratio of cells treated with respective siRNAs. Data represents violin plot with all the data points. ns, P =0.72, 0.62, 0.90 for RhoA, RAC1 and CDC42 siRNA treated cells respectively. (**D**) Quantification of circularity of cells treated with respective siRNAs. Data represents violin plot with all the data points. ns, P =0.09, 0.22, 0.99 for RhoA, RAC1 and CDC42 siRNA treated cells respectively. (**B-D**) One-way ANOVA with Dunnett's multiple comparisons test was performed. n = 40 cells and m = 2 experiments. F-actin, filamentous actin; Cntl, control. ns, not significant.

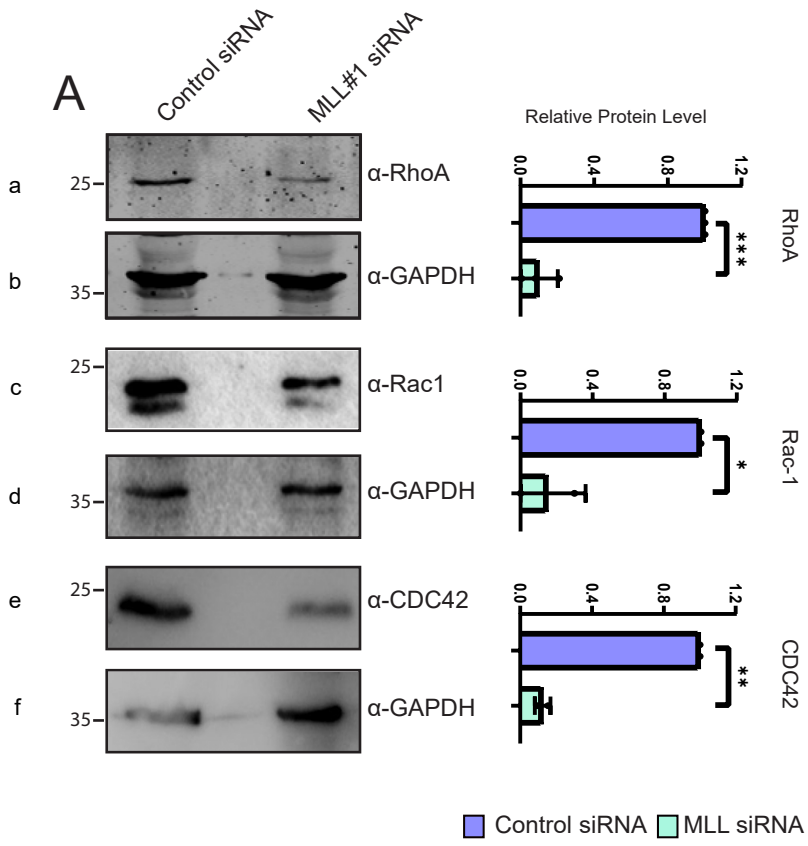

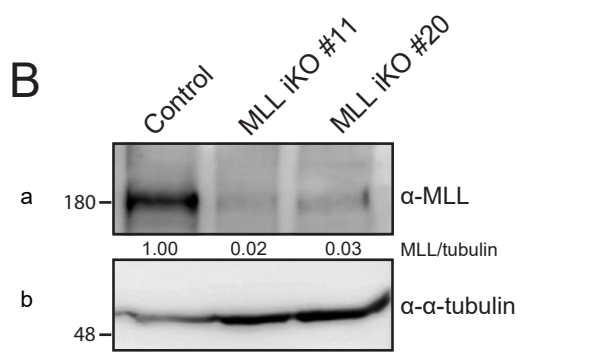

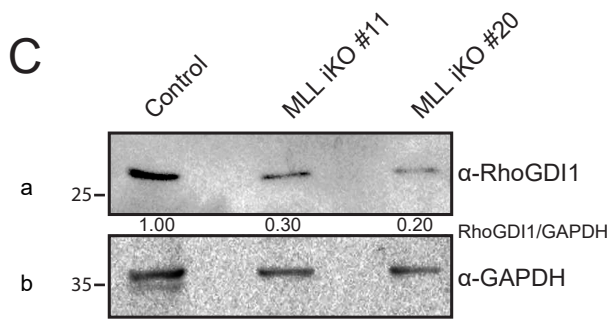

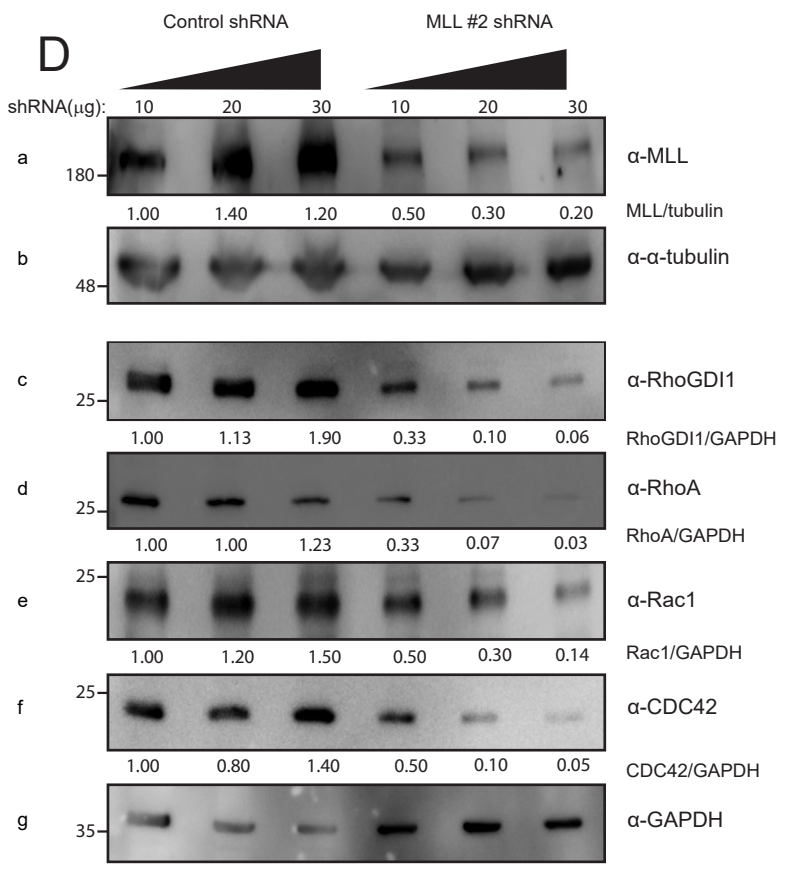

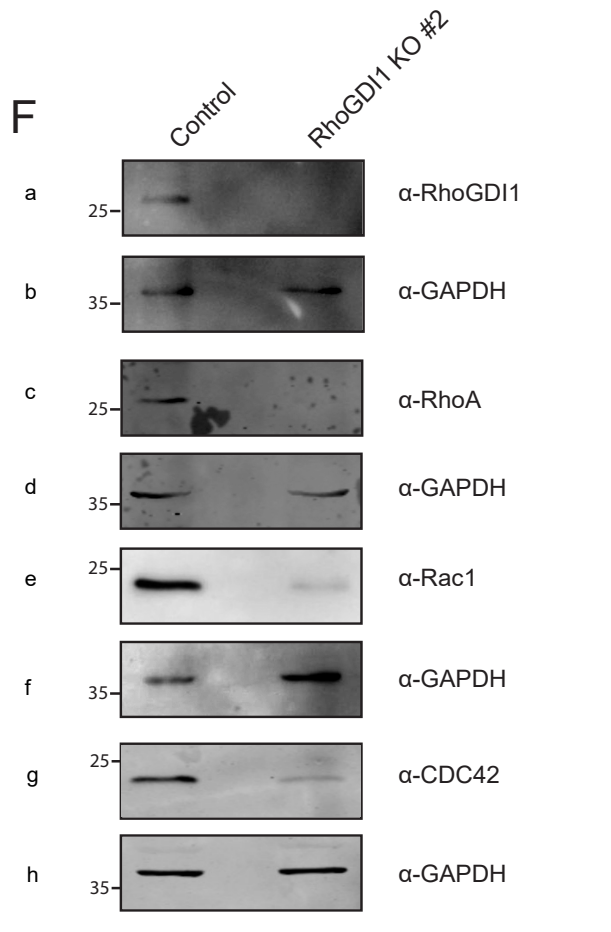

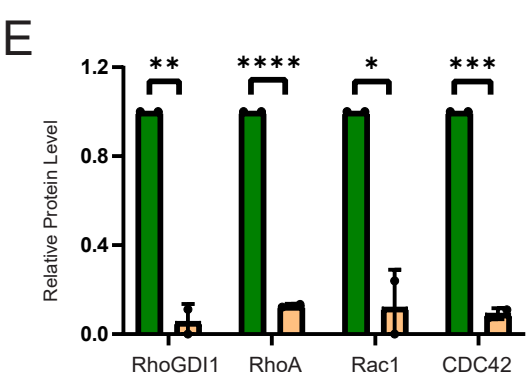

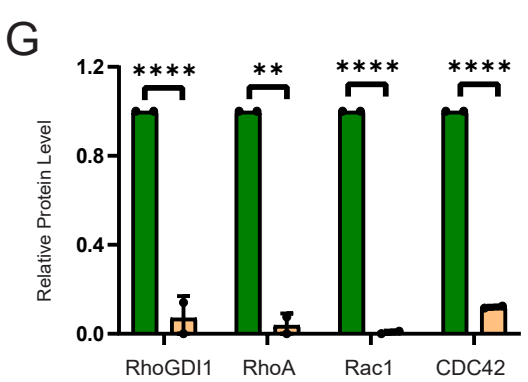

Chinchole Supplementary Figure 4

Fig. S4. MLL regulates the protein levels of RhoGDI1.

(A) MDA-MB-231 cells treated with either control or MLL#1 siRNAs, were harvested after 72 h, lysed and immunoblotted. The blots were probed with various antibodies as indicated on the right. Panels a, c and e show the endogenous protein levels of RhoA, Rac1 and CDC42 respectively upon MLL depletion. The blots shown in panels b, d and f were probed with anti-GAPDH antibody. Numbers on the left indicate molecular weight markers in kDa. Quantifications of protein levels relative to loading control are shown on the right of the blots. Data represents mean ± SD. ***P = 0.0001, *P = 0.0296 and ** P = 0.0012 for RhoA, Rac1 and CDC42 respectively. (Student's unpaired two-tailed t test; m=2 experiments). **(B, C)** Control HEK293 and MLL knock out cell lines #11 and #20 were lysed in NETN buffer and immunoblotted. The blots were probed with antibodies against MLL (**B**, panel a), RhoGDI1 (**C** panel a), and loading control, α-tubulin (**B** panel b) and GAPDH (**C**, panel b). The MLL/tubulin (**B**) and RhoGDI1/GAPDH (**C**) ratios are indicated. **(D)** U2OS cells treated with 10, 20 or 30 µg of control or MLL shRNA#2 were lysed and immunoblotted. Blots were probed with antibodies against MLL, RhoGDI1, RhoA, Rac1 and CDC42 in panels, a, c, d, e and f respectively, as indicated. The blots shown in panels b and g were probed with anti- α-tubulin and ani-GAPDH antibodies respectively. The MLL/tubulin and Rho GTPases/GAPDH ratios are indicated. **(E)** Quantification of protein levels relative to loading control of immunoblots from Figure **5E** are shown. Data represents mean ± SD. **P = 0.0035, ****P <0.0001, *P = 0.018, ***P= 0.0004. Student's unpaired two-tailed ttest; m= 2. **(F)** Control U2OS and RhoGDI1 knock out #2 cells were lysed and immunoblotted. The blots were probed with anti RhoGDI1 (panel a), RhoA (panel c), RAC1 (panel e) and CDC42 (panel g) antibodies respectively. Loading control, GAPDH is shown in panels b, d, f and h for respective blots. **(G)** Quantification of relative protein levels from immunoblots in **F** are shown. Data represents mean ± SD. ****P <0.0001 for RhoGDI1, Rac1 and CDC42. **P = 0.002 for RhoA. Student's unpaired two-tailed t test; m= 2. (A-D, F) Numbers on the left indicate molecular weight markers in kDa; KO, knock out.

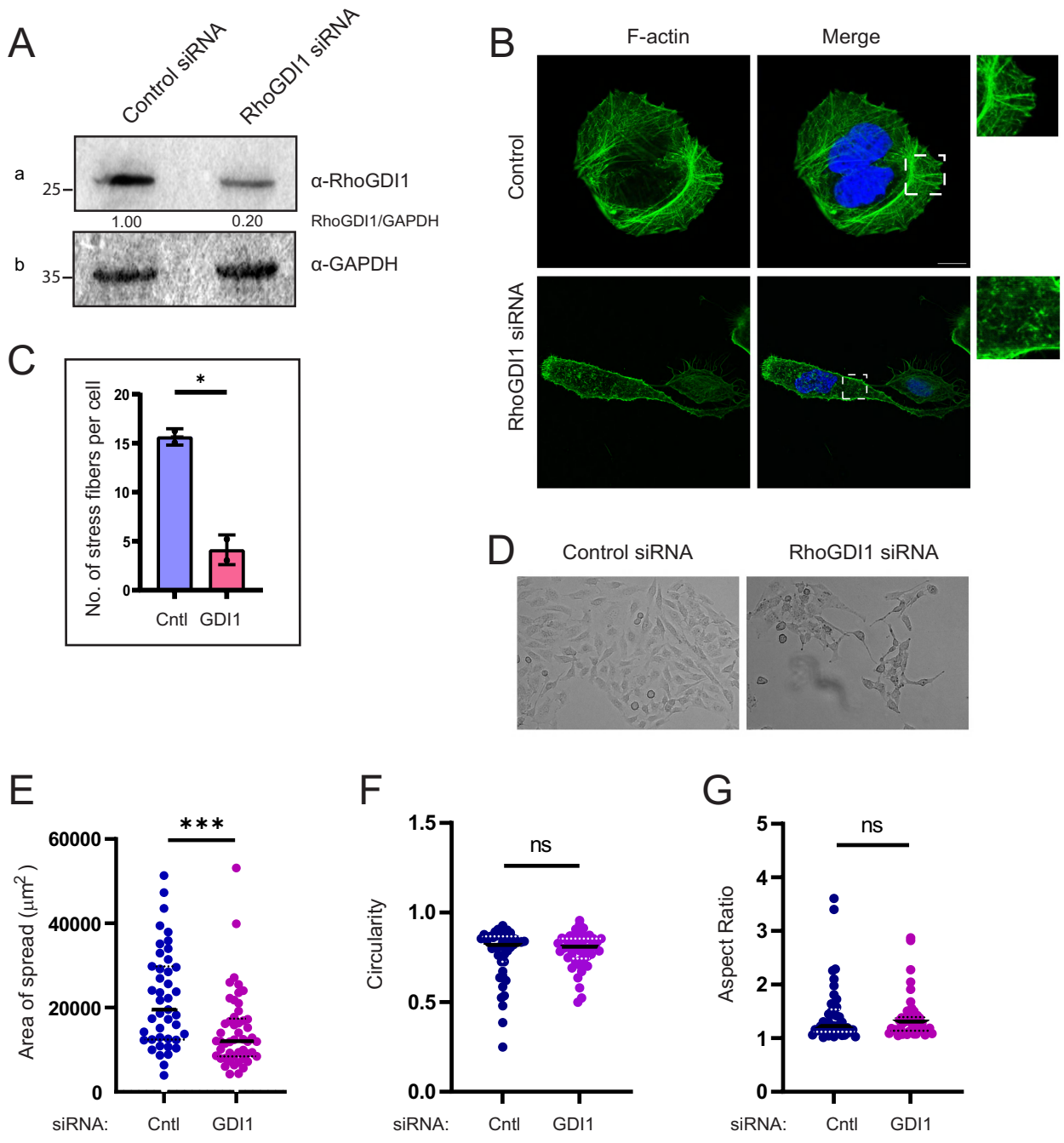

Fig. S5. Depletion of RhoGDI1 affects actin stress fiber formation and cell spreading.

(A) U2OS cells were treated with control or RhoGDI1 siRNAs for 72 h, lysed and immunoblotted. Blots were probed with RhoGDI1 (panel a) and GAPDH (panel b) antibodies. Numbers on the left indicate molecular weight markers in kDa. The RhoGDI1/GAPDH ratio is indicated **(B)** U2OS cells were seeded on cover slips and treated with either control or RhoGDI1 siRNA for 72 h prior to fixation for immunofluorescence. Actin stress fibers stained with stained with rhodamine-conjugated phalloidin is shown in control siRNA (upper panel) and RhoGDI1 siRNA (lower panel) treated cells respectively. Insets are shown adjacent to IF images. White squares indicate region highlighted in insets. Scale bars: 10 μm. **(C)** Quantification of number of stress fibers per cell from **B** is shown. Data represents mean ± SD.

*P = 0.01 (Student's unpaired two-tailed t test; n = 40 cells, m = 2 experiments). Data in wild type U2OS is same as Figure **3E**, as these experiments were done together. **(D)** U2OS cells were treated with control and RhoGDI1 siRNA for 72 h and bright field images were captured at 10x magnification in Zeiss Axiovert CFL 40 microscope. **(E)** U2OS cells treated with control and RhoGDI1 siRNA were spread on fibronectin coated cover slips for 4 h and the area of spread of the cells was quantified. ***P =0.0005. **(F)** Quantification of circularity of control and RhoGDI1 siRNA treated U2OS cells. ns P =0.43. **(G)** Quantification of aspect ratio of control and RhoGDI1 siRNA treated U2OS cells. ns P =0.50 **(E-G)** Data represents violin plot with all data points. Student's unpaired two-tailed t test; n = 40 cells and m = 2 experiments. F-actin, filamentous actin; Cntl, control; GDI1, RhoGDI1; No., number; ns, not significant.

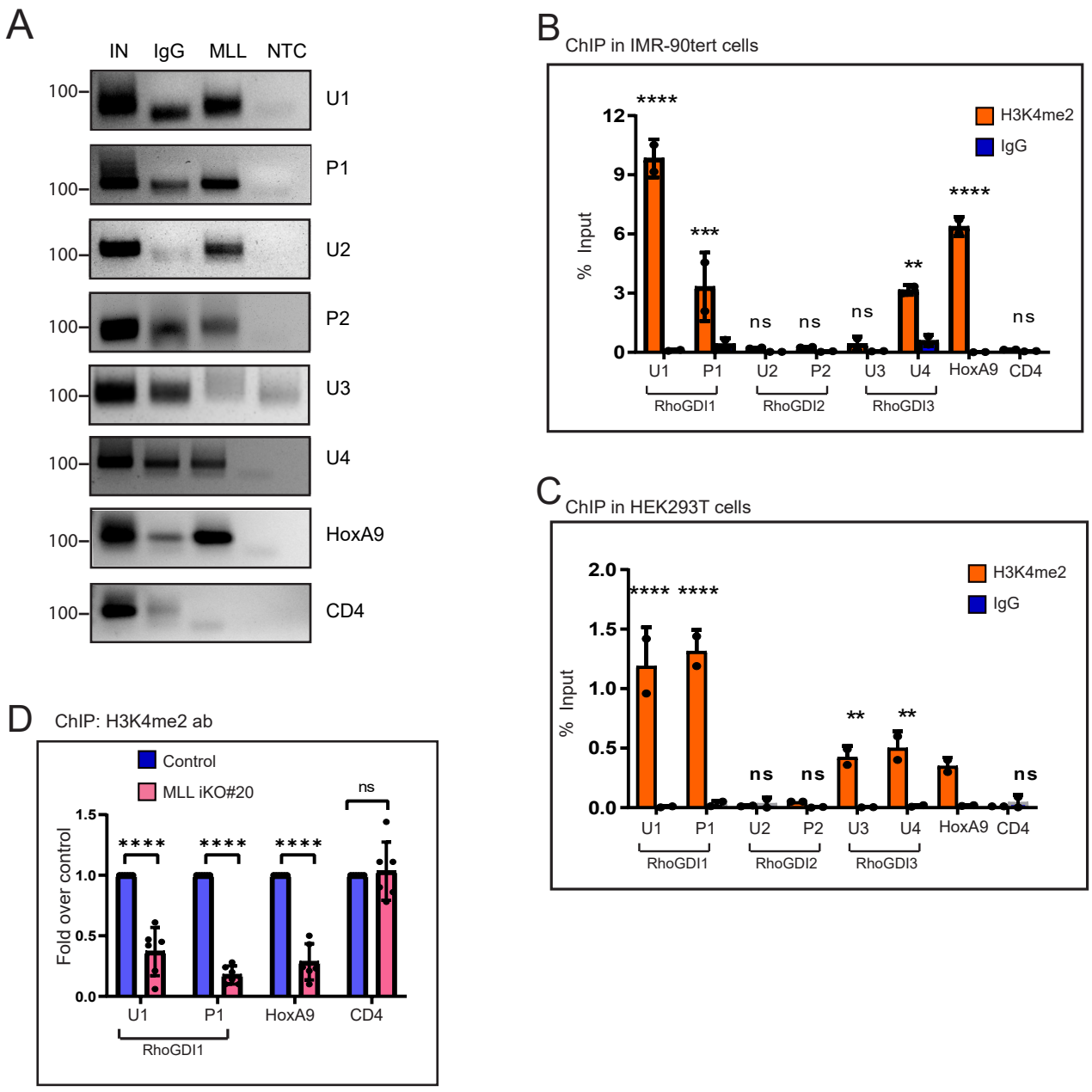

Fig. S6. MLL binds to RhoGDI1 promoter to deposit H3K4 trimethylation marks.

(A) HEK293 cells were subjected to ChIP PCR analysis using anti-MLL and IgG antibodies. The ChIP samples were subsequently used for RT q-PCR amplification. Agarose gel image of the amplicons obtained from RTq-PCR are shown. Primers used for the amplification are indicated on the right. Numbers indicated on the right are molecular weight marker in base pair. **(B-C)** ChIP was performed cells using H3K4me2 and IgG antibody in IMR-90tert **(B)** and HEK293T **(C)** cells. (**D**) ChIP assay was performed in HEK293 control (Cas-9 expressing) and MLL knockout cell lines using H3K4me2 antibody. The immunoprecipitated DNA was quantified with RT-qPCR and the results are plotted as the percentage enrichment relative to the input in **B and C** and as fold change with respect to control in **D,** as described in main text. The antibodies used are indicated in the top right corner of each box. The error bars represent mean ± S.D. two-way ANOVA, *P ≤0.05, **P ≤0.01, *** P ≤0.001, ****P ≤0.0001, ns: not significant, P > 0.05. All the experiments are done at least twice. IN, input; NTC, no template control.

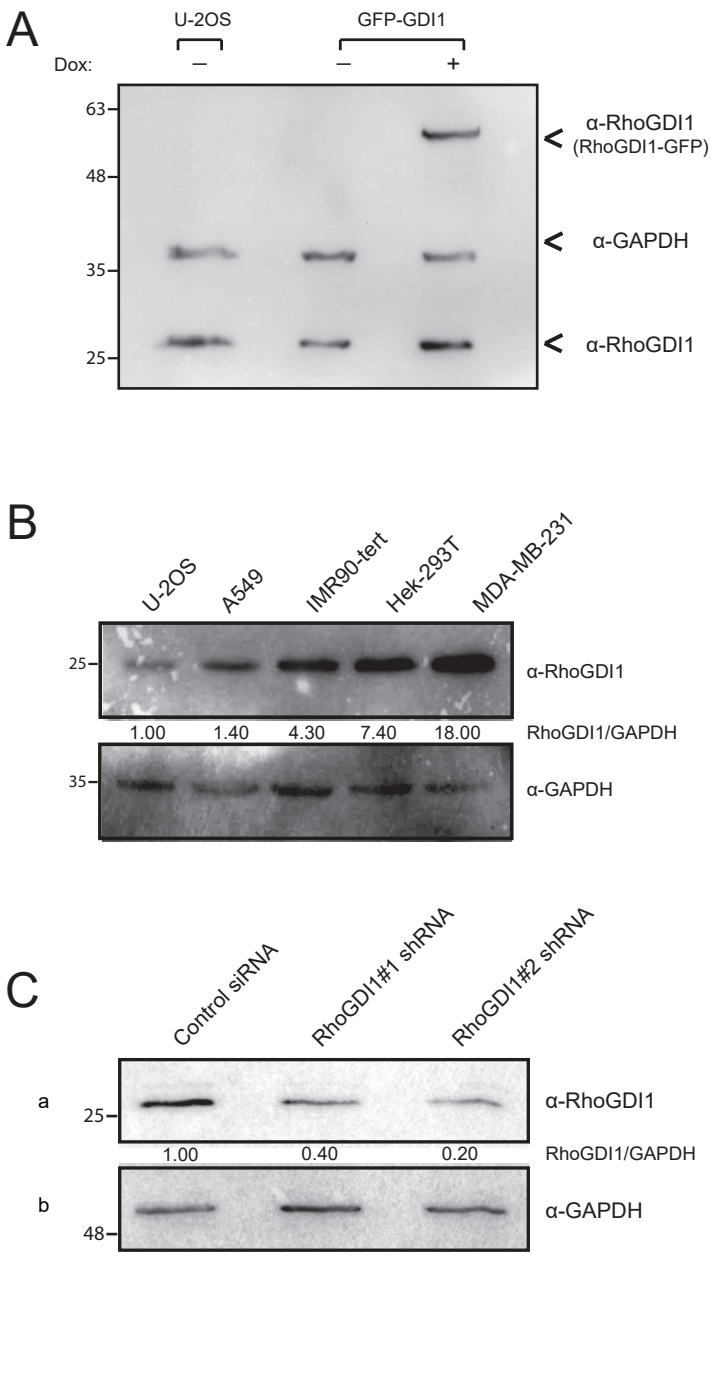

Fig. S7. Endogenous expression of RhoGDI1 in different cell lines.

(A) Western blot analysis of whole cell lysates from U2OS cells as well as U2OS cells over-expressing GFP tagged RhoGDI1 (GFP-GDI1) is shown. The expression of GFP-RhoGDI1 is induced by Doxycycline (Dox). The immunoblots were probed with anti-RhoGDI1 antibody (which detected both recombinant RhoGDI1-GFP and endogenous RhoGDI1) and anti-GAPDH antibody is shown. (**B**)Whole cell lysates were prepared from U2OS, A549, IMR- 90tert, HEK293T and MDA-MB-231 cell lines and immunoblotted. Blots were probed using anti-RhoGDI1 antibody (upper panel) and anti-GAPDH antibody (lower panel). **(C)** MDA-MB-231 cells were treated with control shRNA or RhoGDI1 shRNA#1 or #2 and incubated for 48 h. Cells were harvested, lysed and immunoblotted. Blots were probed with anti-RhoGDI1 (panel a) and anti-GAPDH (panel b) antibodies. Numbers indicated on the left are the molecular weight markers. (**B-C**) The RhoGDI1/GAPDH ratios are indicated. (**D**) U2OS cells constitutively expressing GFP-RhoGDI1 for 72 h were fixed for IF and stained using F-actin (green). Nucleus was stained with DAPI (blue). Expression of GFP-RhoGDI1 is shown with 'red' pseudo-colour. Magnified views of the dashed boxes are shown. White arrows indicate stress fibers. Scale bar: 10 µm.

Fig. S8. Blot Transparency

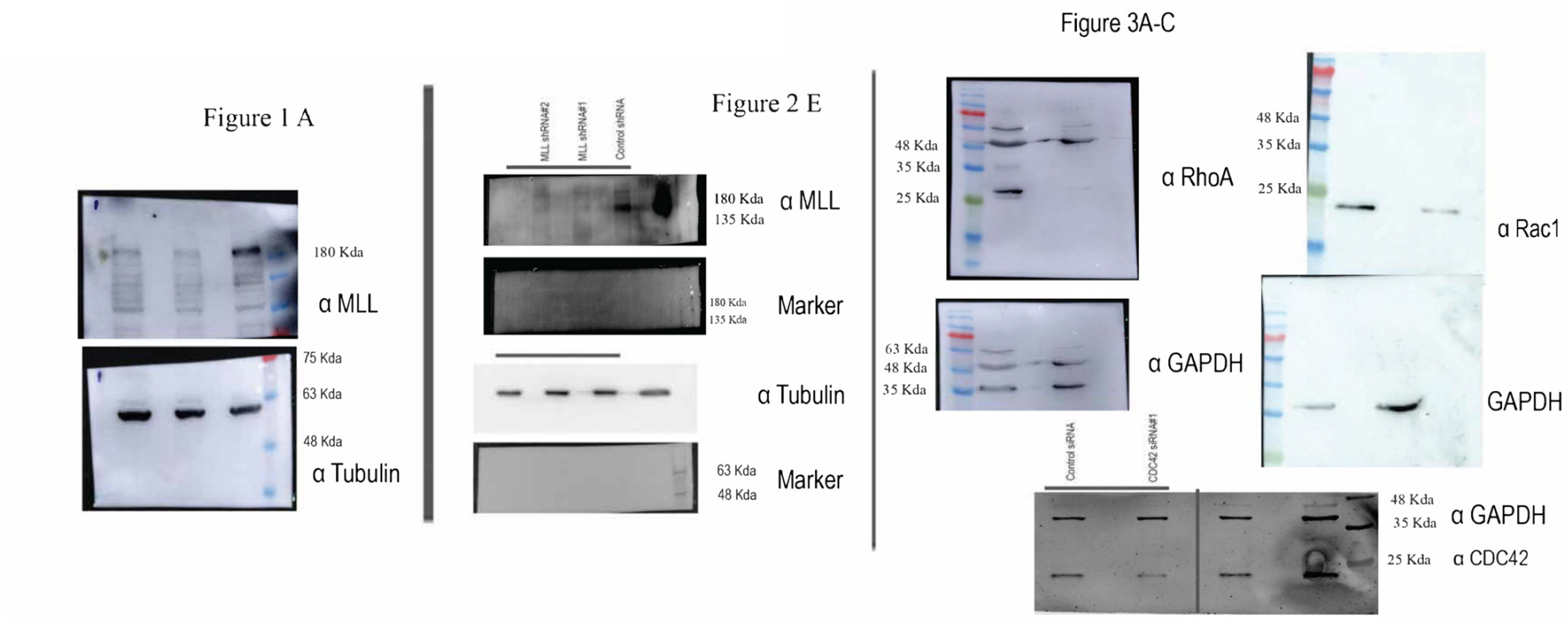

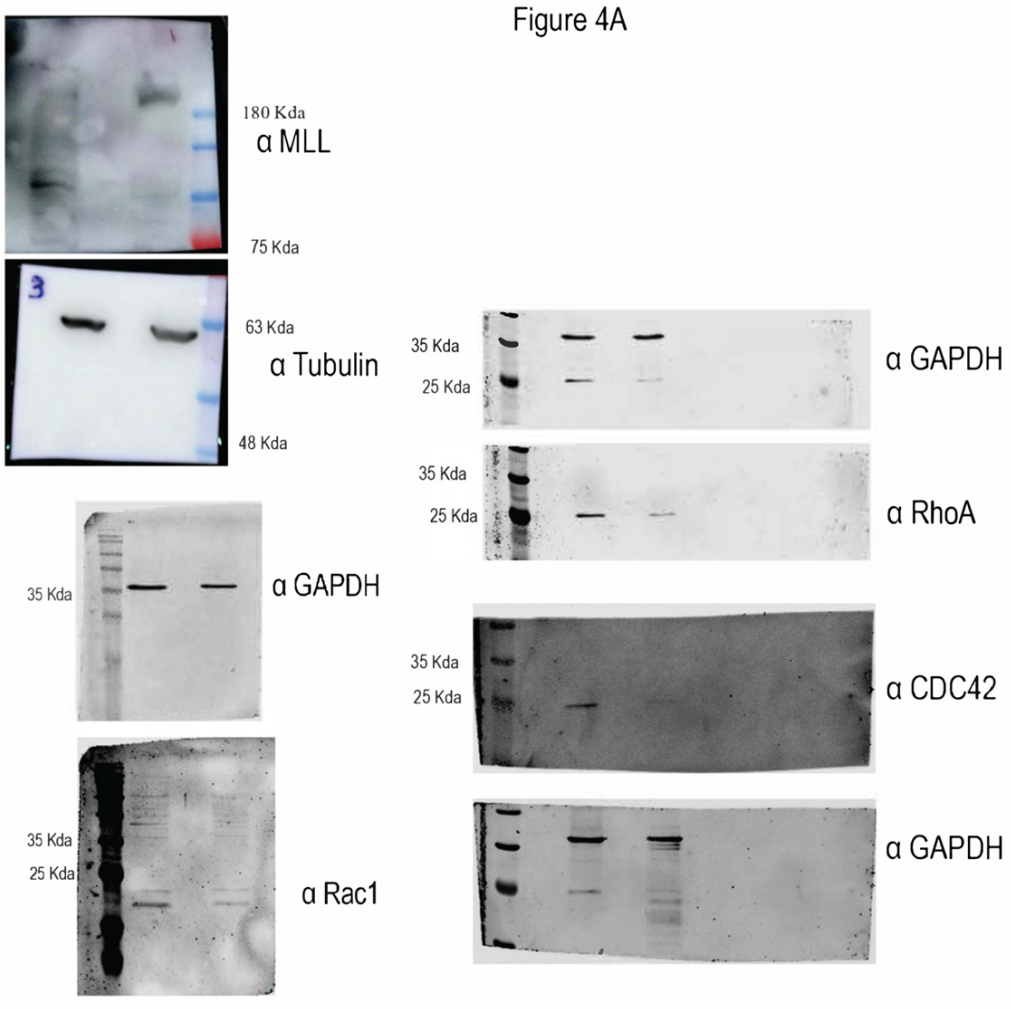

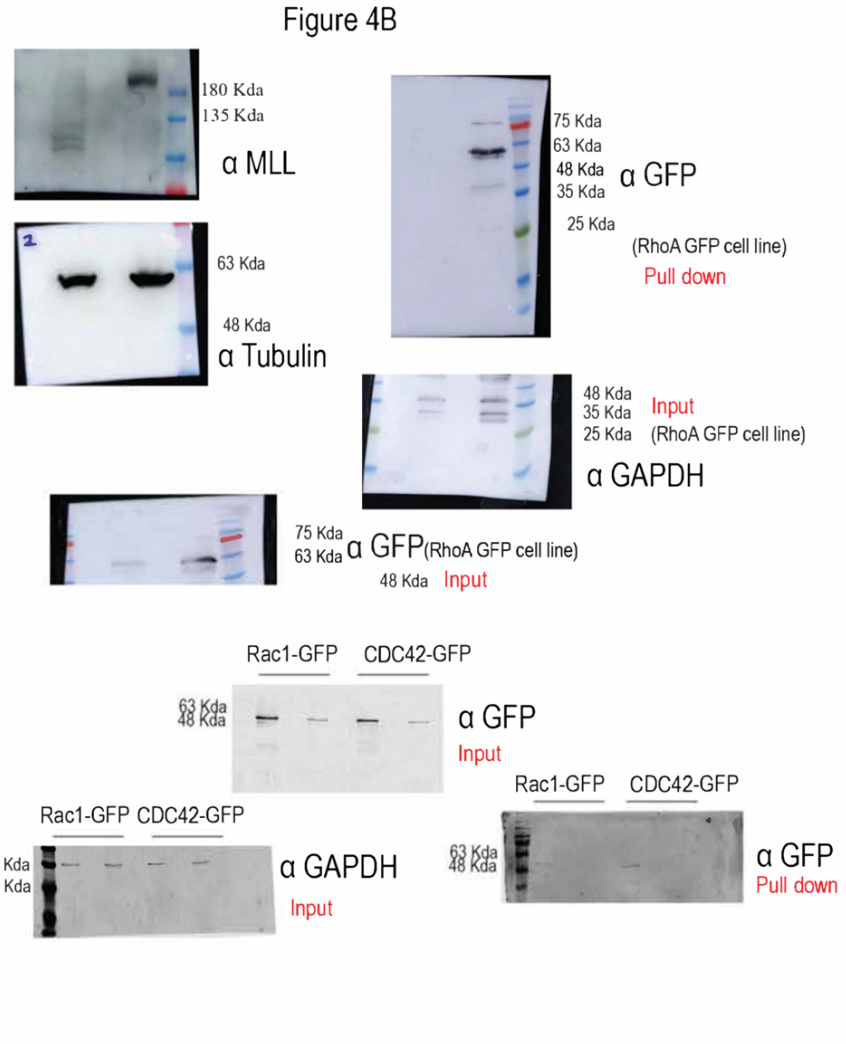

Figure 5A

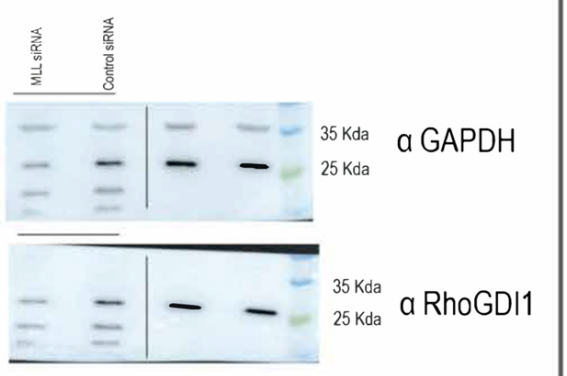

Figure 5B

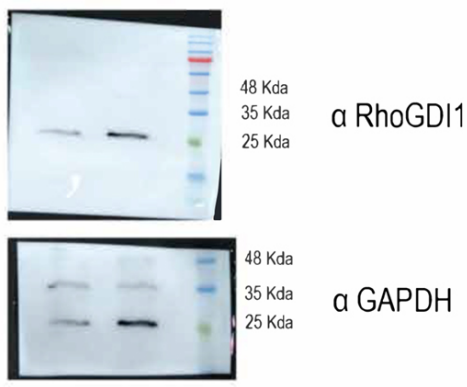

Figure 5E

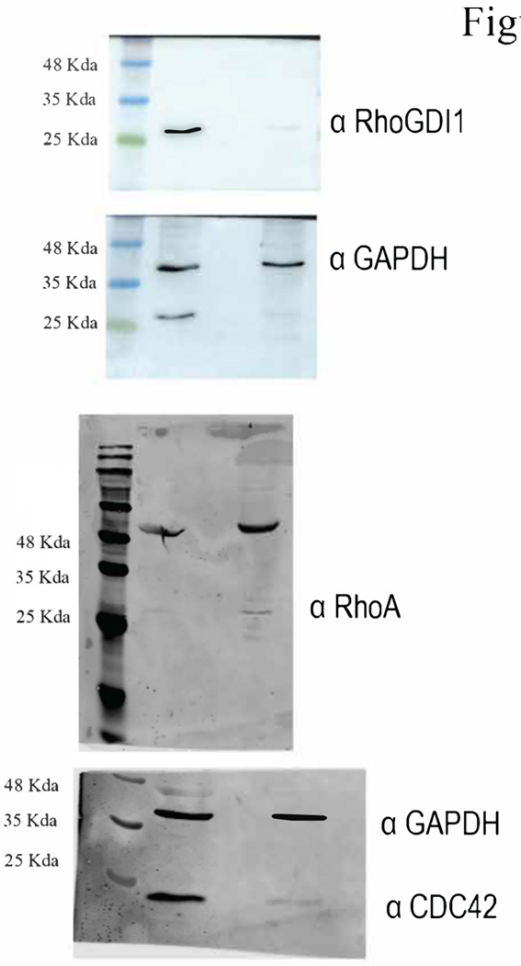

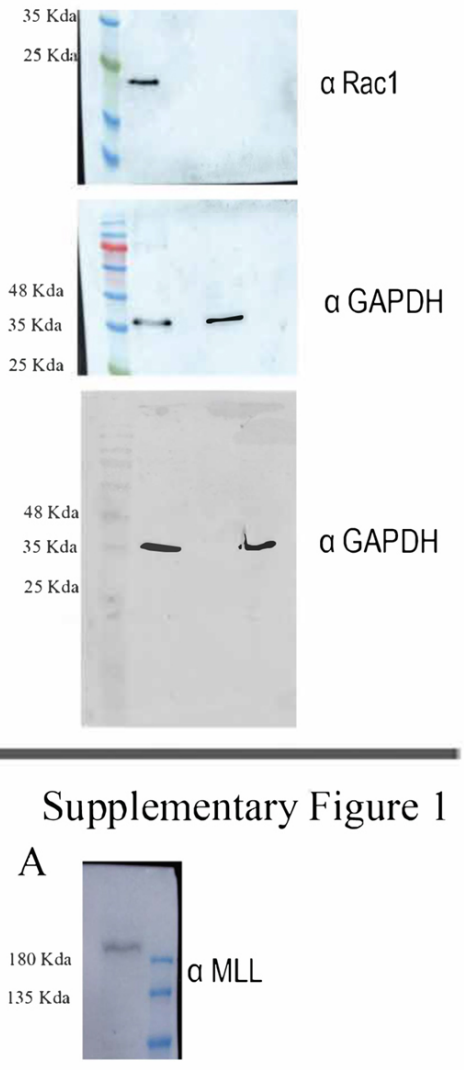

Supplementary Figure 1

Figure 7A

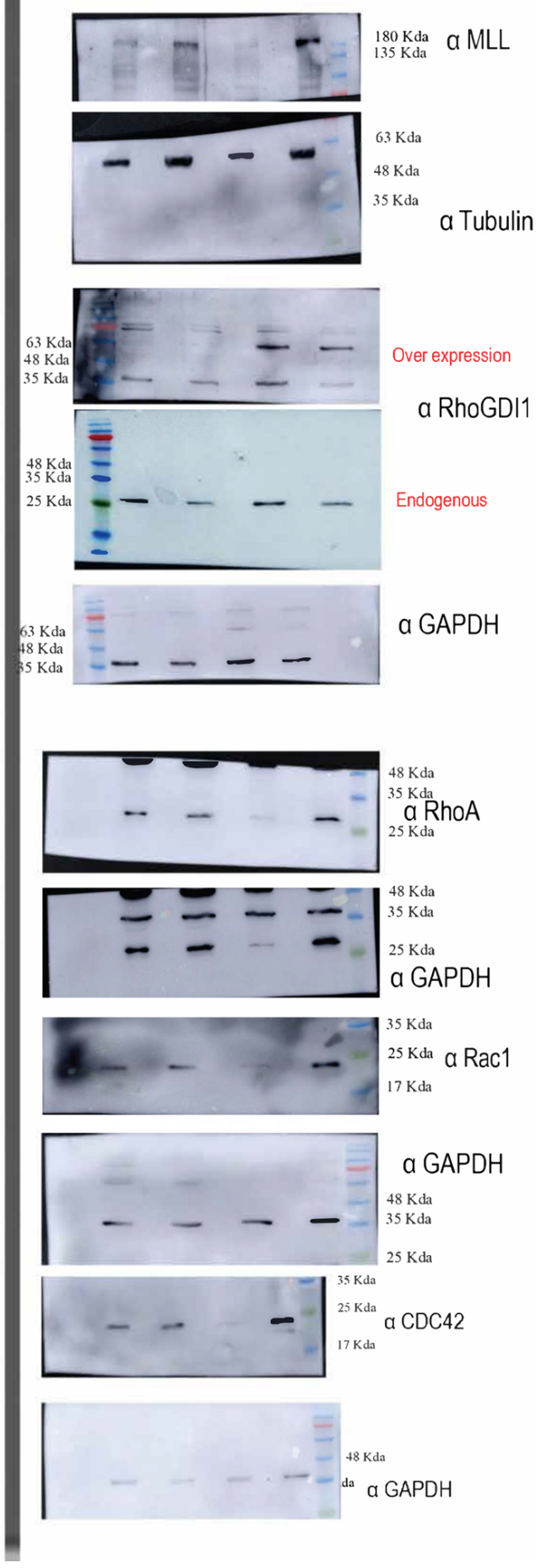

Supplementary Figure 4A

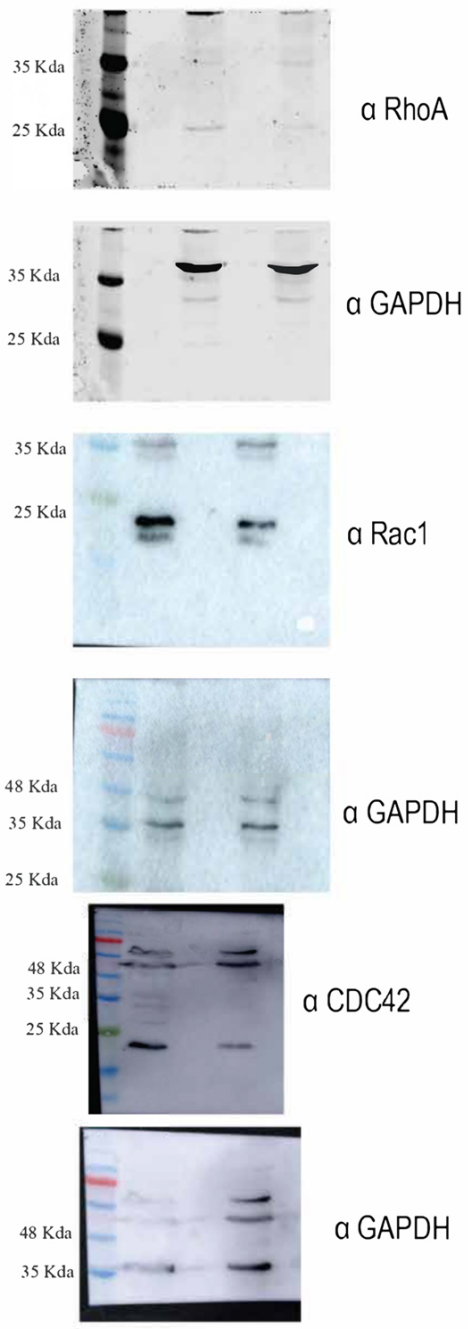

Supplementary Figure 4B

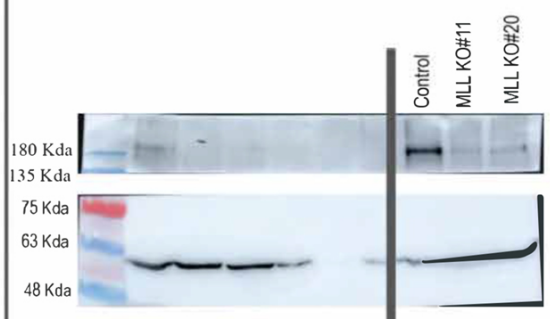

Supplementary Figure 4C

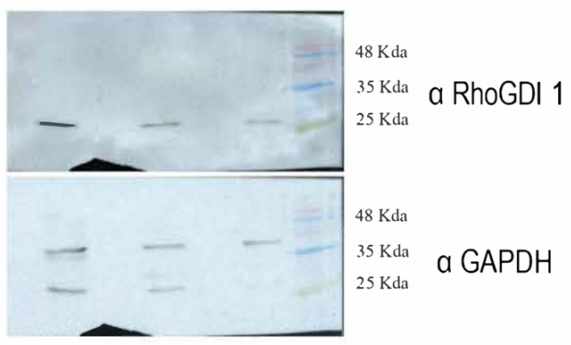

Supplementary Figure 5A

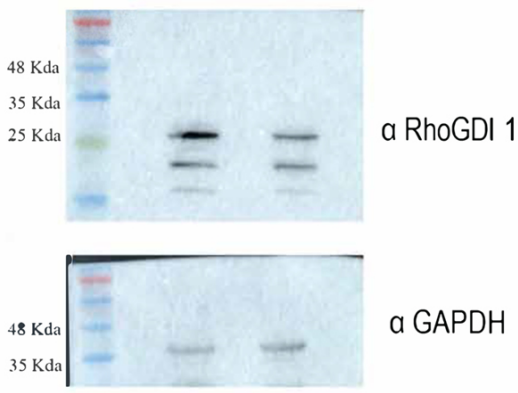

Supplementary Figure 7B

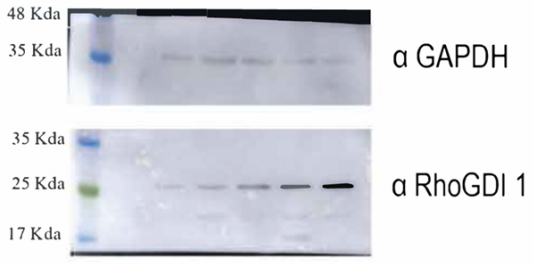

Supplementary Figure 4F

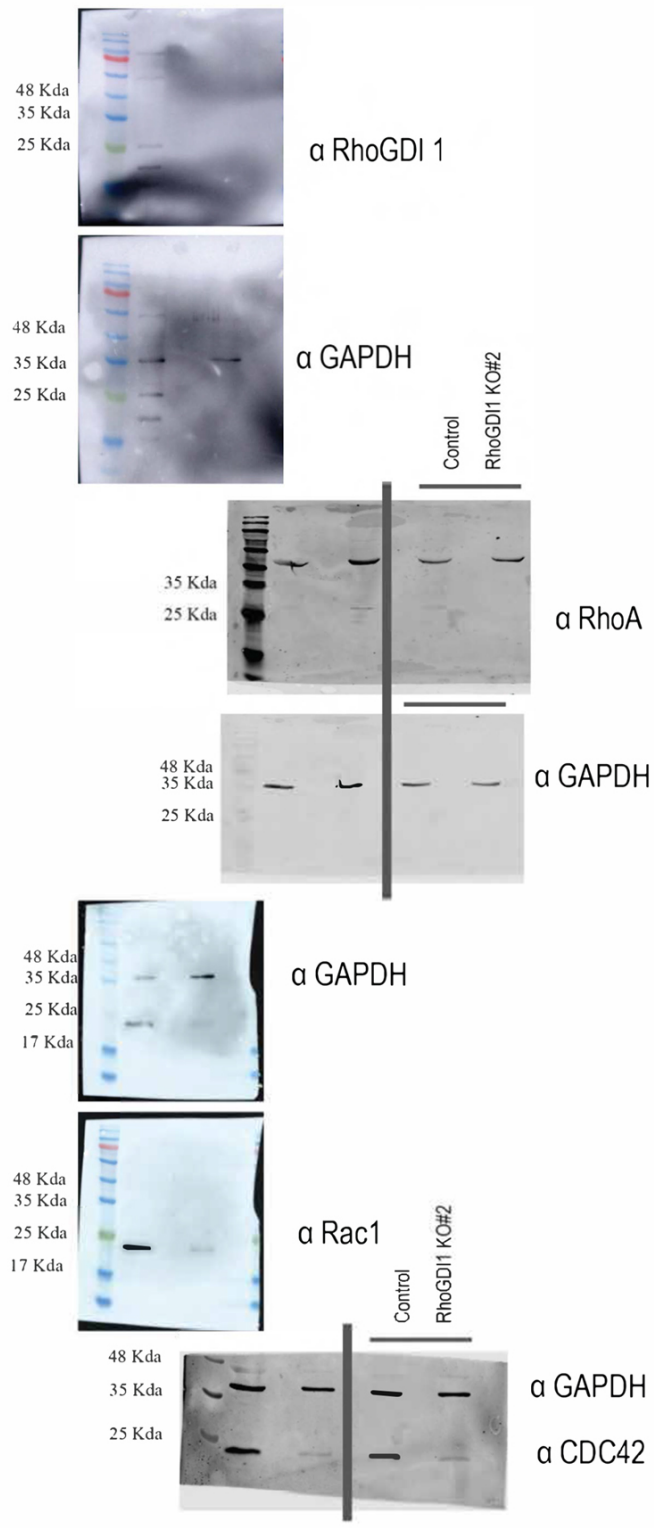

Supplementary Figure 4D

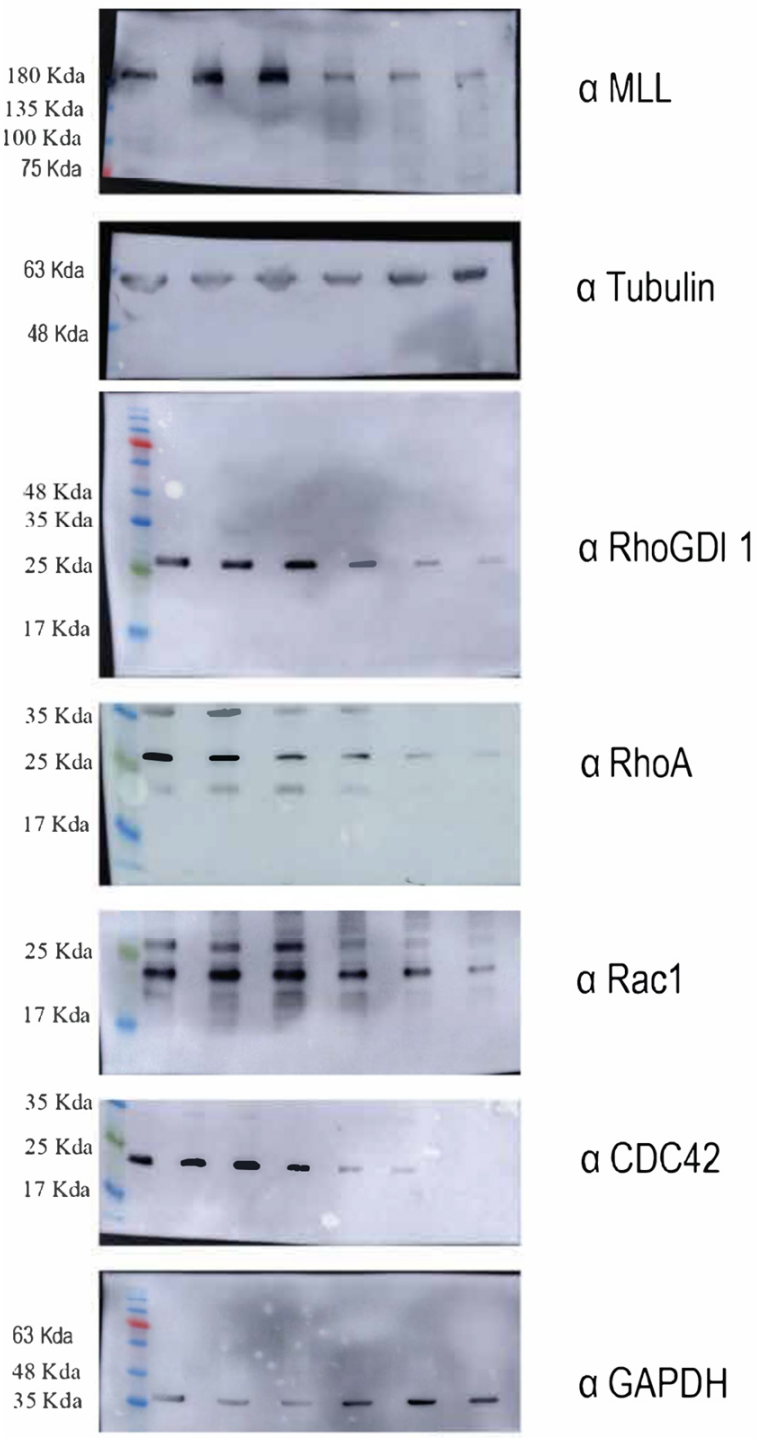

Supplementary Figure 7A

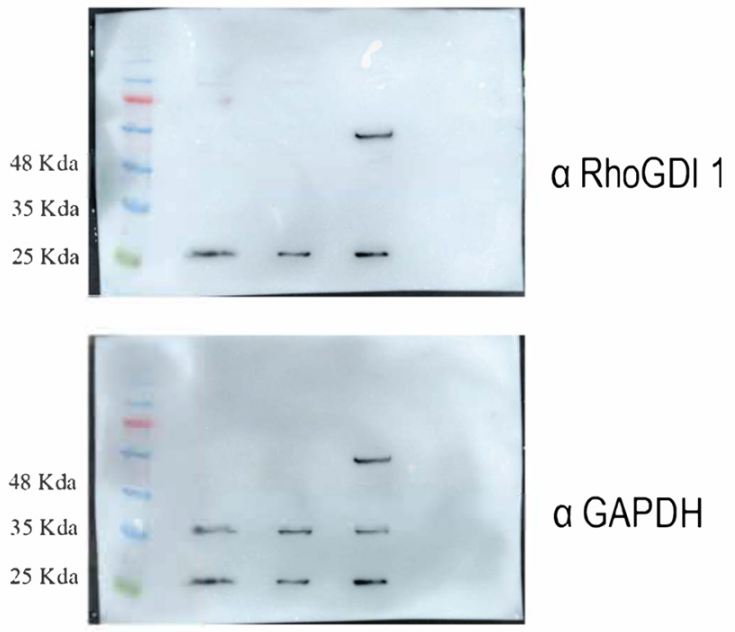

Supplementary Figure 7C

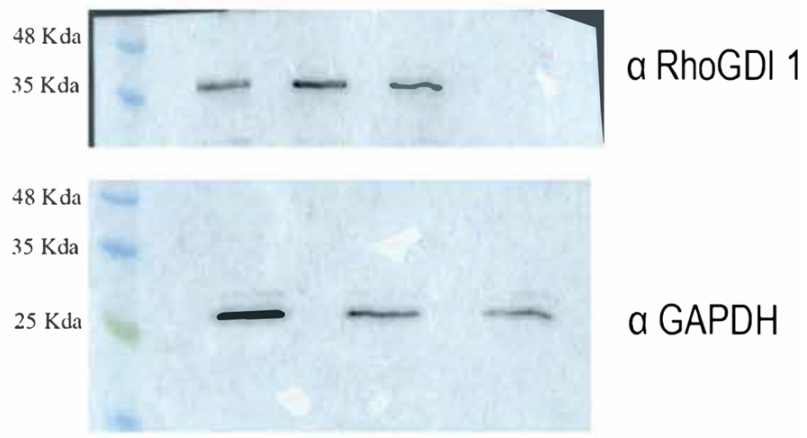

Table S1. Primers used for transcript analysis

Primer Names	Sequences
GAPDH qRT	F: 5'-ATGTTCGTCATGGGTGTGAA-3' R: 5'-GAGGCAGGGATGATGTTCTG-3'
MLL qRT	F: 5'-ATCGTCCACCGCAAATGCTTCTA-3' R: 5'-AGCCATGCCAATCTCATCTTGTT-3'
RhoA qRT	F: 5'-AAGGACCAGTTCCCAGAGGT-3' R: 5'-TTCTGGGGTCCACTTTTCTG-3'
Rac1 qRT	F: 5-'CGCAAACAGATGTGTTCTTA-3' R: 5'-CTAGGATGATGGGAGTGTTG-3'
CDC42 qRT	F: 5'-CTGAAGGCTGTCAAGTATGT-3' R: 5'-GAGAGATGTTCATAGCAGCA-3'
RhoGDI1 qRT	F: 5'-TAGGATCCCGGCGCCTAC-3' R: 5'-TTGGGGTCTGCGGAAACG-3'
RhoGDI2 qRT	F: 5'-ACAAAGCAGGGAAGTGTCAGA-3' R: 5'-GTCAGAGTTGAGAGACAGAGGC-3'
RhoGDI3 qRT	F: 5'-GGACCAGGTGTTTGTCCTGA-3' R: 5'-CCACGGGAGTCACAAACT-3'

Table S2. Primers used for ChIP assay

Primer names	Sequence
RhoGDI1 PROMOTER (P1)	F: 5'-GTGAGCGGAAGTCTCGTG-3' R: 5'-GCCGCGCGGTTCAGGATC-3'
RhoGDI1 UPSTREAM (U1)	F: 5'- GGGCGAATGTGTGGAATCTC-3' R: 5'-CACCGTGAGCAGATGAGGG-3'
RhoGDI2 PROMOTER (P2)	F: 5'-CCAGGGTTTCCTCTTCAAGTAG-3' R: 5'-CTGTCTCTCAACTCTGACTTC-3'
RhoGDI2 UPSTREAM (U2)	F: 5'-GAAGAAAAATCAGCCAAAACTA-3' R: 5'-TCCTTAAACAGATTTTTGGAGT-3'
RhoGDI3 NEGATIVE (U3)	F: 5'-AAGGGCGGGTCTAATTTCTG-3' R: 5'-CTGCGTCTGGATAAGGGAG-3'
RhoGDI3 POSITIVE (U4)	F: 5'-TACTGATGACCGTGAACCTG-3' R: 5'-CTGAGGGAGCTTCTGTCTG-3'
HOXA9	F: 5'-CTCCGCCGCTCTCATTCTCAG-3' R: 5'-GCCAGAAGGGGTGACTGTCC-3'
CD4	F: 5'-TGTGCTCTGCCCAGTTGTCT-3' R: 5'-GCTCATGACCAGTTCCAAGAGAA-3'

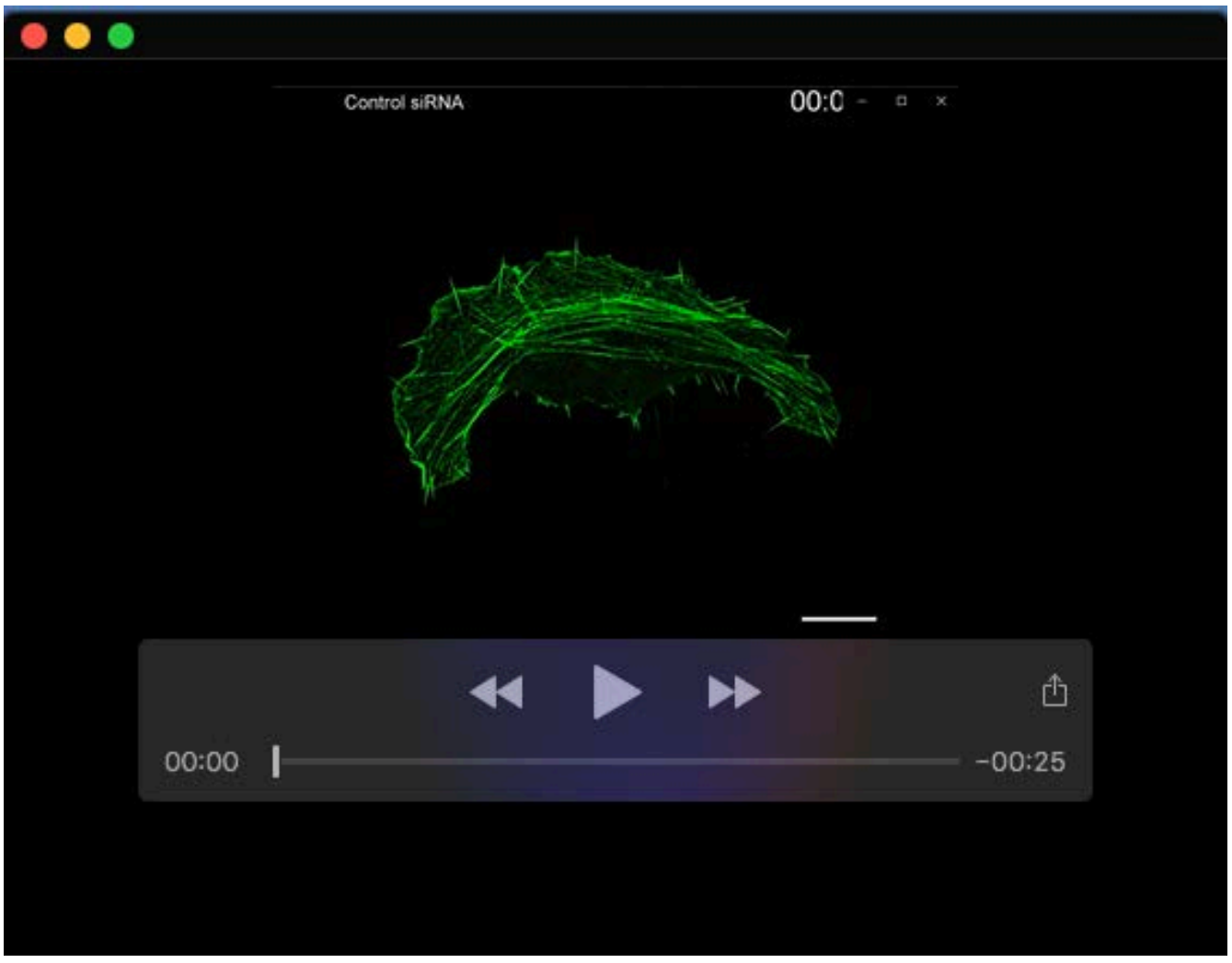

Movie 1. U-2OS cell expressing GFP-Lifeact (green) treated with control siRNA, corresponding to Figure 3G panel a, is shown here. Frame size is 73x73 µm and frame step is 5 s. Scale bar, 10 µm.

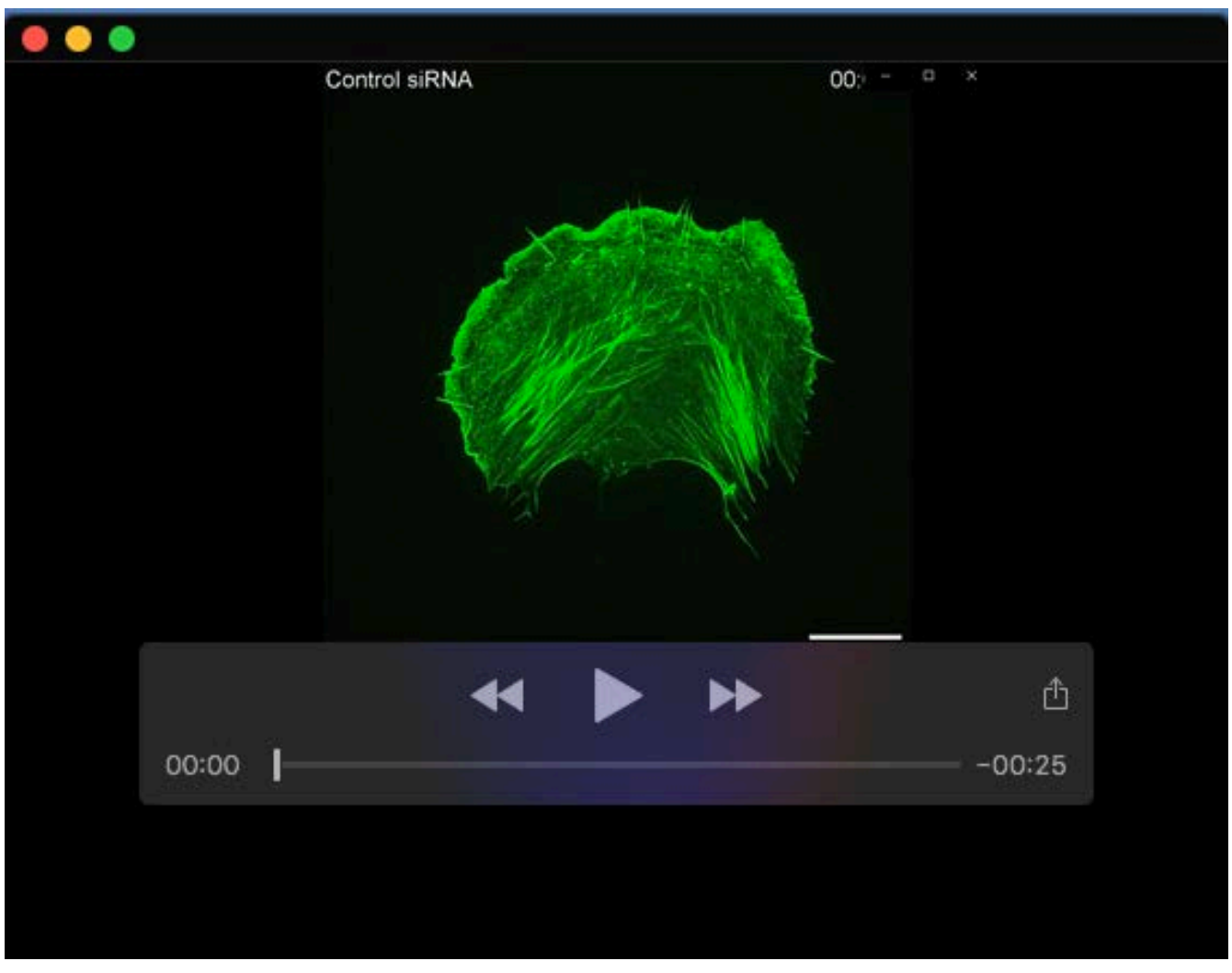

Movie 2.Shown here is U-2OS cell expressing GFP-Lifeact treated with control siRNA, corresponding to Figure 3G panel b, Frame size is 64x64 µm and frame step is 5 s. Scale bar, 10 µm.

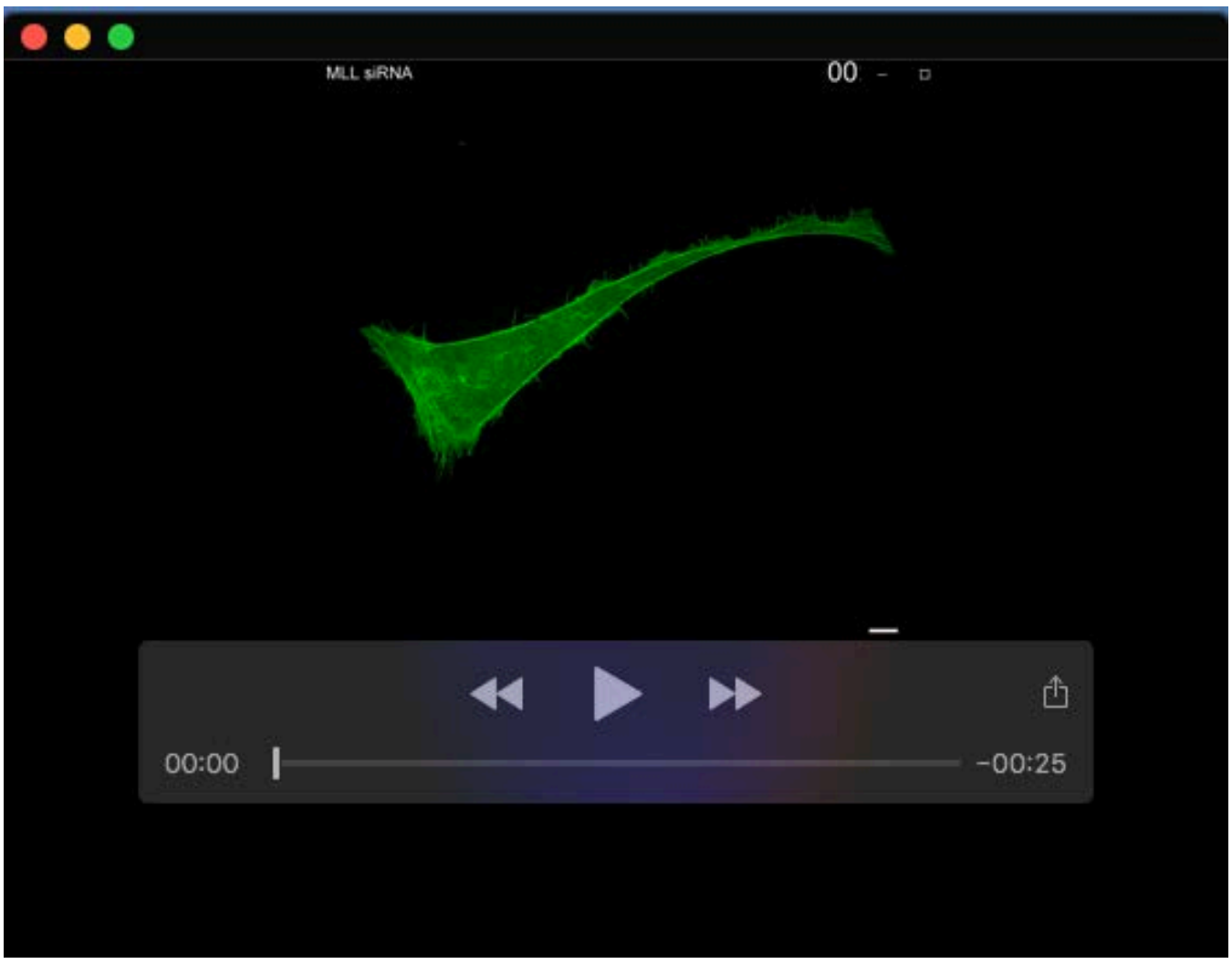

Movie 3. U-2OS cell expressing GFP-Lifeact (green) treated with MLL siRNA#1, corresponding to Figure 3G panel c is shown. Frame size is 128x128 µm and frame step is 5s. Scale bar, 10 µm.

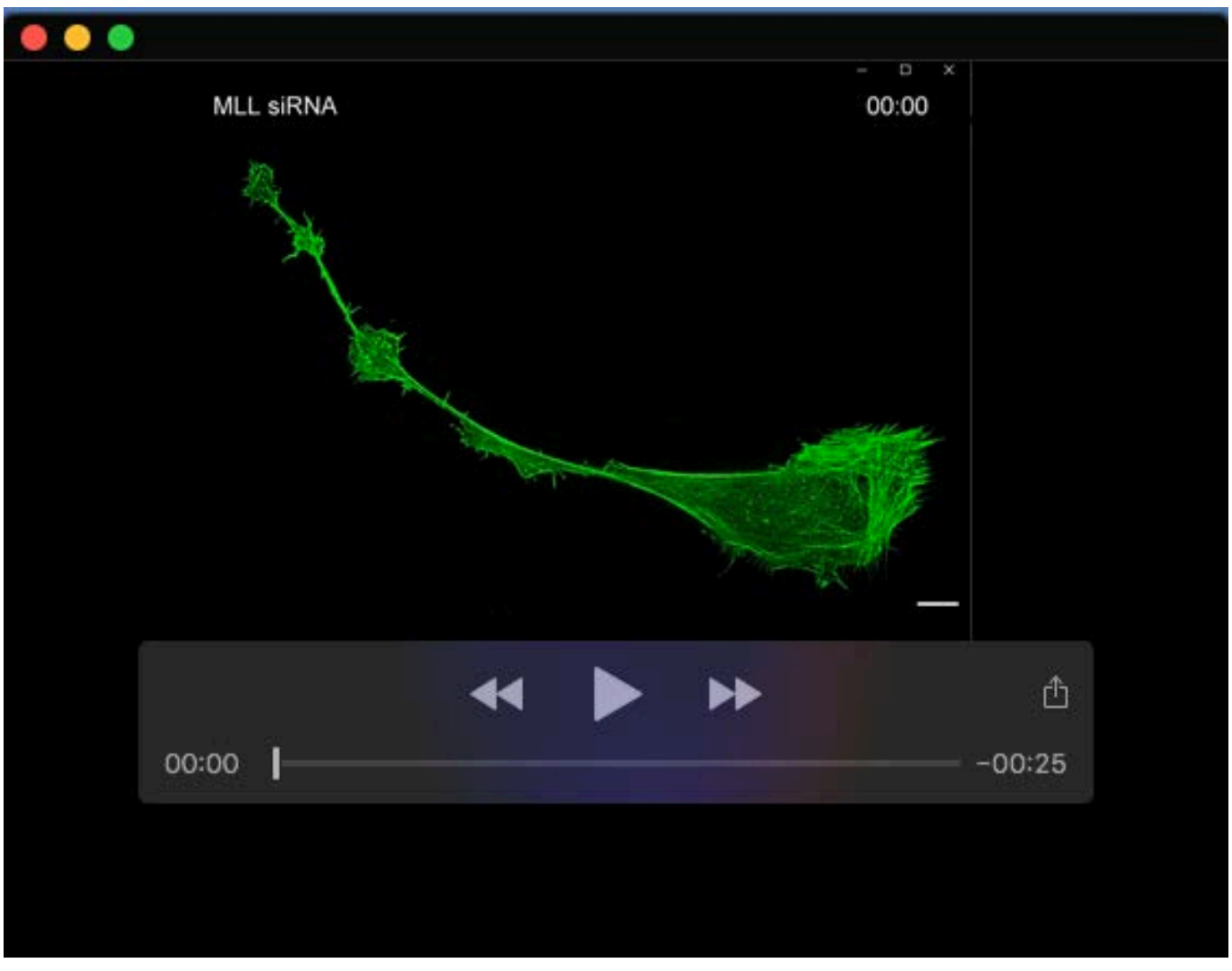

Movie 4. U-2OS cell expressing GFP-Lifeact (green) treated with MLL siRNA#1, corresponding to Figure 3G panel d is shown. Frame size is 186x130 µm and frame step is 5 s. Scale bar, 10 µm.